COUPLED ELECTRO-MECHANICAL SYSTEM MODELING AND EXPERIMENTAL INVESTIGATION OF PIEZOELECTRIC ACTUATOR-DRIVEN ADAPTIVE STRUCTURES

by

Su-Wei Zhou

Dissertation submitted to the Faculty of the

Virginia Polytechnic Institute and State University

in partial fulfillment of the requirements for the degree of

Doctor of Philosophy

in

Mechanical Engineering

APPROVED:

Dr. Craig A. Rogers, Chairman

Dr. Daniel J. Inman

Dr. Harry H. Robertshaw

Dr. O. Hayden Griffin, Jr.

Dr. Chen Liang

August, 1994
Blacksburg, Virginia

COUPLED ELECTRO-MECHANICAL SYSTEM MODELING AND EXPERIMENTAL INVESTIGATION OF PIEZOELECTRIC ACTUATOR-DRIVEN ADAPTIVE STRUCTURES

by

Su-Wei Zhou

Committee Chairman: Dr. Craig A. Rogers

Mechanical Engineering

(ABSTRACT)

Of primary importance to the design and application of adaptive structures is a modeling method to allow for performance prediction and parametric optimization of the integrated system. The statics-based modeling approaches have been applied to model piezoelectric (PZT) actuator-driven adaptive structures. The dynamic interaction between the actuators and their host structures has been ignored, and the system energy conversion can't be predicted. As a matter of fact, PZT actuator-driven smart structures are complex electro-mechanical coupling systems in which electrical energy is converted into mechanical energy and vice-versa. The actuator outputs and the system energy conversion are dominated by the complex electro-mechanical impedance of the system. The entire actuator/substrate system can thus be essentially represented by a coupled impedance-based system model. This research presents such an impedance-based electro-dynamics analytical method and the experimental investigation for integrated PZT/substrate systems. When compared with the conventional static models, the system modeling method has revealed the physical essence and the interconnections among the intelligent elements and

supporting structures. The frequency-dependent behaviors of the actuator and the dynamic response of the integrated system are accurately predicted.

The theoretical model was developed for generic PZT actuator-driven active structures. The actuation force was evaluated as a result of the dynamic interaction between the actuator and the host structure. The model was then extended to include the electrical parameters of the PZT actuator such that the power flow and consumption of the integrated system can be predicted. The system dissipative power was then treated as the equivalent generation source to evaluate a temperature rise and thermal damage of the actuator. To examine the utility and generality of the system modeling method, the developed model was applied to typical two-dimensional structures such as thin plates and thin shells, and to one-dimensional structures such as the circular rings and beams. The design-related mechanical and thermal stress characteristics of the actuators were also specifically investigated.

In addition to the theoretical work, experiments were conducted. The PZT actuator-driven simply-supported plate was built and tested. The velocity response of the integrated plate and the dynamic strain of the PZT actuators were measured. The coupled electro-mechanical admittance of the real system was also directly measured using an impedance analyzer. The predicted solutions agree with the experimental results in all of the tested cases, verifying the theoretical model.

ACKNOWLEDGMENTS

I would like to express my sincere gratitude to Dr. Craig Rogers, my major advisor, for his intellectual advice and financial support throughout this study. I truly appreciate his confidence in me at all stages of my research. His wonderful philosophy on adaptive structures inspires me to explore new ideas in this area. I would also like to specially thank Dr. Dan Inman for his valuable comments on my dissertation and Dr. Chen Liang for his help to the study, and for both of them kind presence on my committee. Drs. Harry Robertshaw and Hayden Griffin also deserve a hearty thanks for kindly serving as members of my committee and for their valuable suggestions throughout this endeavor.

I wish to acknowledge all the staff and students at the Center for Intelligent Material Systems and Structures for their generous assistance and true understanding at all times. My special thanks go to Ms. Beth Howell and Ms. Brenda Neidigh for their time and patience on the careful proof-reading of my papers and dissertations.

I am specially grateful to my wife, Xiao-Feng, for her unconditional support and understanding from the beginning of my interest in continuing my education in the United States, and for helping me endure this stress-filled time. Without her love and great encouragement, the past three years would not have been possible. I am also greatly indebted to my son, Cong, who makes me appreciate the beauty of life and gives me much more energy to accomplish this dissertation. Thank you, my parents and sisters,

for always being a continuous source of support and encouragement in my pursuit of knowledge and a wonderful life.

Finally, I would like to gratefully acknowledge the support of the Office of Naval Research and the Air Force Office of Scientific Research in this study.

Table of Contents

Chapter 4

Chapter 5

Chapter 6

Chapter 7

Lists of Figures

Lists of Tables

Chapter 1

Introduction

1.1 Background

In the past decade, significant research efforts have been devoted to developing adaptive structures or intelligent material systems. Such systems can integrate intelligence and life features into the microstructure of the system to produce adaptive functionality and to also reduce mass and energy (Rogers, 1993). The emergence of intelligent material systems represents a novel and exciting technology in an interdisciplinary scientific and engineering field involving mathematics, materials, mechanics, dynamics, acoustics, and controls. Research in this area has already produced many prominent applications, such as vibration and acoustic control (Bailey and Hubbard, 1985; Rogers, 1990; Zhou, 1991), motion control (Garcia and Inman, 1990), shape alternation (Chaudhry and Rogers, 1991), non-destructive evaluation (Hickman et al. 1990; Zhou et al., 1993; Tappert and

Robertshaw, 1994), failure prevention (Rogers et al., 1990), and system identification (Sun et al., 1994).

From the standpoint of the system architecture, an adaptive structure is an integration of host structures (beams, trusses, plates, shells, and complex structures) with guest components (actuators, sensors, and controllers). One of the most important elements in adaptive structures is an actuator, which acts like muscles in a biological system to implement energy input. An actuator is classified as an induced strain actuator if it produces strains in response to external stimuli such as electricity, magnetism, and heat actuation, etc. The induced strain actuators can be flexibly fabricated with conventional engineering materials to form unified composite structures. This may be one of the most convincing reasons for the induced strain actuators to be more favored than conventional "point" actuators (shakers etc.) in various applications. The fabrication of the induced strain actuators can be surface-bonded, embedded, or attached to the host structures. Such actuators thus provide a powerful means to realize flexible control strategies and to tune the structural response.

The most commonly used induced strain actuators include piezoelectric actuators (PZT and PVDF), magnetostrictive actuators (Terfenol-D), electrostrictive actuators (PMN), and the thermomechanical actuators (shape memory alloys). Among them, piezoelectric (PZT) elements have become increasingly important because piezoelectric elements have

demonstrated competitive characteristics, such as light weight, compact size, and good dynamic output performance. In addition, the ability of piezoelectric materials to transform mechanical energy to electrical energy and vice-versa makes them well suited to be both actuators and sensors. This dissertation will focus on the system modeling and design issues of piezoelectric actuator-driven adaptive structures.

1.2 Introduction to System Modeling

Of primary importance to the design and application of adaptive structures is a modeling method to allow for performance prediction and parametric optimization of the system. How accurately and effectively a real system is described by a mathematical model is always a great challenge to practitioners and designers of engineering structures and materials.

For induced strain actuator-driven intelligent structures, inherent interconnections between host structures and their guest components always exist, such as force equilibrium, deformation compatibility and energy transfer, etc. Figure 1.1 shows a schematic representation of these connections. Use of these essential relations provides a necessary basis for the system modeling.

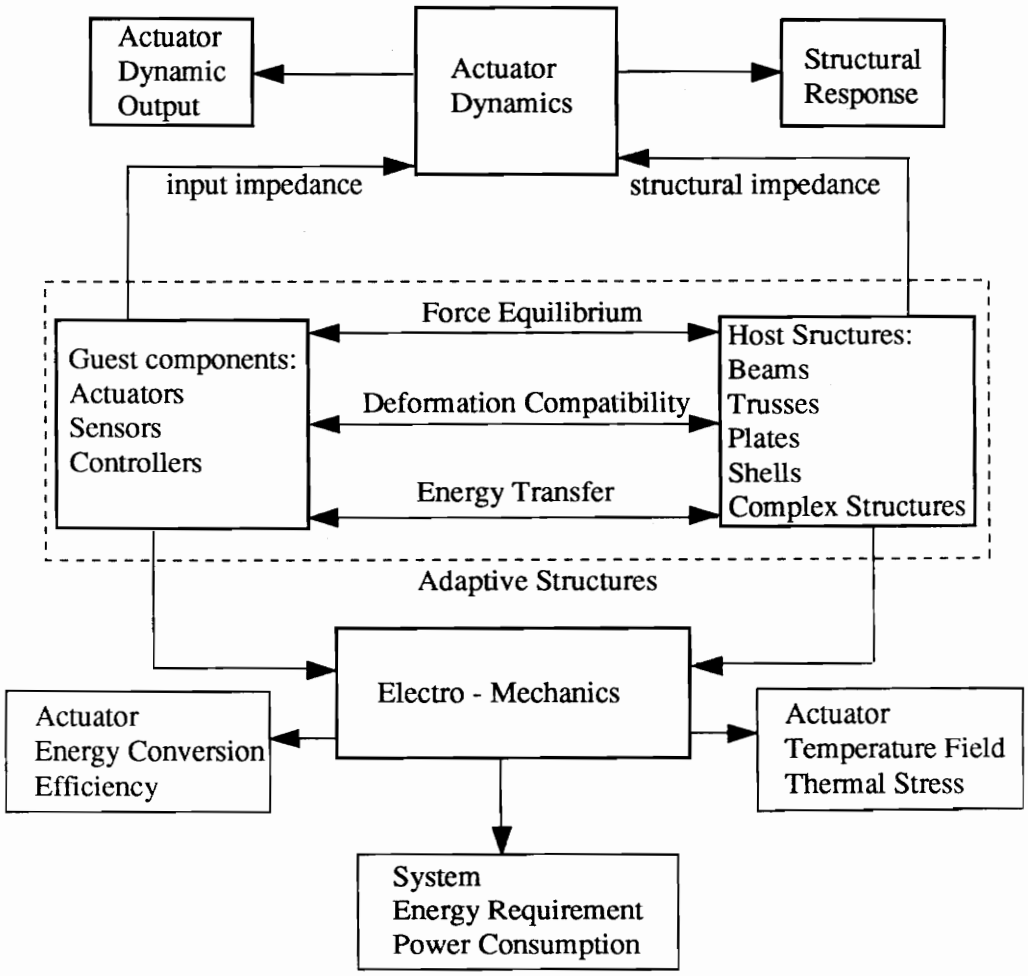

Figure 1.1: Schematic representation of system modeling of adaptive structures.

The actuation mechanism of the induced strain actuators may simply be expressed by a constitutive equation:

$$\varepsilon = \varepsilon_{mech} + \varepsilon_{ther} + \varepsilon_{free} \ , \tag{1.1}$$

where ε is the real induced strain of an actuator; ε_{mech}, ε_{ther}, and ε_{free} are the mechanical strain, the thermal strain, and the free-constrained strain, respectively. The first two terms of the strains are related to the behaviors of the host structures. The third term is the free strain without any mechanical constraints, and is a function of input or stimuli, such as an applied voltage. Equation 1.1 thus gives a substantial strain-input relationship for modeling the induced strain actuator-driven adaptive systems. The formulation are suited for all of induced strain actuators regardless of the type of external stimuli.

1.3 Review of Modeling Integrated Piezoelectric Actuators

Modeling of integrated piezoelectric (PZT) actuators was conducted in the early development and implementation of the PZT actuators in active control systems. The objective is to establish a transduction equation from the input voltage (or electrical field) to the active loading applied by the actuators on host structures. Several different modeling approaches have been developed to determine the induced force or moment outputs of the PZT actuators integrated with one-dimensional beams or two-dimensional plates and shells.

1.3.1 Static Modeling Approach

Figure 1.2 shows the static models using different assumptions of the strain or stress distribution. Bailey and Hubbard (1985) suggested a model of piezoelectric actuators bonded on a cantilevered beam. A constant force output of the actuator was predicted, and it is proportional to the applied voltage. The model is usually called the pin-force model because of the assumption of a pin-force loading applied to the host beam. Crawley and de Luis (1987) conducted a more rigorous study using Bernoulli-Euler beam theory. The model included both the pure bending actuation and the pure extensional actuation as PZT actuators are embedded in and bonded on a one-dimensional beam. In 1989, Dimitriadis et al. (1989) investigated the behavior of a two-dimensional PZT/plate structure actuated in a pure bending mode, and estimated the induced moment loading on the supporting elastic plate. The constant moment was then applied to develop an approximate dynamic model for determining the vibration response of the host plate. Later on, Kim and Jones (1991) refined this model using the assumption that the slope of stress distribution is different through the PZT layer and the plate. The maximization of the effective moment under a constant electric field was also discussed. In addition, Wang and Rogers (1991) presented a linear strain distribution-based model using laminated plate theory. The equivalent active force was determined upon the assumption of free constraint for the expansion or contraction of the PZT patch actuator. The model was suited for both the embedded and surface bonded PZT actuators. In the meantime,

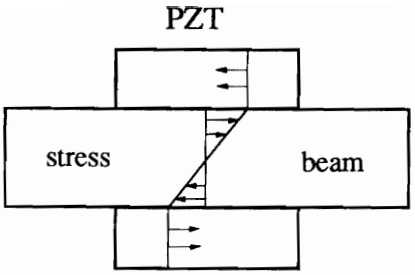

(a)

A model of the integrated beams,
(Bailey and Hubbard, 1985).

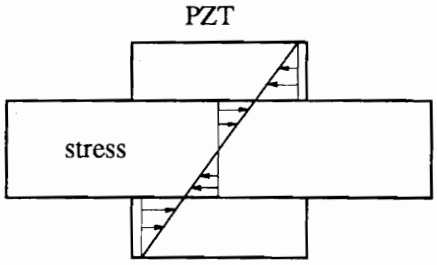

(b)

A model for the integrated plates,
(Dimitraidis, Fuller, and Rogers, 1989).

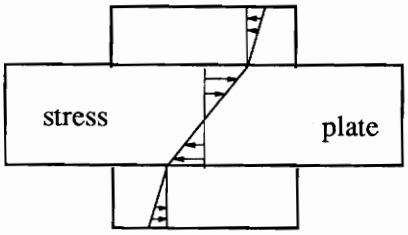

(c)

A model for the plates,
(Kim and Jones, 1991).

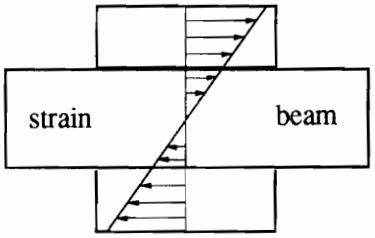

(d)

A model for the integrated beams,
(Crawley and Anderson, 1990).

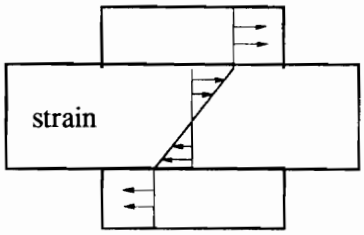

(e)

A model for the integrated beams and plates,
(Crawley and de Luis, 1987, for the beams; Crawley and de Luis, 1991, for the plates;
Wang and Rogers, 1990, for the plates; Lee, 1990, for the plates).

Figure 1.2: The geometric representation of the static models using different assumption of induced strain or stress for integrated PZT actuators.

Lazarus and Crawley (1989), and Crawley and de Luis (1991) expanded their one-dimensional model to two-dimensional isotropic and anisotropic plates. A cantilever plate was built and tested to verify the ability of the model to predict the induced strains. Crawley and Anderson (1990) also improved their model by assuming the linear strain distribution cross both the PZT actuator and the beam. Another rigorously theoretical investigation of integrated piezoelectric structures was conducted by Lee (1990). The formulations for the reciprocal relationship of the piezoelectric sensors and actuators were derived. The electromechanical actuation and mechanoelectrical sensing behavior of the piezoelectric laminate was formulated.

In addition to the smart beam and plate structures, piezoelectric actuator-driven shell structures were widely studied. Tzou (1989) investigated actively-controlled cylinders using layered shell theory; in his study, a completely distinct layer of the piezoelectric material was used to make up a composite cylinder. A more convenient and feasible configuration of PZT actuators bonded on the surface of cylinders was researched by Sonti and Jones (1991) as well as Lester and Lefebvre (1991). In their modeling, the assumption was made that the dimension of the PZT patch in circumferential direction is kept small relative to the cylinder radius, thus the curvature effects could be neglected. The models developed from thin plate theory could then be used in smart shell structures. Lester and Lefebvre (1991) investigated both out-of-plane and in-plane piezoelectric actuation for controlling sound radiation and transmission related to vibrating cylinders.

Sonti and Jones (1991) compared the performance of the controlled cylinder using the piezo-actuator control patch and a point control force for both on- and off-resonance cases.

The static models mentioned above have different formulations for predicting the static force or moment output of the piezoelectric actuators. Nevertheless, a similarity exists amongst these models, that is, the predicted active loading of the PZT actuator is always a constant force or moment. The static models have also been used as an approximate dynamic loading in dynamic analysis. The static modeling approaches, however, do not consider the added dynamic stiffening effect and inertial mass loading of the PZT actuators. The dynamic interaction between the PZT actuator and the host structure is ignored. The static analysis usually leads to the conclusion that the amplitude of the excitation force of the PZT actuator is independent of frequency and host structural dynamics.

1.3.2 Dynamic Modeling Approach

To avoid the disadvantage of the static models, dynamic analytical approaches were suggested to describe the integrated PZT/substrate structures.

Inman (1990) investigated the phenomenon of the control/structure interaction (CSI) for the lumped dynamic system, as shown in Fig. 1.3. It was assumed that the actuators used for control have second-order dynamics. The effects of added actuator dynamics to the state feedback in vibration suppression problems were considered in the modeling. The stability of the integrated control system was specifically discussed.

Another dynamic model was proposed by Hagood et al. (1990). The model based on Rayleigh-Ritz energy formulation was developed for the PZT actuator-driven control system. The parasite mass and stiffness of the integrated PZT patch was included in the governing equation of the system:

$$(M+M_p)\ddot{r}+(K+K_p)r-\Theta v=B_f f \ , \tag{1.2}$$

where r and v represent the generalized displacement coordinate and voltage coordinate, respectively. Θ denotes electromechanical coupling matrix and B_f is the forcing matrix. **f** is the vector of external point forces. The model was applied to the cases of both direct voltage-driven electrodes and direct charge-driven electrodes. The actively controlled cantilevered beam was tested and the favorable results were obtained. However, actuator force loading is not explicitly expressed as a function of the actuator input impedance and the host structural mechanical impedance. As the active control force needs to be calculated, the blocking force was used so that the induced force loading is still independent of the dynamics of the host structure and frequency.

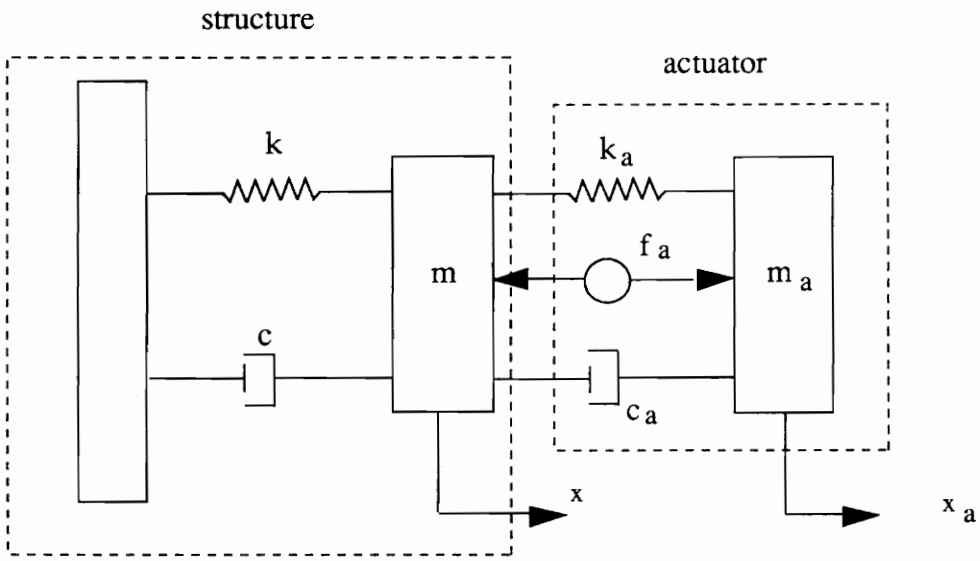

Figure 1.3: The model of control/structure interaction (CSI) for a single-degree-of-freedom systems (Inman, 1990).

1.3.3 Impedance Modeling Approach

A more realistic and accurate model of an adaptive structure must include the dynamic interaction between actuators and host structures. When a control voltage is applied to the PZT patch along the polarization direction, an active force is generated as a result of the mechanical interaction between the actuator and the structure. At this point, the PZT actuator itself is also driven by the force. The mass loading and stiffening effect of the PZT patch should be considered. This added dynamic effect plays an important role in the actuation on the host structure and may significantly change the mechanical resonant frequencies of the original system. Therefore, a dynamic model that relates the actuator dynamics to the host structure dynamics is desired.

Liang et al. (1993) used the PZT actuator-driven one-degree-of-freedom spring-mass-damping system to obtain the dynamic output of the PZT actuator:

$$F_x = -\frac{Z_{xx}}{Z_{pxx}+Z_{xx}} Y_p^* S_p d_{31} E \ , \tag{1.3}$$

where Z_{xx} is the mechanical impedance of the spring-mass-damping system, defined as :

$$Z_{xx} = \frac{F_x}{\dot{x}} = c + \frac{m\omega^2 - k}{\omega} i \ , \tag{1.4}$$

in which $i=(-1)^{(1/2)}$; ω is the excitation frequency is the damping factor; k is the stiffness; m is the mass, as shown in Fig. 1.4. Z_{pxx} in Eq. (1.3) is the input impedance of the PZT actuator; S_p, Y^*_p and d_{31} are the cross section area, the Young's modulus, and the

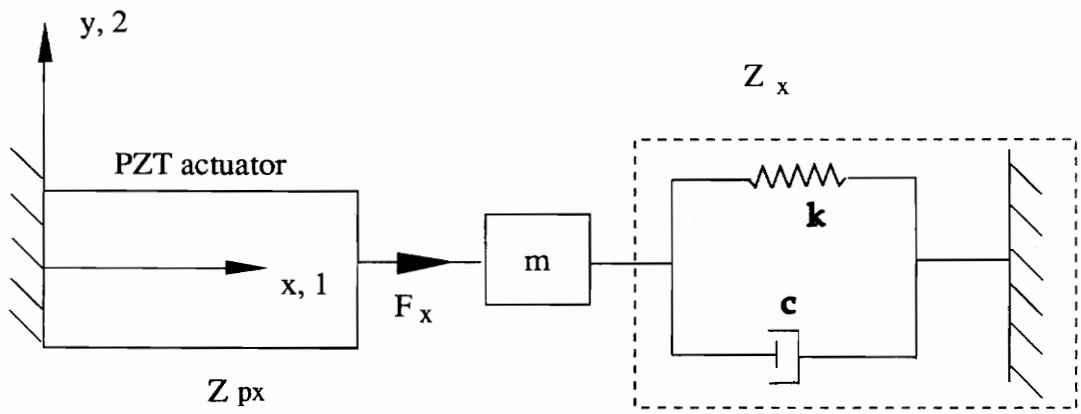

Figure 1.4: The impedance model of piezoelectric actuator-driven spring-mass-damping systems (Liang et al., 1993).

piezoelectric constant of the PZT actuator, respectively; E is the applied electric field. The force output of the PZT actuator, apparently, is dependent on the actuator input impedance, the host structural impedance, and frequency.

The model was then applied to similar one-dimensional structures, such as beams (Stein et. al., 1993) and circular rings (Rossi et. al., 1993). In Rossi's work (1993), the experiments were conducted to measure the velocity response of the cylindrical ring. The predicted and measured results agree well, which demonstrates the accuracy and potential of the impedance model in the design and applications of the PZT actuators.

However, the previous studies on the dynamic modeling approach have so far been limited to the modeling of one-dimensional structures. For general two-dimensional structures, such as thin shells and thin plates, the mechanical impedance coupling in different coordinate directions occurs. The cross impedance of the host structure may have an impact on the actuator dynamics. Moreover, the actuator energy conversion, the system power requirement, the actuator temperature rise and thermal damage, and the induced stress characteristics have not been fully addressed yet. Therefore, a generic and rigorous investigation based upon coupled electro-dynamics is highly required for general intelligent structures.

1.4 Research Objectives

Piezoelectric actuator-driven adaptive structures are complex electro-mechanical coupling systems in which electrical energy is converted into mechanical energy and vice-versa. The mechanical energy, then, is eventually transformed into internal heat in actuators/sensors and host structures. The system energy conversion and power consumption are dominated by the complex electro-mechanical impedance of the system. The dynamic interaction between the actuators and the host structures is governed by the actuator input impedance and the mechanical impedance of the structure. Therefore, the entire actuator/substrate system can be essentially represented by a coupled impedance model. Such a model will include overall system characteristics and the inherent connections among these parameters: mechanical properties, dynamic performance, and electrical parameters of active elements and host structures.

The objective of this research is to develop a generic electro-mechanical system modeling method for piezoelectric actuator-driven intelligent structures. The dynamic essence and the interconnections amongst intelligent elements and their supporting structures will be revealed. The investigation will focus on the development of a unified model to quantitatively analyze comprehensive issues in smart structures, including the actuator output dynamics, the mechanical stress and thermal stress characteristics of the PZT actuators, and the system power requirement and energy conversion efficiency.

In addition to theoretical work, the experiments will be conducted in this study. A real PZT patch actuator-driven simply-supported plate will be built and tested. The dynamic strain of the PZT actuators, the velocity response of the integrated plate, and the coupled electro-mechanical admittance of the system will be directly measured. An extensive comparison of experimental results and the corresponding theoretical solutions will be made to demonstrate the accuracy of the theoretical model.

The coupled electro-mechanical system modeling method will provide a new interdisciplinary prospective on adaptive structures and give a more accurate description of complex electro-mechanical active material systems. The potential of this modeling technique will be demonstrated for designing energy-efficient smart structures, actuators, and their associated power electronics and for optimizing the actuator location and thickness. The concept and method developed from this study will benefit the implementation and innovation of other induced strain actuators, such as shape memory alloy actuators, electrostrictive actuators, and magnetostrictive actuators etc.

In this dissertation, the newly developed theory is presented in Chapter 2 for shell structures, and in Chapter 3 for plate structures. The emphasis of these two chapters is to accurately predict the dynamic output performance of the PZT actuator and the dynamic response of the host structures. Chapter 4 highlights the analysis of energy conversion and power consumption of integrated piezoelectric structures based on the

coupled electro-mechanical admittance. Chapter 5 applies the generic model to deal with the design issues of the integrated piezoelectric actuators, especially the dynamics mechanical stress behaviors of the PZT actuators. Chapter 6 develops a heat transfer model to estimate the temperature rise and thermal stress of integrated PZT actuators. The parametric studies are conducted through Chapter 2 to Chapter 6. The experiments are described and conducted in Chapters 3, 4, and 5, respectively. The summary of this research is finally given in Chapter 7 along with the recommendations for future work.

1.5 Concluding Remarks

- The statics-driven approaches are limited to the prediction of static mechanical behaviors of the system. An approximate dynamic analysis expanded from the static models is not sufficient to fully understand the dynamic essence of PZT actuator-driven systems. The system power consumption and actuator energy conversion can't be predicted in the static models either.

- The dynamic model includes the added mass and stiffness of integrated PZT patches in the governing equation of the system. However, the induced force loading can't be predicted as a result of the dynamic interaction between the PZT actuator and the supporting structure.

- The impedance modeling approach demonstrates its potential and ability in the design and modeling of adaptive structures. More extensive and rigorous investigation is substantially required to develop a coupled electro-mechanical analysis method for generic two-dimensional intelligent structures.

1.6 References

Bailey, T. and J. E. Hubbard, Jr., 1985, "Distributed Piezoelectric Polymer Active Vibration Control of a Cantilever Beam", Journal of Guidance, Control, and Dynamics, Vol. 8, No. 5; pp. 605-611.

Chaudhry, Z. and Rogers, C. A., 1991, "Bending and Shape Control of Beams Using SMA Actuators", Journal of Intelligent Material Systems and Structures, Vol. 2, No. 4; pp. 581-602.

Crawley, E. F. and J. de Luis, 1987, "Use of Piezoelectric Actuators as Elements of Intelligent Structures", AIAA Journal, Vol. 25, No. 10; pp. 1373-1385.

Crawley, E. F. and E H. Anderson, 1990, "Detailed Models of Piezoceramic Actuation of Beams", Journal of Intelligent Material Systems and Structures, Vol. 1, No. 1; pp. 4-25.

Crawley, E. F. and K. B. Lazarus, 1991, "Induced Strain Actuation of Isotropic and Anisotropic Plates", AIAA Journal, Vol. 29, No. 6; pp. 944-951.

Dimitriadis, E. K., C. R. Fuller, and C. A. Rogers, 1989, "Piezoelectric Actuators for Distributed Noise and Vibration Excitation of Thin Plates, ASME Failure Prevention and Reliability, DE-VOL. 16, 1989; pp. 223-233.

Garcia, E. and D. Inman, 1990, "Advantages of Slewing an Active Structure", Journal of Intelligent Material Systems and Structures, Vol. 1, No. 3; pp. 261-272.

Hickman, G. A., Gerardi, J. J., and Feng, Y., 1990, "Application of Smart Structures to Aircraft Health Monitoring", Proceedings of First Joint U.S./Japan Conference on

Adaptive Structures, Maui, Hawaii, March 19-23; pp. 966-984.

Inman, D. J., 1990, "Control/Structure Interaction: Effects of Actuators Dynamics", Mechanics and Control of Large Flexible Structures, edited by J. L. Junkins, AIAA, Inc., Washington, DC; pp. 507-533.

Lee, C. K., 1990, "Theory of Laminated Piezoelectric Plates for the Design of Distributed Sensors/Actuators. Part I: Governing Equations and Reciprocal Relationships", Journal of Acoustic Society of American, 87 (3); pp. 1144-1158.

Lester, H. C. and S. Lefebvre, 1991, "Piezoelectric Actuator Models for Active Sound and Vibration Control of Cylinders", Recent Advances in Active Control of Sound and Vibration, Blacksburg, VA; pp. 3-26.

Liang, C., F. P. Sun, and C. A. Rogers, 1993, "Dynamic Output Characteristics of Piezoceramic Actuators", Proceedings of Smart Structures and Intelligent Systems, SPIE, Albuquerque, NM, VOL. 1917; pp. 286-298.

Rogers, C. A. and H. H. Robertshaw, 1988, "Shape memory Alloy Reinforced Composites", Engineering Science Reprints 25, ESP25.88027, Society of Engineering and Science.

Rogers, C. A., 1990, "Active Vibration and Structural Acoustic Control of Shape Memory Alloy Hybrid Composites: Experimental Results", Proceedings of International Congress on Recent Developments in Air- and Structure-Borne Sound and Vibration, Auburn University, March 6-8, 1990; pp. 695-708.

Rogers, C. A., 1990, "Intelligent Material Systems and Structures", Proceedings of First Joint U.S./Japan Conference on Adaptive Structures, Maui, Hawaii, March 19-23.

Rogers, C. A., C. Liang, and S. Li, 1991, "Active Damage Control of Hybrid Material Systems Using Induced Strain Actuators", Proceedings of the AIAA/ASME/ASCE/AHS 32th SDM Conference, Baltimore, MD, April 8-10, 1991, AIAA Inc., Washington, DC; pp. 1190-1203.

Rossi, A., C. Liang, and C. A. Rogers, 1993, "Coupled Electro-Mechanical Analysis of a Piezoceramic Actuator Driven System - An Application to a Circular Ring", Proceedings of the AIAA/ASME/ASCE/AHS 34th SDM Conference, La Jolla, CA, pp.3618-3624.

Sonti, V. R. and J. D. Jones, 1991, "Active Vibration Control of Thin Cylindrical Shells Using Piezo-Electric Actuators", Proceedings of Recent Advances in Active Control of

Sound and Vibration, Blacksburg, VA, pp. 27-38.

Stein, S., C. Liang, and C. A. Rogers, "Power Consumption of Piezoelectric Actuators in Underwater Active Structural Acoustic Control", Proceedings of the Second Conference on Recent Advances in Active Control of Sound and Vibration, Blacksburg, VA, April 28-30, 1993; pp. 240-251.

Sun, F. P., C. Liang, and C. A. Rogers, 1994, "Modal Analysis Using Collocated PZT Actuator/Sensor--An Electromechanical Approach", Proceedings of Smart Structures and Intelligent Systems, SPIE, Orlando, FL, February 13-18, 1994; in press.

Tappert, P. M. and H. H. Robertshaw, 1994, "Manipulations of Dynamic Response Data for Use in Inductive Learning Methods to Identify Damage", Proceedings of Smart Structures and Intelligent Systems, SPIE, Orlando, FL, February 13-18, 1994; in press.

Tzou, H. S., 1989, "Theoretical Development of a Layered Shell with Internal Distributed Controllers", ASME Failure Prevention and Reliability, DE-Vol. 16, pp. 241-249.

Wang, B. T. and C. A. Rogers, 1991, "Modeling of Finite-Length Spatially Distributed Induced Strain Actuators for Laminate Beams and Plates", Proceedings of the AIAA/ASME/ASCE/AHS 32th SDM Conference, Baltimore, MD, April 8-10, pp. 1511-1520.

Zhou, S. W., 1991, "Active Magnetostrictive Mounts for Base Vibration Isolation Systems", Research Report, Center for Intelligent Material Systems and Structures, Virginia Polytechnic Institute and State University, January 3, 1991; pp. 1-25.

Zhou, S. W., C. Liang, and C. A. Rogers, 1993, "An In-Situ Sensory Technique for In-Service Monitoring--Measurement of the Complex Young's Modulus of Polymers", Proceedings of Smart Sensing, Processing, and Instrumentation, SPIE, Albuquerque, NM, February 1-4, 1993, Vol. 1918; pp. 14-23.

Chapter 2

Modeling of Piezoelectric Actuators Integrated with Thin Shell Structures

2.1 Introduction

The use of piezoelectric materials (PZT) as actuators and sensors in intelligent shell structures has been drawing much attention in the active controls community. One investigation devoted to the modeling of actively-controlled cylinders was based on the layered shell theory (Tzou et al., 1989); in this study, a completely distinct layer of the piezoelectric material was used to make up a composite cylinder. A more convenient and feasible configuration of PZT actuators in adaptive structures is the use of segmented piezoelectric patches bonded on the surface of host structures. For the modeling of these PZT actuators locally coupled with shell structures, static approaches have been used to estimate the induced loading. Sonti and Jones (1991) investigated the performance of the

controlled cylinder using the piezo-actuator control patch and a point force for both on- and off-resonance cases; in this work, the output performance of the PZT actuator was not addressed. The assumption was made that the dimension of the PZT patch in the circumferential direction is kept small relative to the cylinder radius, the curvature effects could thus be neglected. The models developed from thin plate theory could then be used in smart shell structures. Lester and Lefebvre (1991) applied the same assumption in the study and researched both out-of-plane and in-plane piezoelectric actuation for controlling sound radiation and transmission related to vibrational cylinders. It is typically assumed in the static model that the added mass and stiffness of PZT are insignificant and the dynamic interaction between the PZT actuator and the host structure is ignored. Thus, the input impedance of the actuators and the mechanical impedance of the host structures are not incorporated in the modeling. The static analysis usually leads to the conclusion that the amplitude of the excitation force of the PZT actuator is frequency independent.

However, a rigorous investigation must account for the dynamic properties of the actuators, and the actuators have their own mechanical impedance. When an active force provided by the PZT actuator is applied to a host structure, the PZT itself is driven by the force. Therefore, the mechanical resonance of an integrated PZT/substrate system is the combination of the dynamic behavior of the PZT and that of the actuated structure.

Rossi et al. (1993) modeled a PZT actuator-driven circular ring using the impedance analytical approach. The frequency-dependent dynamic output of the PZT actuator is predicted. The experiments were also performed to validate the theoretical model. Nevertheless, the previous studies related to the dynamic modeling have so far been limited to the one-dimensional shell structures. For general two-dimensional shell structures, the mechanical impedance coupling in different coordinate directions occurs. Therefore, an extended investigation is highly required so as to develop a coupled impedance analysis applicable to two-dimensional shell structures (Zhou et al., 1993 and Zhou et al., 1994).

The work in this chapter focuses on the development of a generic method for the dynamic modeling of two-dimensional PZT actuators surface-bonded to a thin cylindrical shell. The impedance characteristics of a simply-supported cylinder corresponding to the excitation of a pair of pure bending moments will be presented, from which the dynamic output moments (or forces) of PZT actuators can be accurately predicted. Direct comparisons will be made between a conventional static modeling approach and the impedance method in order to identify the critical differences between these modeling methods for a cylindrical structure. The case studies will demonstrate that the mechanical impedance matching between PZT actuators and host structures has an impact on the output performance of actuators.

2.2 Mathematical Model of Integrated PZT/Shell Structures

A physical model of a thin cylindrical shell excited by PZT actuators is shown in Fig. 2.1. The PZT patches are assumed to be perfectly bonded on the internal and external surfaces of the cylinder so that a pure bending moment excitation can be locally created. Figure 2.2 displays the corresponding impedance model. The dynamic behavior of the cylinder in the x and θ direction is represented by the direct impedance Z_{xx} and $Z_{\theta\theta}$ as well as the cross impedance $Z_{x\theta}$ and $Z_{\theta x}$ at a driving point, respectively, which can be defined as:

$$Z_{xx(\theta\theta)} = \frac{F_{x(\theta)}}{\dot{x}(\dot{\theta})} \quad or \quad Z_{x\theta(\theta x)} = \frac{F_{\theta(x)}}{\dot{x}(\dot{\theta})} \ , \tag{2.1}$$

where $F_{x(\theta)}$ is the driving force; and $\dot{x}$ $\dot{\theta}$ are the in-plane velocity response of the structure. Under the actuation of the moments, M_x and M_θ, the angular velocity response of the cylinder at the edge of the bonded PZT patches may be described by:

$$\nabla\beta_x = \left(\frac{\partial \dot{w}}{\partial x}\right)_{x=x_2} - \left(\frac{\partial \dot{w}}{\partial x}\right)_{x=x_1} = -(H_{xx}M_x + H_{\theta x}M_\theta) \tag{2.2a}$$

$$\nabla\beta_\theta = \left(\frac{\partial \dot{w}}{R\partial\theta}\right)_{\theta=\theta_2} - \left(\frac{\partial \dot{w}}{R\partial\theta}\right)_{\theta=\theta_1} = -(H_{x\theta}M_x + H_{\theta\theta}M_\theta) \ , \tag{2.2b}$$

where $\nabla\beta$ is the total angular velocity of the cylinder; R is the radius of the cylinder. The minus sign indicates that the structural reactions are equal and opposite to the output forces of the PZT actuator; H_{xx} and $H_{\theta\theta}$ are the direct admittance of the cylinder at the driving points; and $H_{x\theta}$ and $H_{\theta x}$ are the cross admittance of the cylinder and responsible for the coupling of the input moments in the x and θ directions. The moment admittance

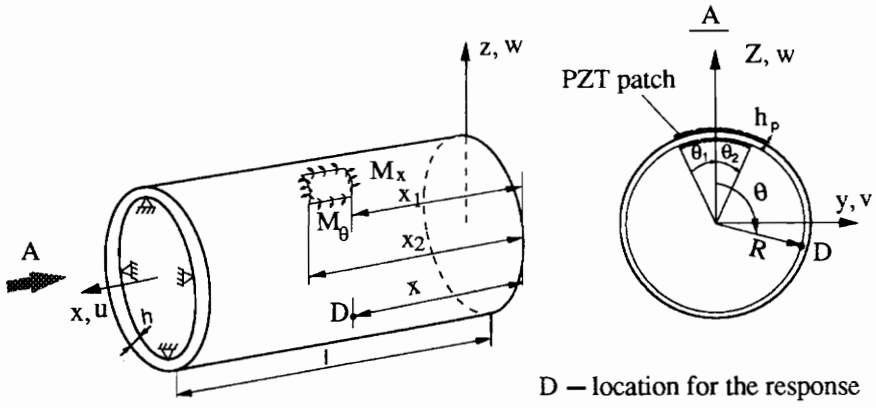

Figure 2.1: A thin cylindrical shell with surface-bonded PZT actuators.

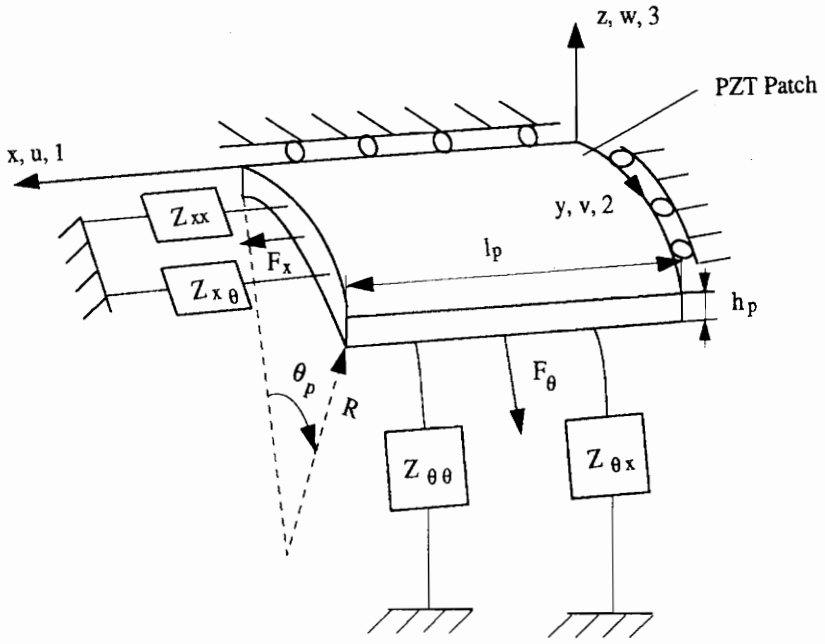

Figure 2.2: A physical model of a PZT actuator integrated with a thin shell structure represented by the mechanical impedance.

is defined as:

$$H_{lk}=\frac{\nabla\dot{\beta}_k}{M_l} \qquad (l,k=x,y)\ . \tag{2.3}$$

Figure 2.3 shows the geometric deformation of the cylinder in the x direction under the actuation of M_x. The similar deformation occurs in the θ direction. Considering the relationship between the translational displacement and the angular deformation of the cylinder, the in-plane displacement, u and v, can be expressed by:

$$u=\frac{h+h_p}{2}\left[\left(\frac{\partial w}{\partial x}\right)_{x=x_2}-\left(\frac{\partial w}{\partial x}\right)_{x=x_1}\right] \tag{2.4a}$$

$$v=\frac{h+h_p}{2}\left[\left(\frac{\partial w}{R\partial\theta}\right)_{\theta=\theta_2}-\left(\frac{\partial w}{R\partial\theta}\right)_{\theta=\theta_1}\right]\ , \tag{2.4b}$$

where h and h_p are the thicknesses of the cylinder and the PZT actuator, respectively. The corresponding in-plane velocity, $\dot{u}$ and $\dot{v}$, are then given by:

$$\dot{u}=\frac{h+h_p}{2}\left[\left(\frac{\partial \dot{w}}{\partial x}\right)_{x=x_2}-\left(\frac{\partial \dot{w}}{\partial x}\right)_{x=x_1}\right] \tag{2.5a}$$

$$\dot{v}=\frac{h+h_p}{2}\left[\left(\frac{\partial \dot{w}}{R\partial\theta}\right)_{\theta=\theta_2}-\left(\frac{\partial \dot{w}}{R\partial\theta}\right)_{\theta=\theta_1}\right]\ . \tag{2.5b}$$

Using the relation of the in-plane force and the out-of-plane moment: $M_{x(\theta)}=(h+h_p)F_{x(\theta)}$ and substituting Eq. (2.5) into Eq. (2.2) results in:

$$\begin{pmatrix}F_x\\F_\theta\end{pmatrix}=-\frac{2}{(h+h_p)^2}\begin{pmatrix}H_{xx} & H_{\theta x}\\H_{x\theta} & H_{\theta\theta}\end{pmatrix}^{-1}\begin{pmatrix}\dot{u}\\\dot{v}\end{pmatrix}=-\begin{pmatrix}Z_{xx} & Z_{x\theta}\\Z_{\theta x} & Z_{\theta\theta}\end{pmatrix}\begin{pmatrix}\dot{u}\\\dot{v}\end{pmatrix}=-[Z]\begin{pmatrix}\dot{u}\\\dot{v}\end{pmatrix}, \tag{2.6}$$

where the structural impedance Z_{lk} $(l,k = x,\theta)$ can be derived from classic shell theory and will be developed later. $\dot{u}$ and $\dot{v}$ need to be solved so that the output force can be quantitatively predicted.

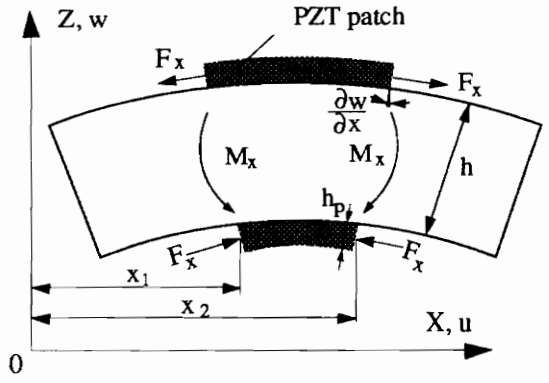

Figure 2.3: The angular deformation of a cylinder in the x direction, actuated by a pair PZT patches in pure bending mode.

When an external electric field is applied to PZT patches along the polarization direction (3), the equation of motion of the PZT actuator shown in Fig. 2.2 may be expressed by:

$$\rho_p \frac{\partial^2 u}{\partial t^2} = Y_{p11}^E \frac{\partial^2 u}{\partial x^2} \tag{2.7a}$$

$$\rho_p \frac{\partial^2 v}{\partial t^2} = Y_{p22}^E \frac{\partial^2 v}{R\partial \theta^2} \ , \tag{2.7b}$$

where the subscript p refers to the parameters of the PZT actuator, and 11 and 22 denote the coordinates of PZT materials; ρ is the mass density; and Y^E is the Young's modulus. The solution of Eq. (2.7) is described by:

$$u = \left[A\sin(k_{p11}x) + B\cos(k_{p11}x)\right] e^{j\omega t} \tag{2.8a}$$

$$v = \left[C\sin(k_{p22}R\theta) + D\cos(k_{p22}R\theta)\right] e^{j\omega t} \ , \tag{2.8b}$$

where A, B, C and D are unknowns and can be determined by the boundary conditions; j symbolizes the imaginary part of a complex number; ω is the input angular frequency. Considering the isotropy of the PZT material in the *1* and *2* directions yields the wave number:

$$k_p^2 = k_{p11}^2 = k_{p22}^2 = \omega^2 \frac{\rho_p}{Y_p^E} \ . \tag{2.9}$$

Applying the displacement boundary conditions, $u_{x=0}=0$ and $v_{\theta=0}=0$ to Eq. (2.8), leads to $B=D=0$. The unknowns, A and C , can be determined from the constitutive equation of the PZT actuator at $x=l_p$ and $\theta=\theta_p$:

$$\begin{pmatrix}\varepsilon_x\\ \varepsilon_y\end{pmatrix}=\begin{pmatrix}\dfrac{\partial u}{\partial x}\\ \dfrac{\partial v}{R\partial\theta}\end{pmatrix}=\begin{pmatrix}\dfrac{1}{Y_p^E R\theta_p h_p} & -\dfrac{\nu_p}{Y_p^E l_p h_p}\\ -\dfrac{\nu_p}{Y_p^E R\theta_p h_p} & \dfrac{1}{Y_p^E l_p h_p}\end{pmatrix}\begin{pmatrix}F_x\\ F_\theta\end{pmatrix}+\begin{pmatrix}d_{31}\\ d_{32}\end{pmatrix}E\ , \tag{2.10}$$

where l_p, θ_p, and $d_{31(2)}$ are the length, the angle, and the piezoelectric constant of the PZT actuator, respectively. Note that the Poisson's ratio of the PZT material, ν_p is introduced so that the mechanical coupling of the in-plane motion in different directions (x, θ) of the PZT actuator can be included in the modeling. Substituting Eqs. (2.6) and (2.8) into Eq. (2.10) and taking the algebraic operation to rearrange A and C yield:

$$\begin{pmatrix}C_l(1-\dfrac{\nu_p}{\alpha}\dfrac{Z_{x\theta}}{Z_{pxx}}+\dfrac{Z_{xx}}{Z_{pxx}}) & C_\theta(\alpha\dfrac{Z_{\theta x}}{Z_{p\theta\theta}}-\nu_p\dfrac{Z_{\theta\theta}}{Z_{p\theta\theta}})\\ C_l(\dfrac{1}{\alpha}\dfrac{Z_{x\theta}}{Z_{pxx}}-\nu_p\dfrac{Z_{xx}}{Z_{pxx}}) & C_\theta(1-\nu_p\alpha\dfrac{Z_{\theta x}}{Z_{p\theta\theta}}+\dfrac{Z_{\theta\theta}}{Z_{p\theta\theta}})\end{pmatrix}\begin{pmatrix}A\\ C\end{pmatrix}=\begin{pmatrix}d_{31}\\ d_{32}\end{pmatrix}E\ , \tag{2.11}$$

where $C_l=k_p cos(k_p l_p)$ and $C_\theta=k_p cos(k_p R\theta_p)$; $\alpha=l_p/(R\theta_p)$ is the ratio of the length to the width of the PZT patch; Z_{pxx} and $Z_{p\theta\theta}$ are the input impedances of the PZT actuator in the x and θ directions, defined as:

$$Z_{pxx}=\frac{F_x}{\dot{x}}=K_{px}\frac{k_p l_p}{\tan(k_p l_p)}\frac{1}{j\omega} \tag{2.12a}$$

$$Z_{p\theta\theta}=\frac{F_\theta}{\dot{\theta}}=K_{p\theta}\frac{k_p R\theta_p}{\tan(k_p R\theta_p)}\frac{1}{j\omega} \tag{2.12b}$$

with the static extension stiffnesses of the actuator in the x and θ directions, $K_{px}=Y^E_p R\theta_p h_p/l_p$ and $K_{p\theta}=Y^E_p l_p h_p/(R\theta_p)$. Solving for A and C from Eq. (2.11) and substituting it into Eq. (2.8), the displacement and velocity responses of the PZT actuator are obtained. The dynamic force output of the PZT actuator can then be determined from

Eq. (2.6):

$$F_x = \bar{F}_x e^{j\omega t} = -j\omega \left(AS_l Z_{xx} + CS_\theta Z_{x\theta}\right) e^{j\omega t} \tag{2.13a}$$

$$F_\theta = \bar{F}_\theta e^{j\omega t} = -j\omega \left(AS_l Z_{\theta x} + CS_\theta Z_{\theta\theta}\right) e^{j\omega t}, \tag{2.13b}$$

where $S_l = sin(k_p l_p)$ and $S_\theta = sin(k_p R\theta_p)$. Accordingly, the amplitude of the line moments per unit length created by the pair of PZT patches, $\bar{M}_{x,(\theta)}$ (in N·m/m), can be determined as:

$$\bar{M}_x = \frac{\bar{F}_x (h+h_p)}{R\theta_p} = -j\frac{\omega (h+h_p)\left(AS_l Z_{xx} + CS_\theta Z_{x\theta}\right)}{R\theta_p} \tag{2.14a}$$

$$\bar{M}_\theta = \frac{\bar{F}_\theta (h+h_p)}{l_p} = -j\frac{\omega (h+h_p)\left(AS_l Z_{\theta x} + CS_\theta Z_{\theta\theta}\right)}{l_p}. \tag{2.14b}$$

The distributed line moments are thus expressed by:

$$M_x = \bar{M}_x [\delta(x-x_1) - \delta(x-x_2)]\,[h(\theta-\theta_1) - h(\theta-\theta_2)] e^{j\omega t} \tag{2.15a}$$

$$M_\theta = \bar{M}_\theta [\delta(\theta-\theta_1) - \delta(\theta-\theta_2)]\,[h(x-x_1) - h(x-x_2)] e^{j\omega t}, \tag{2.15b}$$

where $\delta(x)$ and $\delta(\theta)$ are the Direc Delta functions; $h(x)$ and $h(\theta)$ are the Heaviside functions; x_1, x_2, θ_1 and θ_2 are the location coordinate of the edge of PZT patches on the cylinder, as illustrated in Fig. 2.1.

Since the coefficients A and C, as well as the mechanical impedance of the cylinder in Eq. (2.14), are functions of driving frequency, the moment outputs of the PZT actuator are frequency dependent. If the cross impedance $Z_{x\theta}$ and $Z_{\theta x}$ in Eq. (2.11) is assumed to be zero and the Poisson's effect of the PZT material is ignored, a decoupled analysis is then obtained for one-dimensional rings. The formulation for the force output of the PZT actuator expressed in Eq. (2.13) is reduced to:

$$F_\theta = -\frac{Z}{Z+Z_p} Y_p^E S_p d_{32} E \ , \tag{2.16}$$

where Z is the mechanical impedance of the ring, Z_p is the input impedance of the PZT actuator, and S_p is the cross section area of the PZT actuator. Equation (2.16) is same as the formulation that was derived from the circular rings by Rossi et al. (1993). The two-dimensional impedance analysis, therefore, is applicable to one-dimensional structures.

Thus far, the dynamic forces and moments of the PZT actuator have been obtained based upon the impedance characteristics of the PZT and the cylinder. The input impedance of the PZT actuator is given by Eq. (2.12). The mechanical impedance matrix [**Z**] of the cylinder expressed in Eq. (2.6) depends on the location of the actuators, the structural configuration, the boundary condition, and the physical properties, and it can be determined from classic shell theory. The next section will address the calculation of the admittance of the cylinder actuated by line moments.

2.3 Admittance Calculation of a Cylinder

The general solution of the response of a thin shell excited by line moments can be determined by solving the following Love equations (Soedel, 1981):

$$L_u(u,v,w) - \lambda \dot{u} - \rho h \ddot{u} = -q_u - \frac{1}{2R}\frac{\partial M_n}{\partial \theta} \tag{2.17a}$$

$$L_v(u,v,w)-\lambda\dot{v}-\rho h\ddot{v}= -q_v-\frac{1}{2}\frac{\partial M_n}{\partial x} \tag{2.17b}$$

$$L_w(u,v,w)-\lambda\dot{w}-\rho h\ddot{w}= -q_w-\frac{1}{R}\left(R\frac{\partial M_x}{\partial x}+\frac{\partial M_\theta}{R\partial\theta}\right), \tag{2.17c}$$

where q_i *(i=u,v,w)* is the pressure applied along the x, y, and z directions normal to the surface of the shell, respectively. The twisting moment M_n is applied about the normal *(z)* direction; λ is an equivalent viscous damping factor; and the operator L_i (i=u,v,w) can be evaluated from an eigenvalue analysis. Since the transverse modes in a very shallow shell are the dominant modes, it is assumed that the inertial effects in the in-plane directions are neglected and the loading is applied normally to the surface of the shells (Soedel, 1981; Leissa, 1973). In current case, the ratio of the thickness to the radius of the cylinder is assumed to be 1/100 and the theory for thin shells is thus applied. Only Eq. (2.17c) is considered in the modeling. The modal expansion series solution of Eq. (2.17c) is expressed by:

$$w=\sum_{m=1}^{\infty}\sum_{n=0}^{\infty}p_{mn}W_{mn}(x,\theta) \tag{2.18}$$

where m and n refer to the axial and circumferential mode numbers; p_{mn} is the modal participation factor; $W_{mn}(x,\theta)$ is the eigenfunction. The operator L_w in Eq. (2.17c) is evaluated from the eigenvalue analysis:

$$L_w(w)= -\rho h\omega_{mn}^2 w\ , \tag{2.19}$$

where ω_{mn} is the natural frequency of the cylinder. Substituting Eqs. (2.18) and (2.19) into Eq. (2.17c) and assuming $q_w=0$ results in:

$$\sum_{m=1}^{\infty}\sum_{n=0}^{\infty}(\rho h\ddot{p}_{mn}+\lambda\dot{p}_{mn}+\rho h\omega_{mn}^{2}p_{mn})W_{mn}(x,\theta)=\frac{1}{R}\left(R\frac{\partial M_x}{\partial x}+\frac{\partial M_\theta}{R\partial\theta}\right) . \tag{2.20}$$

For a simply-supported cylinder, the eigenfunction $W_{mn}(x,\theta)$ can be described by:

$$W_{mn}(x,\theta)=\sin\frac{m\pi}{l}x\cos n(\theta-\psi) , \tag{2.21}$$

where ψ is the relative angular location of the input moment with respect to the coordinate system and l is the length of the cylinder. Substituting Eq. (2.21) into Eq. (2.20) and using the usual modal expansion technique yields:

$$\ddot{p}_{mn}+2\zeta_{mn}\dot{p}_{mn}+\omega_{mn}^{2}p_{mn}=F_{mn}e^{j\omega t} , \tag{2.22}$$

where the equivalent forcing function, F_{mn}, is the form of:

$$F_{mn}=\frac{1}{\rho hN_{mn}}\int_0^l\int_0^{2\pi}W_{mn}(x,\theta)\left(R\frac{\partial M_x}{\partial x}+\frac{\partial M_\theta}{R\partial\theta}\right)dxd\theta \tag{2.23}$$

where

$$N_{mn}=\int_0^l\int_0^{2\pi}\sin^2\frac{m\pi x}{l}\cos^2 n(\theta-\psi)Rdxd\theta=\begin{cases}Rl\pi/2 & (n\neq 0)\\ Rl\pi & (n=0)\end{cases} . \tag{2.24}$$

In the case of $\psi = 0$, Eq. (2.23) becomes

$$F_{mn1}=\frac{C_x}{\rho hN_{mn}}\left(\frac{R\pi m}{ln}\bar{M}_x+\frac{ln}{R\pi m}\bar{M}_\theta\right)(\sin n\theta_1-\sin n\theta_2) , \tag{2.25}$$

where $C_x=\cos(m\pi x_1/l)-\cos(m\pi x_2/l)$. In the case of $\psi = \pi/2n$,

$$F_{mn2}=\frac{C_x}{\rho hN_{mn}}\left(\frac{Rm\pi}{ln}\bar{M}_x+\frac{ln}{Rm\pi}\bar{M}_\theta\right)(\cos n\theta_2-\cos n\theta_1) . \tag{2.26}$$

In particular, when $\psi=0$ and $n=0$, the effective force function is reduced to:

$$F_{m0}=\frac{C_x}{\rho h}\frac{m}{l^2}(\theta_1-\theta_2)\bar{M}_x . \tag{2.27}$$

The solution of the governing equation (2.22) is expressed by:

$$p_{mn}(t)=\frac{F_{mn}e^{j(\omega t-\phi_{mn})}}{\omega_{mn}^2\sqrt{\left(1-(\omega/\omega_{mn})^2\right)^2+4\zeta_{mn}^2(\omega/\omega_{mn})^2}} \tag{2.28}$$

with the phase shift,

$$\phi_{mn}=\tan^{-1}\frac{2\zeta_{mn}(\omega/\omega_{mn})}{1-(\omega/\omega_{mn})^2}\ , \tag{2.29}$$

where ζ_{mn} is the modal damping coefficient. The transverse displacement response of the cylinder is thus obtained:

$$w(x,\theta,t)=\sum_{m=1}^{\infty}\sum_{n=0}^{\infty}\frac{(F_{mn1}\cos n\theta+F_{mn2}\sin n\theta)\sin\frac{m\pi}{l}x\,e^{j(\omega t-\phi_{mn})}}{\omega_{mn}^2\sqrt{\left(1-(\omega/\omega_{mn})^2\right)^2+4\xi_{mn}^2(\omega/\omega_{mn})^2}} \tag{2.30}$$

Substituting Eq. (2.30) into Eq. (2.2) and recalling the definition of the admittance in Eq. (2.3), the direct admittance at the middle point of the edge of the PZT actuator can be determined as:

$$H_{xx}=\frac{4\omega\pi}{\rho hR\theta_p l^3}\sum_{m=1}^{\infty}\sum_{n=1}^{\infty}\left(\frac{m^2C_x^2\sin[n(\theta_2-\theta_1)/2]}{n\Delta_{mn}}\right)e^{j(\pi/2-\phi_{mn})} \tag{2.31}$$

and

$$H_{\theta\theta}=\frac{4\omega}{\rho hl_p\pi^2R^3}\sum_{m=1}^{\infty}\sum_{n=1}^{\infty}\left(\frac{n^2C_xS_x[1-\cos n(\theta_1-\theta_2)]}{m\Delta_{mn}}\right)e^{j(\pi/2-\phi_{mn})}\ , \tag{2.32}$$

where $S_x=sin[m\pi(x_1+x_2)/(2l)]$ and Δ_{mn} is given by:

$$\Delta_{mn} = \omega_{mn}^2 \sqrt{\left(1-(\omega/\omega_{mn})^2\right)^2 + 4\xi_{mn}^2(\omega/\omega_{mn})^2} \tag{2.33}$$

Similarly, the cross admittances are obtained by:

$$H_{x\theta} = \frac{4\omega}{\rho h \theta_p R^2 l^2} \sum_{m=1}^{\infty} \sum_{n=1}^{\infty} \left(\frac{mC_x S_x [1-\cos n(\theta_1-\theta_2)]}{\Delta_{mn}} \right) e^{j(\pi/2-\phi_{mn})} \tag{2.34}$$

and

$$H_{\theta x} = \frac{4\omega}{\rho h \pi R^2 l l_p} \sum_{m=1}^{\infty} \sum_{n=1}^{\infty} \left(\frac{nC_x^2 \sin\frac{n(\theta_2-\theta_1)}{2}}{\Delta_{mn}} \right) e^{j(\pi/2-\phi_{mn})} \tag{2.35}$$

2.4 Numerical Examples and Discussion

The simply-supported thin cylinder used in the case study is made of aluminum and its geometric configuration is shown in Fig. 2.1. The material properties of aluminum and PZT (G1195) are listed in Table 2.1 and their geometric parameters are given in Table 2.2. In the case study, two geometric parameters, the thickness of the PZT (h_p=*0.2, 0.5, 1.0 mm)* and the location of the PZT on the cylinder (x_1=*310, 100 mm)* are examined. The purpose is to identify the effect of the input impedance of the PZT and the structural impedance on the moment outputs of the PZT actuator and to determine how they influence the response of the cylinder.

Table 2.1: Material Properties of the PZT and Aluminum

	Y^E (N/m^2) $x10^{10}$	ρ (kg/m^3)	ν	d_{31},d_{32} (m/volt) $x10^{-10}$	ζ_{mn}
PZT*	6.3	7650	0.3	-1.66	0.005
Aluminum	6.9	2700	0.33	N/A	0.005

*From Piezo Systems, Inc. (PSI-5A-S3)

Table 2.2: Geometric Size of the PZT Actuator and the Cylinder (unit: mm)

	Length l	Radius R	Angle θ_p(degree)	Thickness h
PZT	80	200	6	0.2, 0.5, 1.0
Cylinder	700	200	360	2.0

For comparison of modeling approaches, the static line moment calculation is based upon a flat PZT patch, because the dimension of the PZT patch in circumferential direction is kept small relative to the cylinder radius, thus the curvature effects can be neglected (Sonti et al., 1991; Lester et al., 1991). This is a reasonable approximation from the experimental point of view. In the current numerical examples, the circumferential size of the PZT patch is much smaller than that of the cylinder, $(R\theta_p)/R=1/10$, hence flat PZT patches are used in the static calculations. There are several formulae for the actuation of PZT patches on two-dimensional structures (Dimitriadis et al., 1988; Wang et al., 1991; Crawley et al., 1991). One formula developed from the laminated plate theory (Wang, 1991) is used here.

Figure 2.4 shows the variation of the amplitude of the force admittance with frequency. The peaks of the curves correspond to the resonant frequencies of the original cylinder. When the PZT actuator is much thinner than the cylinder $(h_p=0.2mm \text{ and } h_p/h=1/10)$, the input impedance levels of PZT are much lower than those of the cylinder, as shown in Fig. 2.5. The corresponding amplitude of the dynamic moments is nearly constant over the whole frequency band, as illustrated in Figs. 2.6 and 2.7 ($h_p=0.2$ mm). This result is expected because relatively small PZT patches "planted" in the substrate do not significantly stiffen the cylinder. On the other hand, the host structural dynamics do not yet apply a strong influence on the actuator moment outputs. In this case, the dynamic interaction between the PZT actuator and the cylinder may be ignored. The active

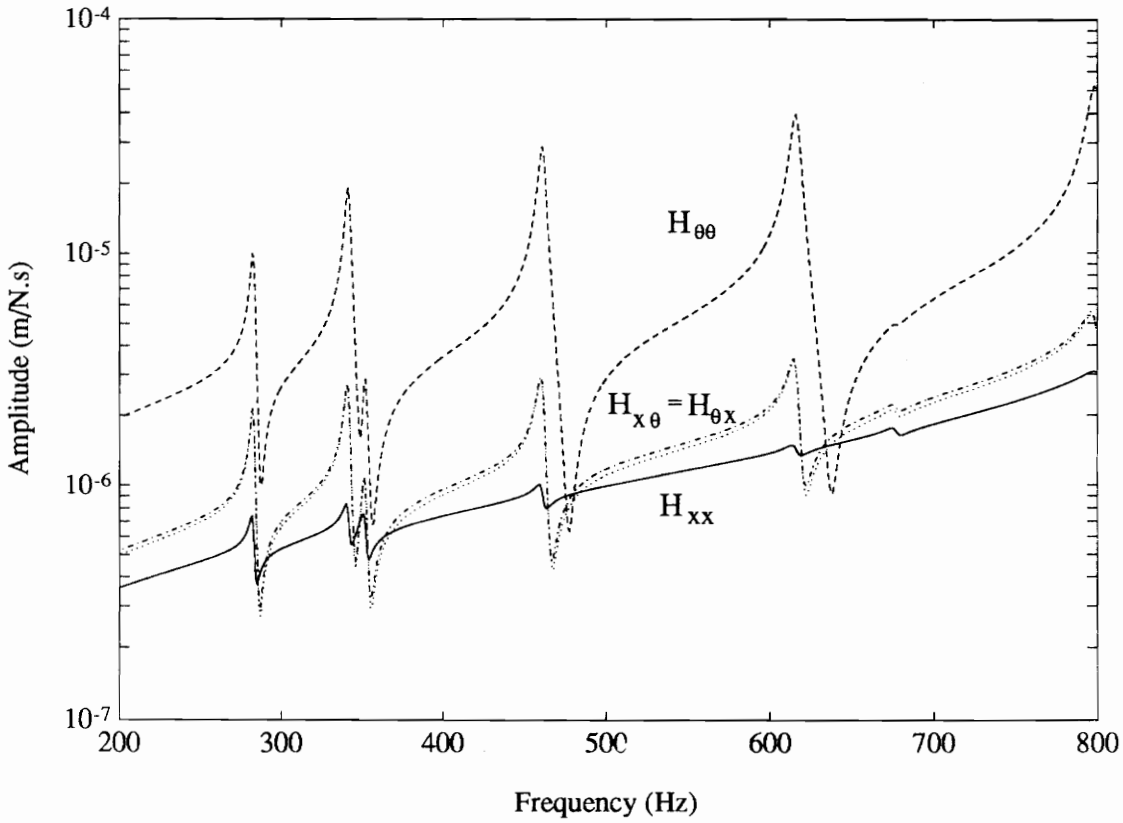

Figure 2.4: The admittance characteristics of a simply-supported cylinder (h_p=0.5 mm).

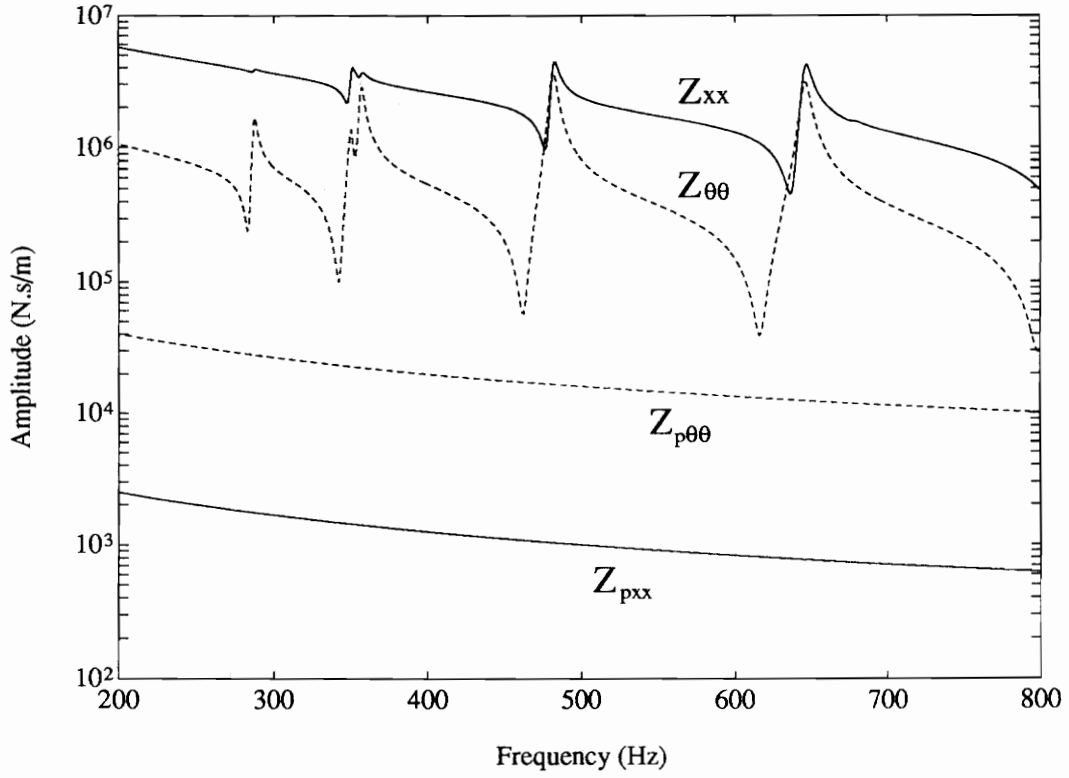

Figure 2.5: The direct impedance of the cylinder and the PZT actuator (h_p=0.2 mm).

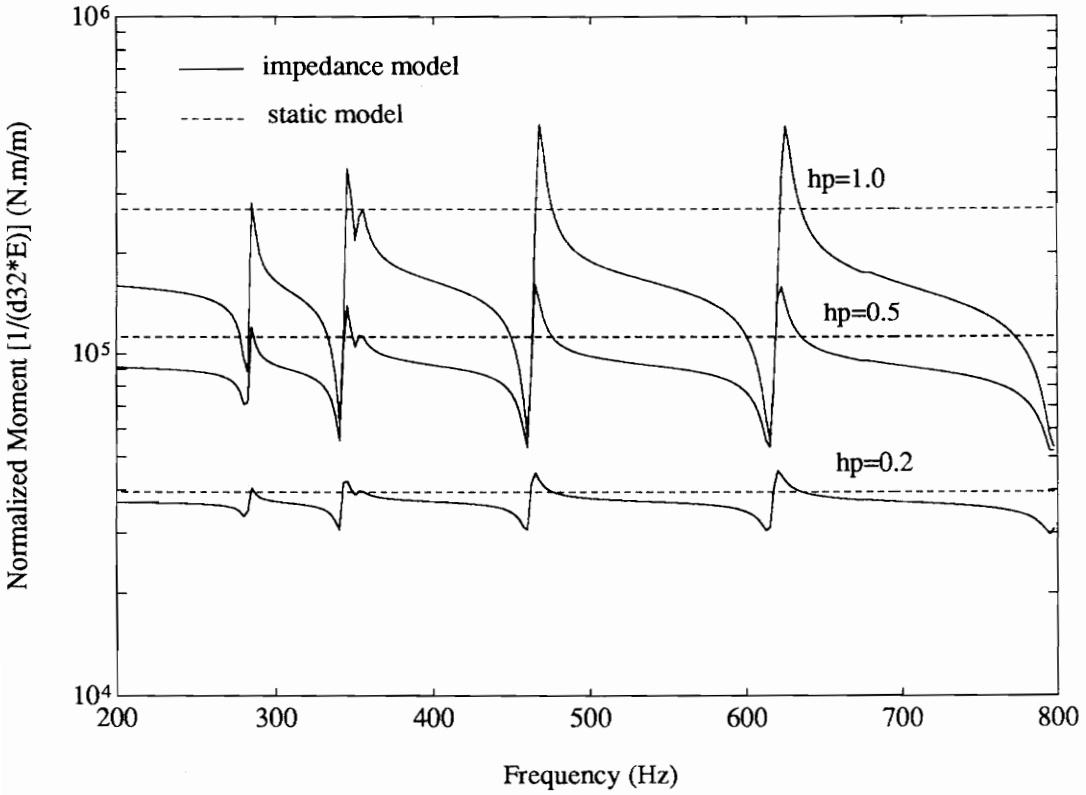

Figure 2.6: The moment outputs of the PZT actuator in the circumferential direction.

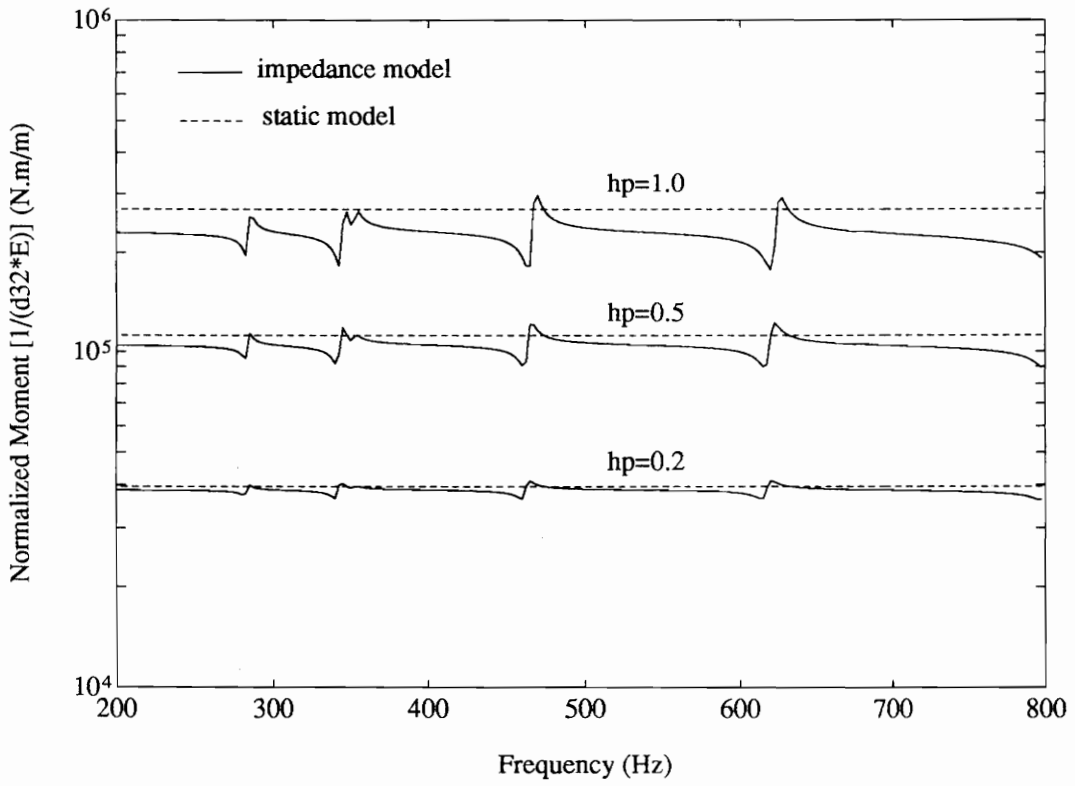

Figure 2.7: The moment outputs of the PZT actuator in the axial direction.

moments given by the static model agrees with that predicted by the impedance model.

With increases in the thickness of the PZT actuator up to h_p=*1.0 mm* (h_p/h=*0.5*), the input impedance of the PZT actuator matches with the structural impedance of the cylinder in the circumferential direction, which is displayed in Fig. 2.8. The moment outputs of the PZT actuator is strengthened. Figure 2.6 demonstrates that the amplitude of the dynamic moments, M_θ, varies significantly around the system resonance from $8.2\text{x}10^4$ to $2.9\text{x}10^5$ (N.m/m) for the first mode and from $5.9\text{x}10^4$ to $3.6\text{x}10^5$ (N.m/m) for the second mode. The static approach, however, gives a constant moment prediction. The thicker the PZT patches, the greater the increment of the amplitude of the moments. It should be noted that although the axial impedance Z_{xx} in Fig. 2.8 is not matched by the input impedance $Z_{p\theta\theta}$, the axial moment output $\bar{M}_x$ also goes up, as shown in Fig. 2.7, because of the coupling effect due to the cross impedance and the Poisson's ratio. In addition, Figures 2.5 and 2.8 show that for the cylinder, the mechanical impedance in the axial direction is different from that in the circumferential direction. This implies that the different actuation is generated in the axial direction and in the circumferential direction, i.e., $\bar{M}_x \neq \bar{M}_\theta$, as illustrated in Figs. 2.6 and 2.7.

The influence of the location of the PZT actuator on the host structure on its dynamic output is examined in Fig. 2.9. When the location of the excitation points changes, the driving point mechanical impedance of the cylinder varies; accordingly, the moment

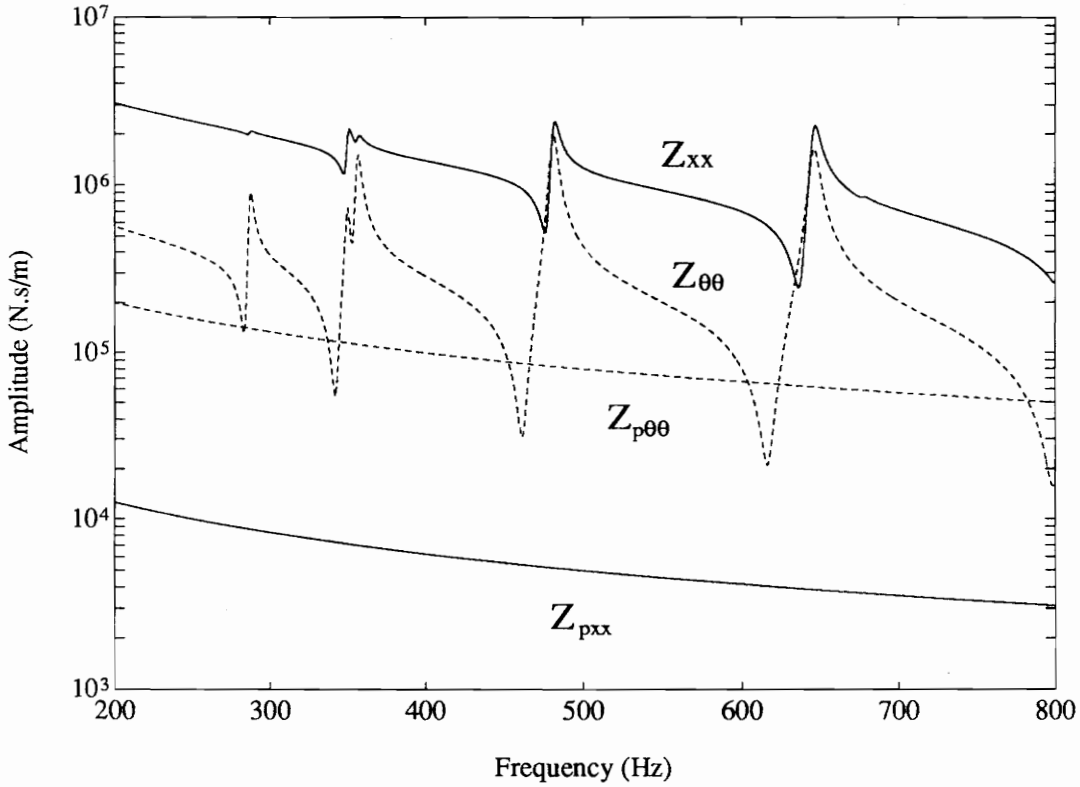

Figure 2.8: The direct impedance of the cylinder and the PZT actuator (h_p=1.0 mm).

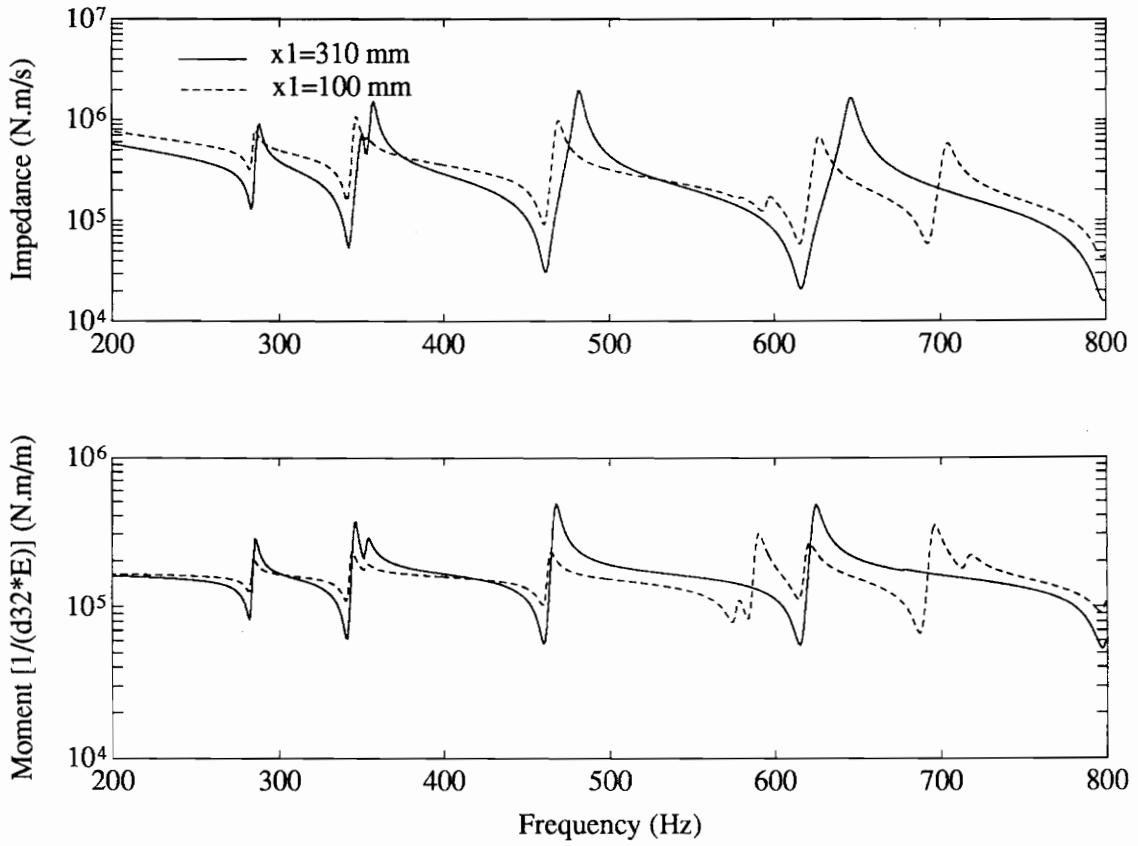

Figure 2.9: The effect of location of the actuator on the circumferential impedance and moment output (h_p=1.0 mm).

output of the PZT actuator changes. Since the frequencies corresponding with the peaks of the moments are the resonant frequencies of the entire PZT/shell system, the variation of the peaks due to the location change of the actuator reflects the dynamic performance shifts of the original cylinder. When the PZT actuator is placed on the different locations on the host cylinder, it applies the different stiffening effect on the system. Hence, the location of the PZT actuator is a critical factor affecting the excitation of the actuator on vibrational modes of the system.

Considering the convenience of comparing different modeling approaches and the practice of a voltage input in structural excitation, a scaled displacement is defined by:

$$w_{normal} = \frac{w}{d_{1,(2)} V} \tag{2.36}$$

so that a pseudo-frequency response function of an integrated structure can be obtained. The displacement response of the cylinder is picked up at $x=300\ mm$ and $\theta=90^0$. As the thickness of the PZT actuator increases, the natural frequencies of the integrated PZT/cylinder system move up, which is accurately predicted in the impedance model. Figure 2.10 displays the differences in the displacement responses of the cylinder predicted by the static model and by the impedance model, respectively. The resonant frequencies of the integrated system are shifted to a higher value compared with that of the original cylinder. The corresponding amplitude of the response decreases. It can be explained that thicker PZT patches bonded on the surface of the cylinder stiffen the cylinder, which

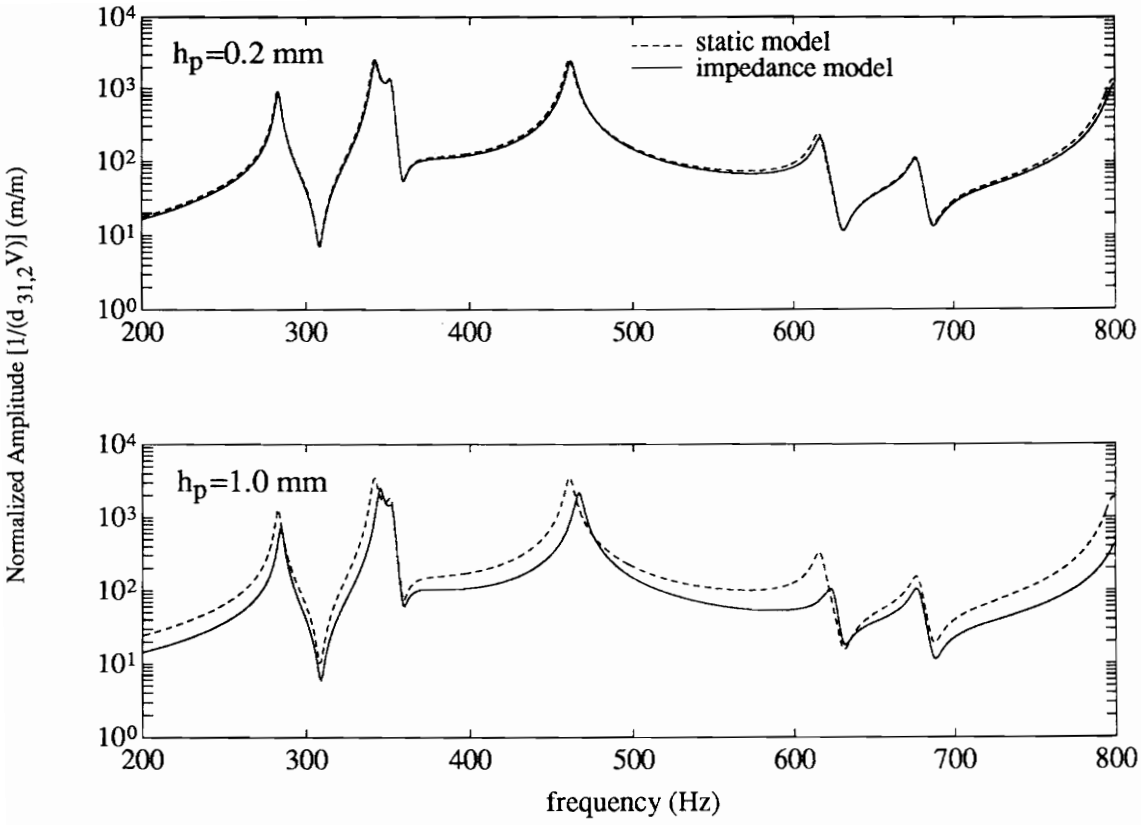

Figure 2.10: A comparison of the displacement response of the cylinder predicted by the static model and the impedance model, respectively (the response at x=310 mm and θ =90^0).

leads to the variations in the performance of the original structure. The intensity of these changes depends on the extent of the impedance matching between the PZT and the cylinder. When the response happen to be picked up at the nodal line of the 4th mode of the original cylinder (h_p=*0.5 mm*, *x=310 mm*, and $\theta=15^0$), a significant difference is observed between the different modeling approaches, as shown in Fig. 2.11. The 4th mode does not show up in the normalized response of the cylinder from the prediction of the static model. The developed impedance model, however, picks up this mode. The explanation of this phenomenon may be found from the pseudo-frequency response function expressed in Eq. (2.36). Usually, the frequency response function (FRF) of a structure is only a function of structural dynamics itself, independent of the excitation force. Nevertheless, in the case of structural actuation using PZT actuators, the excitation force is structural dynamics dependent. When the vibrational response of the structure is divided by input voltage instead of the excitation force (only choice in experimental situations), the pseudo-FRF has to be correlated to the excitation force. As a sensor is located on a nodal line of a specific mode, such as the 4th mode, the static model gives a "flat" response because of the assumption of a "flat" input force. The impedance model, however, gives a "peak" response caused from a "peak" force input. Therefore, the pseudo-frequency response function of the entire structure should reflect this 4th mode. This physical phenomenon was observed in experiments, and the results will be presented in following Chapter 3.

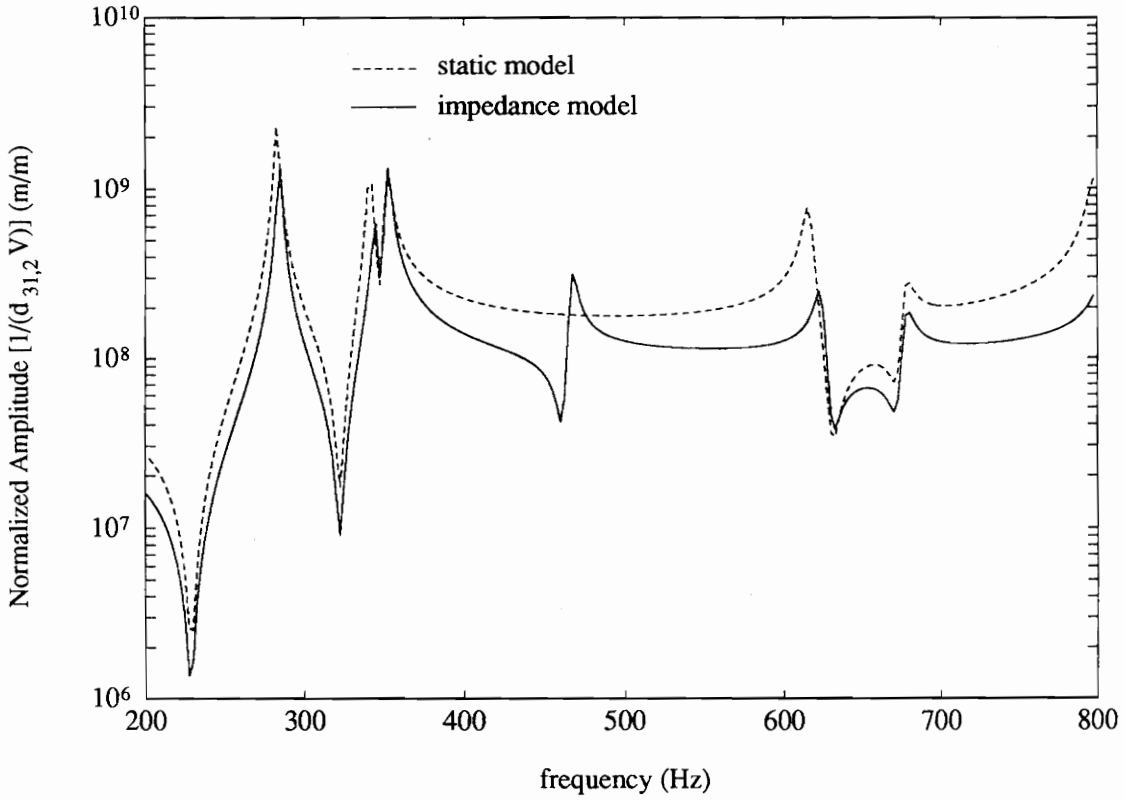

Figure 2.11: A comparison of the displacement response of the cylinder predicted by the static model and the impedance model, respectively (the response at x=310 mm and θ =15^0; h_p=0.5 mm).

2.5 Concluding Remarks

- A theory development using impedance modeling method for the actuation of two-dimensional structures has been performed. The impedance method reveals physics of the dynamic interaction between the actuators and host structures, therefore, it gives more accurate prediction of the output moments of induced strain actuators than the conventional static approach.

- The output moments (or forces) of induced strain actuators are strongly related to the input impedance of the actuators and the mechanical impedance of the host structure, and they are frequency dependent.

- When the actuator input impedance levels approach or match with the host structural impedance levels, the dynamic performance of the original shell structure is altered because of the stiffening effect of the integrated PZT actuators. The intensity of the stiffening effect varies with the location and the thickness of the PZT actuators.

2.6 References

Leissa, W., 1973, Vibration of Shells, NASA, U.S. Government Printing Office, Washington, DC; pp. 31-157.

Lester, H. C. and S. Lefebvre, 1991, "Piezoelectric Actuator Models for Active Sound and Vibration Control of Cylinders", Proceedings of Recent Advances in Active Control of Sound and Vibration, Blacksburg; VA, April 15-17, 1991, Technomic Publishing Co., Inc., Lancaster, PA; pp. 3-26.

Rossi, A., C. Liang, and C. A. Rogers, 1993, "Coupled Electric-Mechanical Analysis of a Piezoceramic Actuator Driven System - An Application to a Circular Ring", Proceedings of the AIAA/ASME/ASCE/AHS 34th SDM Conference, La Jolla, CA, April 19-21, 1993, AIAA, Inc., Washington, DC; pp. 3618-3624.

Soedel, W., 1981, Vibrations of Shells and Plates, Marcel Dekker Inc., New York.

Sonti, V. R. and J. D. Jones, 1991, "Active Vibration Control of Thin Cylindrical Shells Using Piezo-Electric Actuators", Proceedings of Recent Advances in Active Control of Sound and Vibration, Blacksburg, VA, April 15-17, 1991, Technomic Publishing Co., Inc., Lancaster, PA; pp. 27-38.

Tzou, H. S., 1989, "Theoretical Development of a Layered Shell with Internal Distributed Controllers", ASME Failure Prevention and Reliability, ASME, DE-Vol. 16; pp. 241-249.

Wang, B. T., and C. A. Rogers, 1991, "Modeling of Finite-Length Spatially Distributed Induced Strain Actuators for Laminate Beams and Plates", Proceedings of the AIAA/ASME/ASCE/AHS 32th SDM Conference, Baltimore, MD, April 8-10, 1991, AIAA, Inc., Washington, DC; pp. 1511-1520.

Zhou, S. W., C. Liang, and C. A. Rogers, 1994, "Modeling of a Distributed Piezoelectric Actuators Integrated with Thin Shells", The Journal of the Acoustical Society of American, No. 96(3), September 1994; pp. 1605-1612.

Zhou, S. W., C. Liang, and C. A. Rogers, 1993, "Impedance Modeling of Two-Dimensional Piezo-Actuators Bonded on a Cylinder", Proceedings of Adaptive Structures and Material Systems, ASME, New Orleans, LA, Nov. 28-Dec. 3, 1993; pp. 247-256.

Chapter 3

A Dynamic Model of Piezoelectric Actuator-Driven Thin Plates

3.1 Introduction

In the modeling of distributed piezoelectric actuators locally coupled with two-dimensional plate structures, static strain or stress-based analytical approaches have been used to estimate the induced loading (Dimitriadis et al., 1989; Wang et al., 1990; Crawley et al., 1991; Kim et al., 1991). It is typically assumed in the static models that the piezoelectric actuators do not significantly alter the inertia mass and the stiffness of the host structures. The dynamic interaction between PZT actuators and the structures is thus ignored. The static analysis usually leads to the conclusion that the amplitude of the excitation force of the PZT actuator is frequency independent.

When a control voltage is applied to the PZT patch along the polarization direction, the dynamic strain is induced on the host structure. The active force is then generated as a result of the mechanical interaction between the actuator and host structure. The dynamic mass loading and stiffening effect of the PZT patch should be considered. This added dynamic effect plays an important role in the actuation on the host structure and may significantly change the mechanical resonant frequencies of the original system. Therefore, a dynamic model which relates the actuator dynamics to the host structure dynamics is desired. Liang et al. (1993a) suggested an impedance model and derived the formulation of the force output of a piezoelectric actuator-driven one-degree-of-freedom spring-mass-damping system. The impedance modeling approach has been expanded to one-dimensional structures, such as beams (Liang et al., 1993b). For generic two-dimensional plate structures, the mechanical impedance coupling in different coordinate directions should be included and the cross impedance of the host structures has an impact on the actuator dynamics. Therefore, a coupled mechanical impedance model for generic smart plate structures is required.

This chapter will further expand the impedance-based modeling method to piezoelectric actuator-driven two-dimensional plate structures. First, a generic impedance analysis will be developed to obtain the dynamic outputs of the PZT actuator based upon the input impedance of the PZT patch and the mechanical impedance of the host structure. Then, an analytical solution for the admittance and impedance of a simply-supported thin plate

excited by a pair of moments will be derived. Furthermore, a vibration excitation experiment is conducted on the plate to verify the theoretical model. The comparison of the conventional static approach and the impedance method is also performed to demonstrate the significant difference between these two types of modeling approaches.

3.2 A Dynamic Model for Integrated PZT/Plate Structures

Figure 3.1 illustrates the equivalent dynamic model of a PZT actuator-driven two-dimensional structure. The dynamic performances of the host structure in the x and y directions is represented by the direct impedance Z_{xx} and Z_{yy} as well as the cross impedance Z_{xy} and Z_{yx}, respectively.

When a voltage is applied to the PZT patch along the polarization direction (3), the dynamic displacement is induced in both the x (u) and y (v) directions. The active force provided by the PZT actuator, F_x and F_y may be expressed by:

$$\begin{pmatrix} F_x \\ F_y \end{pmatrix} = -\begin{pmatrix} Z_{xx} & Z_{xy} \\ Z_{yx} & Z_{yy} \end{pmatrix}\begin{pmatrix} \dot{u} \\ \dot{v} \end{pmatrix}, \tag{3.1}$$

where the minus sign indicates that the structural reactions are equal and opposite to the output forces of the PZT actuator; and $\dot{u}$ $\dot{v}$ are the in-plane velocity response of the PZT actuator. The equation of motion of the PZT actuator may be described by:

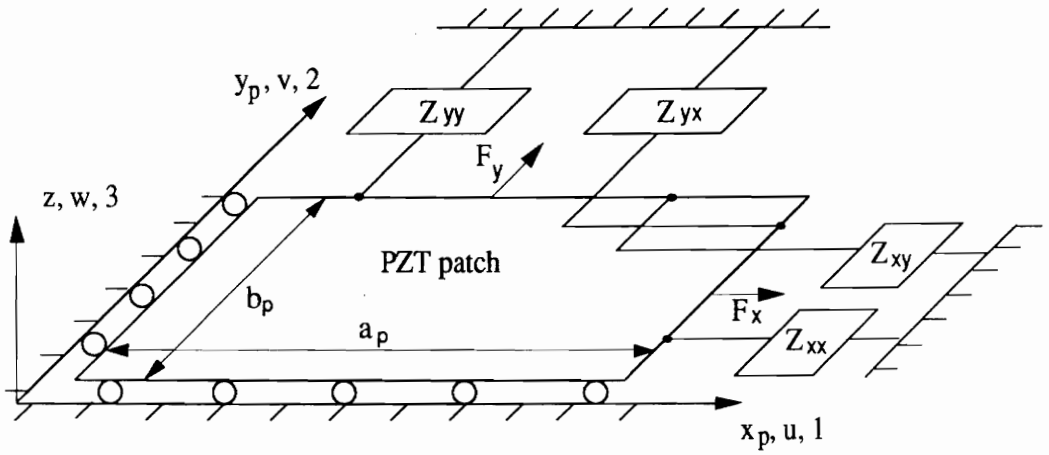

Z_{xx} , Z_{yy} — direct impedance of a two-dimensional structure
Z_{xy} , Z_{yx} — cross impedance of a two-dimensional structure

Figure 3.1: A model of dynamic interaction between a PZT actuator and a thin plate structure represented by mechanical impedance.

$$\rho_p \frac{\partial^2 u}{\partial t^2} = Y_{p11}^E \frac{\partial^2 u}{\partial x^2} \tag{3.2a}$$

$$\rho_p \frac{\partial^2 v}{\partial t^2} = Y_{p22}^E \frac{\partial^2 v}{\partial y^2} \ , \tag{3.2b}$$

in which the subscript p refers to the parameters of the PZT patch and the subscript *11 (22)* indicates the direction of the piezoelectric material; ρ is the mass density; and Y^E is the complex Young's modulus at a constant field:

$$Y^E = Y(1 + j\eta) \ , \tag{3.3}$$

where η is the structural loss factor; j is the complex number; and Y is the real Young's modulus. The displacement response of the PZT actuator is written as:

$$u = \left[A \sin(k_{p11} x) + B \cos(k_{p11} x)\right] e^{j\omega t} \tag{3.4a}$$

$$v = \left[C \sin(k_{p22} y) + D \cos(k_{p22} y)\right] e^{j\omega t} \ , \tag{3.4b}$$

where A, B, C and D are unknowns and can be determined by the boundary conditions. Considering the isotropy of the PZT material gives the wave number, $k_{p11(22)}$:

$$k_p = k_{p11} = k_{p22} = \omega \sqrt{\frac{\rho_p}{Y_p^E}} \ , \tag{3.5}$$

where ω is the input angular frequency. Applying the displacement boundary condition, $u_{x=0}=0$ and $v_{y=0}=0$ to Eq. (3.4) leads to $B=D=0$. The displacement response of the PZT actuator is reduced to:

$$u = A \sin(k_p x) e^{j\omega t} \tag{3.6a}$$

$$v = C \sin(k_p y) e^{j\omega t} \ . \tag{3.6b}$$

The unknowns A and C may be evaluated from the constitutive equation of the PZT patch

at $x=a_p$ and $y=b_p$, as shown in Fig. 3.1:

$$\begin{pmatrix}\varepsilon_x\\ \varepsilon_y\end{pmatrix}=\begin{pmatrix}\frac{\partial u}{\partial x}\\ \frac{\partial v}{\partial y}\end{pmatrix}=\begin{pmatrix}\frac{1}{Y_p^E b_p t_p} & -\frac{\nu_p}{Y_p^E a_p t_p}\\ -\frac{\nu_p}{Y_p^E b_p t_p} & \frac{1}{Y_p^E a_p t_p}\end{pmatrix}\begin{pmatrix}F_x\\ F_y\end{pmatrix}+\begin{pmatrix}d_{31}\\ d_{32}\end{pmatrix}E\ , \tag{3.7}$$

where $\varepsilon_{x(y)}$ is the dynamic strain; a_p, b_p, and t_p are the length, the width, and the thickness of the PZT patch, respectively; d_{31} and d_{32} are the piezoelectric constants of the PZT material in the 1 and 2 directions; $E=V/t_p$ is the electric field; and V is the applied voltage. Note that the Poisson's ratio of the PZT material, ν_p is introduced so that the mechanical coupling of the in-plane motions in the x and y directions of the PZT actuator can be included in the modeling. Substituting Eqs. (3.1) and (3.6) into Eq. (3.7) and taking the algebraic operation to rearrange A and C yields:

$$\begin{pmatrix}k_p\cos(k_p a_p)(1-\frac{\nu_p}{\alpha}\frac{Z_{xy}}{Z_{pxx}}+\frac{Z_{xx}}{Z_{pxx}}) & k_p\cos(k_p b_p)(\alpha\frac{Z_{yx}}{Z_{pyy}}-\nu_p\frac{Z_{yy}}{Z_{pyy}})\\ k_p\cos(k_p a_p)(\frac{1}{\alpha}\frac{Z_{xy}}{Z_{pxx}}-\nu_p\frac{Z_{xx}}{Z_{pxx}}) & k_p\cos(k_p b_p)(1-\nu_p\alpha\frac{Z_{yx}}{Z_{pyy}}+\frac{Z_{yy}}{Z_{pyy}})\end{pmatrix}\begin{pmatrix}A\\ C\end{pmatrix}=\begin{pmatrix}d_{31}\\ d_{32}\end{pmatrix}E\ , \tag{3.8}$$

where $\alpha=a_p/(b_p)$ is the ratio of the length to the width of the PZT patch; and Z_{pxx} and Z_{pyy} are the short-circuit input impedance of the PZT actuator in the x and y directions, defined as:

$$Z_{pxx}=\frac{F_x}{\dot{u}}=-j\frac{K_{px}}{\omega}\frac{k_p a_p}{\tan(k_p a_p)} \tag{3.9a}$$

$$Z_{pyy}=\frac{F_y}{\dot{v}}=-j\frac{K_{py}}{\omega}\frac{k_p b_p}{\tan(k_p b_p)}\ , \tag{3.9b}$$

with the static extension stiffness of the PZT actuator in the x and y directions, K_{px} and

K_{py}:

$$K_{px} = \frac{Y_p^E b_p t_p}{a_p} \tag{3.10a}$$

$$K_{py} = \frac{Y_p^E a_p t_p}{b_p} \ . \tag{3.10b}$$

Solving for A and C from Eq. (3.8), the dynamic force output of the PZT actuator is determined from Eq. (3.1) with the substitution of the velocity response:

$$\begin{pmatrix} F_x \\ F_y \end{pmatrix} = \begin{pmatrix} \bar{F}_x \\ \bar{F}_y \end{pmatrix} e^{j\omega t} = -j\omega \begin{pmatrix} Z_{xx} & Z_{xy} \\ Z_{yx} & Z_{yy} \end{pmatrix} \begin{pmatrix} A\sin(k_p a_p) \\ C\sin(k_p b_p) \end{pmatrix} e^{j\omega t} \ . \tag{3.11}$$

Accordingly, the amplitude of the line moments per unit length created by a pair of the PZT actuators, $\bar{M}_{x,(y)}$ (in N·m/m), can be obtained by:

$$\begin{pmatrix} \bar{M}_x \\ \bar{M}_y \end{pmatrix} = (h+t_p) \begin{pmatrix} \bar{F}_x/b_p \\ \bar{F}_y/a_p \end{pmatrix} = -j\omega \frac{h+t_p}{a_p b_p} \begin{pmatrix} a_p Z_{xx} & a_p Z_{xy} \\ b_p Z_{yx} & b_p Z_{yy} \end{pmatrix} \begin{pmatrix} A\sin(k_p a_p) \\ C\sin(k_p b_p) \end{pmatrix} , \tag{3.12}$$

where h is the thickness of the host structure. The distributed line moments are thus expressed by:

$$M_x = \bar{M}_x [\delta(x-x_1) - \delta(x-x_2)]\,[h(y-y_1) - h(y-y_2)] e^{j\omega t} \tag{3.13a}$$

$$M_y = \bar{M}_y [\delta(y-y_1) - \delta(y-y_2)]\,[h(x-x_1) - h(x-x_2)] e^{j\omega t} \ , \tag{3.13b}$$

where $\delta(x)$ and $\delta(y)$ are the Direc delta functions; $h(x)$ and $h(y)$ are the Heaviside functions; x_1, x_2, y_1 and y_2 are the location coordinates of the edge of PZT patches on the plate, as illustrated in Fig. 3.2. Notice that the coefficients A and C as well as the mechanical impedance of the host structure in Eq. (3.12) are functions of frequency Therefore, the moment outputs of PZT actuator must be frequency dependent.

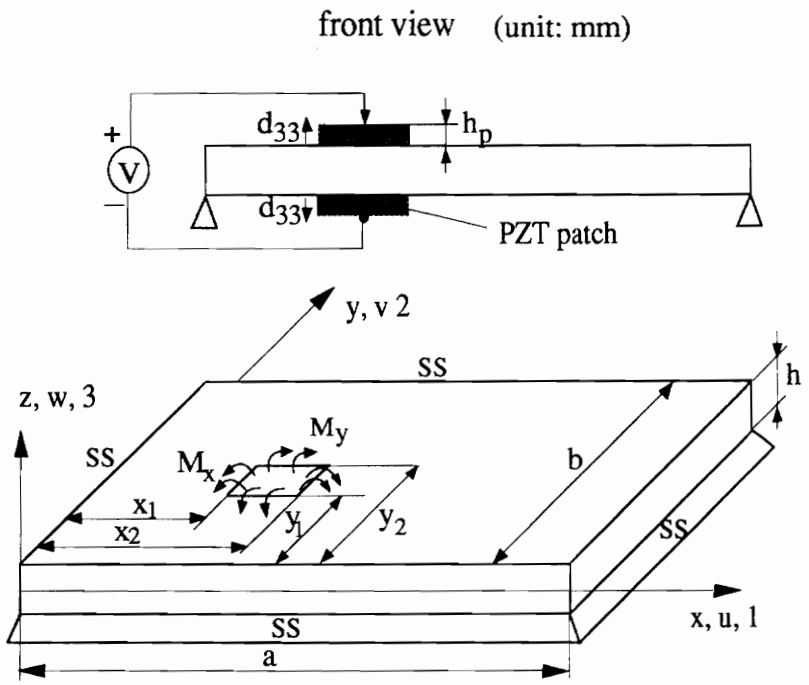

Figure 3.2: Geometric configuration of a simply-supported (ss) thin plate with surface-bonded PZT actuators.

Thus far, the dynamic forces and moments of the PZT actuator have been obtained based upon the impedance characteristics of the PZT itself and the host structure. This dynamic model is also called the impedance model. The input impedance of the PZT actuator is given by Eq. (3.9). The mechanical impedance of the host structure depends on the location of the actuation and the geometric configuration, the physical and material properties, and the boundary condition of the structure. As a numerical example, the next section will address how to calculate the admittance of a simply-supported thin plate actuated by the line moments. For complex structures, although a close form solution is difficult to obtain, the structural impedance can be determined from either experiments or finite element analysis.

3.3 Admittance Analysis of a Thin Plate Actuated by Line Moments

The geometric representation of a simply-supported thin plate with a pair of PZT actuators is shown in Fig. 3.2. The PZT patches are assumed to be perfectly bonded on the top and bottom surfaces of the plate. When the PZT actuators are actuated out-of-phase, a pure bending moment excitation is created at the edges of the PZT patches.

Under the actuation of M_x and M_y, the total angular velocity response of the plate at the edge of the PZT patches may be written as:

$$\nabla\beta_x = -[(\frac{\partial \dot{w}}{\partial x})_{x=x_2} - (\frac{\partial \dot{w}}{\partial x})_{x=x_1}] = -(H_{xx}M_x + H_{yx}M_y) \tag{3.14a}$$

$$\nabla\beta_y = -[(\frac{\partial \dot{w}}{\partial y})_{y=y_2} - (\frac{\partial \dot{w}}{\partial y})_{y=y_1}] = -(H_{xy}M_x + H_{yy}M_y) \ , \tag{3.14b}$$

where H_{xx} and H_{yy} are the direct moment admittances of the plate. H_{xy} and H_{yx} are the cross moment admittances of the plate and indicate mechanical impedance coupling of the host structure in the x and y directions. The moment admittance here is defined as:

$$H_{lk} = \frac{\nabla\beta_k}{M_l} \qquad (l,k=x,y) \ . \tag{3.15}$$

Using the relation of the force and the moment, $M_{x(y)}=(h+h_p)F_{x(y)}$ as well as the geometric relation of $u(v)=(h+h_p)\bullet\nabla\beta_{x(y)}/2$, as illustrated in Fig. 3.3, Eq. (3.14) is rewritten in terms of the force admittance matrix:

$$\begin{pmatrix} F_x \\ F_y \end{pmatrix} = -\frac{2}{(h+h_p)^2}\begin{pmatrix} H_{xx} & H_{yx} \\ H_{xy} & H_{yy} \end{pmatrix}^{-1}\begin{pmatrix} \dot{u} \\ \dot{v} \end{pmatrix} = -\begin{pmatrix} Q_{xx} & Q_{yx} \\ Q_{xy} & Q_{yy} \end{pmatrix}^{-1}\begin{pmatrix} \dot{u} \\ \dot{v} \end{pmatrix} . \tag{3.16}$$

The coefficient $2/(h+h_p)^2$ in Eq. (3.16) is developed for transformation of the moment admittance to the in-plane force admittance. The corresponding force impedance matrix is thus determined by:

$$\mathbf{Z} = \begin{pmatrix} Z_{xx} & Z_{xy} \\ Z_{yx} & Z_{yy} \end{pmatrix} = \begin{pmatrix} Q_{xx} & Q_{yx} \\ Q_{xy} & Q_{yy} \end{pmatrix}^{-1} . \tag{3.17}$$

Under the actuation of distributed moments normal to the surface of the plate, the governing equation for the forced transverse motion of the plate may be written based upon Love's theory and Hamilton principle (Soedel, 1981):

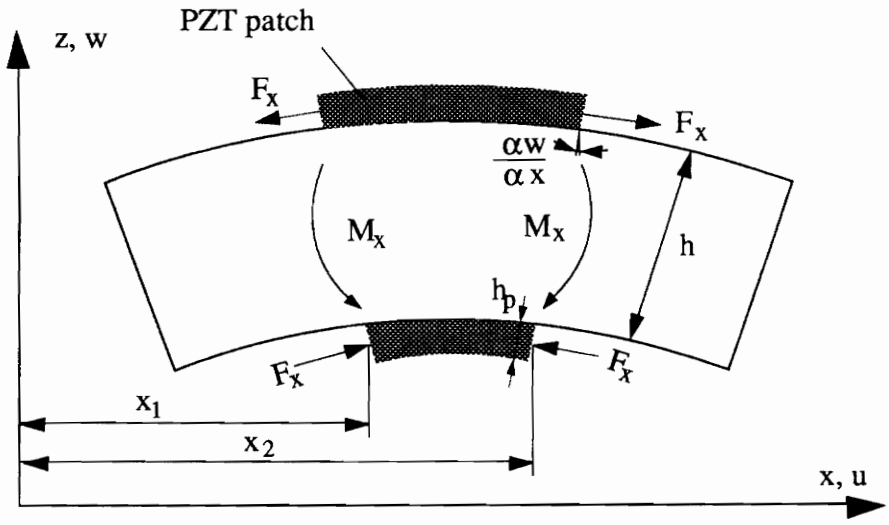

Figure 3.3: Geometric deformation of a plate actuated by a pair of moments in the x direction.

$$L(w)-\rho h\ddot{w}=-\left(\frac{\partial M_x}{\partial x}+\frac{\partial M_y}{\partial y}\right), \tag{3.18}$$

where w is the transverse displacement response of the plate. $L(w)$ is the Love operator, which can be evaluated from the eigenvalue analysis:

$$L(w)=-\rho h\omega_{mn}^2 w, \tag{3.19}$$

where ω_{mn} is the complex resonant frequency of the plate because the damping factor of the system is introduced through the complex Young's modulus in Eq. (3.3). The subscript m and n refer to the mode numbers in the x and y directions. The forced response of the plate may be expressed by the modal expansion series solution:

$$w=\sum_{m=1}^{\infty}\sum_{n=1}^{\infty}p_{mn}W_{mn}(x,y), \tag{3.20}$$

where p_{mn} is the modal participation factor which determines the amount of participation of each mode in the total transverse dynamic response. W_{mn} is the eigenfunction. Substituting Eqs. (3.19) and (3.20) into Eq. (3.18) results in:

$$\sum_{m=1}^{\infty}\sum_{n=1}^{\infty}(\rho h\ddot{p}_{mn}+\rho h\omega_{mn}^2 p_{mn})W_{mn}(x,y)=\frac{\partial M_x}{\partial x}+\frac{\partial M_y}{\partial y}. \tag{3.21}$$

For a simply-supported plate, the eigenfunction $W_{mn}(x,y)$ can be described by:

$$W_{mn}(x,y)=\sin\frac{m\pi}{a}x\cos\frac{n\pi}{b}y, \tag{3.22}$$

where a and b are the length and the width of the plate. Substituting Eq. (3.22) into Eq. (3.21) and using the usual modal expansion technique yields:

$$\ddot{p}_{mn}+\omega_{mn}^2 p_{mn}=F_{mn}e^{i\omega t}, \tag{3.23}$$

where the equivalent forcing function, F_{mn} is the form of

$$F_{mn}=\frac{1}{\rho h N_{mn}}\int_0^a\int_0^b W_{mn}(x,y)\left(\frac{\partial M_x}{\partial x}+\frac{\partial M_y}{\partial y}\right)dxdy\ , \tag{3.24}$$

and

$$N_{mn}=\int_0^a\int_0^b \sin^2\frac{m\pi x}{a}\cos^2\frac{n\pi y}{b}\,dxdy=\frac{ab}{4}\ . \tag{3.25}$$

Applying Eqs. (3.13) and (3.22) into Eq. (3.24) yields:

$$F_{mn}=\frac{4}{ab\rho h}\left(\frac{bm}{an}\bar{M}_x+\frac{an}{bm}\bar{M}_y\right)\left(\cos\frac{m\pi}{a}x_2-\cos\frac{m\pi}{a}x_1\right)\left(\cos\frac{n\pi}{b}y_1-\cos\frac{n\pi}{b}y_2\right)\ . \tag{3.26}$$

The steady-state solution of the forced vibration of the plate is thus obtained by:

$$w(x,y,t)=\sum_{m=1}^{\infty}\sum_{n=1}^{\infty}\frac{F_{mn}\sin\frac{m\pi}{a}x\sin\frac{n\pi}{b}y\,e^{j\omega t}}{\omega_{mn}^2-\omega^2}\ , \tag{3.27}$$

where x and y are the location coordinates at which the response is picked up. The resonant frequency, ω_{mn}, is determined from the homogenous equation of the transverse motion of the plate:

$$\omega_{mn}=\pi^2\sqrt{\frac{D}{\rho h}}\left(\left(\frac{m}{a}\right)^2+\left(\frac{n}{b}\right)^2\right), \tag{3.28}$$

where

$$D=\frac{h^3 Y^E}{12(1-\nu^2)} \tag{3.29}$$

is the flexural stiffness of the plate.

Recalling the definition of the admittance in Eq. (3.15) and the relation of $Q_{lk}=(h+t_p)^2H_{lk}/2$ $(l,k=x,y)$, the direct force admittance of the plate at the edge of the PZT patch is obtained

by:

$$Q_{xx}=\frac{2\pi(h+t_p)^2\omega}{\rho h a^3 b_p}\sum_{m=1}^{\infty}\sum_{n=1}^{\infty}\left(\frac{m^2(\cos\frac{m\pi x_1}{a}-\cos\frac{m\pi x_2}{a})^2\sin\frac{n\pi(y_1+y_2)}{2b}(\cos\frac{n\pi y_1}{b}-\cos\frac{n\pi y_2}{b})}{n(\omega_{mn}^2-\omega^2)}\right)e^{j\pi/2} \quad (3.30)$$

and

$$Q_{yy}=\frac{2\pi(h+t_p)^2\omega}{\rho h b^3 a_p}\sum_{m=1}^{\infty}\sum_{n=1}^{\infty}\left(\frac{n^2(\cos\frac{m\pi x_1}{a}-\cos\frac{m\pi x_2}{a})\sin\frac{m\pi(x_1+x_2)}{2a}(\cos\frac{n\pi y_1}{b}-\cos\frac{n\pi y_2}{b})^2}{m(\omega_{mn}^2-\omega^2)}\right)e^{j\pi/2}. \quad (3.31)$$

Similarly, the cross admittance is determined by:

$$Q_{xy}=\frac{2\pi(h+t_p)^2\omega}{\rho h a^2 b b_p}\sum_{m=1}^{\infty}\sum_{n=1}^{\infty}\left(\frac{m(\cos\frac{m\pi x_1}{a}-\cos\frac{m\pi x_2}{a})\sin\frac{m\pi(x_1+x_2)}{2a}(\cos\frac{n\pi y_1}{b}-\cos\frac{n\pi y_2}{b})^2}{\omega_{mn}^2-\omega^2}\right)e^{j\pi/2} \quad (3.32)$$

and

$$Q_{yx}=\frac{2\pi(h+t_p)^2\omega}{\rho h a b^2 a_p}\sum_{m=1}^{\infty}\sum_{n=1}^{\infty}\left(\frac{n(\cos\frac{m\pi x_2}{a}-\cos\frac{m\pi x_1}{a})^2\sin\frac{n\pi(y_1+y_2)}{2b}(\cos\frac{n\pi y_1}{b}-\cos\frac{n\pi y_2}{b})}{(\omega_{mn}^2-\omega^2)}\right)e^{j\pi/2}. \quad (3.33)$$

3.4 Dynamic Output Characteristics of Integrated PZT Actuators

In the static models, the amplitude of the moment outputs of the actuator are assumed to be independent of the frequency and the dynamic behavior of the host structure. In addition, the same amplitude of the moment is assumed to be in both the x and y directions even though the mechanical impedance of the structure may be quite different.

There are several static models for the actuation of PZT patches on two-dimensional plate structures (Dimitriadis et al., 1989; Wang et al., 1990; Crawley et al., 1991; Kim et al., 1991). One of them was developed from the stress-based pure bending model (Dimitriadis et al., 1989) is used in this paper to compare with the dynamic model.

A simply-supported thin plate as shown in Fig. 3.2 is used in the numerical calculation. The thin plate is made of aluminum and the PZT material is G1195. Their geometric parameters are listed in Table 3.1. The basic material properties are same as those listed in Table 2.1.

Figure 3.4 demonstrates the difference of moment outputs of the actuator predicted by the dynamic model and the static model. In the dynamic model, the amplitude of the moment varies significantly near the resonant frequencies of the system because of the dynamic interaction between the actuator and the plate. This interaction can be explained by the impedance matching, as shown in Fig. 3.5. When the input impedance of the PZT actuator approaches and matches the structural impedance of the plate, the moment output of the actuator varies significantly. Therefore, the actuation is greatly strengthened. In the static model, however, the amplitude of the moment output is constant over the whole frequency band as shown in Fig. 3.4 and the dynamic output of the actuator can not be predicted. In addition, Figure 3.5 shows that the mechanical impedance of the plate is different in the x and y directions because of the asymmetric geometry of the plate.

Table 3.1: Geometric Parameters of the PZT Actuator and the Plate

	Length a	Width b	Thickness h	Location x_1	Location y_1
PZT	50.8	50.8	0.19	50.8	25.4
plate	304.8	203.2	1.53	N/A	N/A

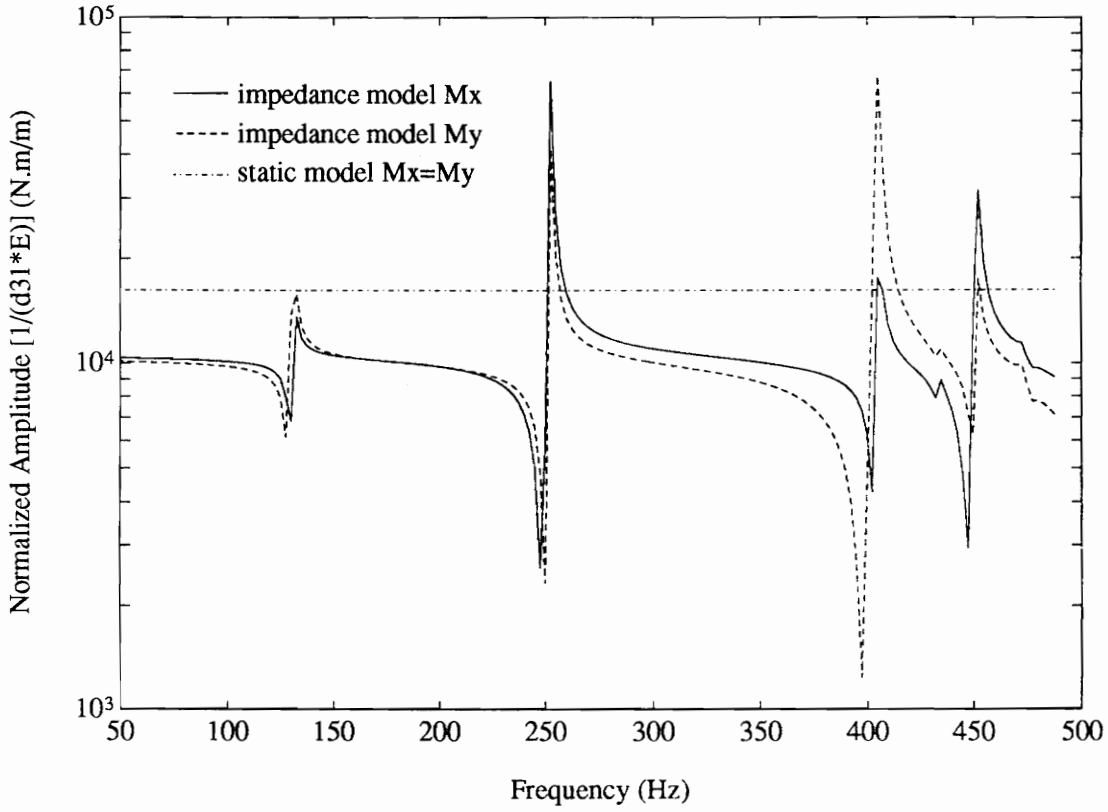

Figure 3.4: The moment outputs predicted by the impedance model and the conventional static model, respectively.

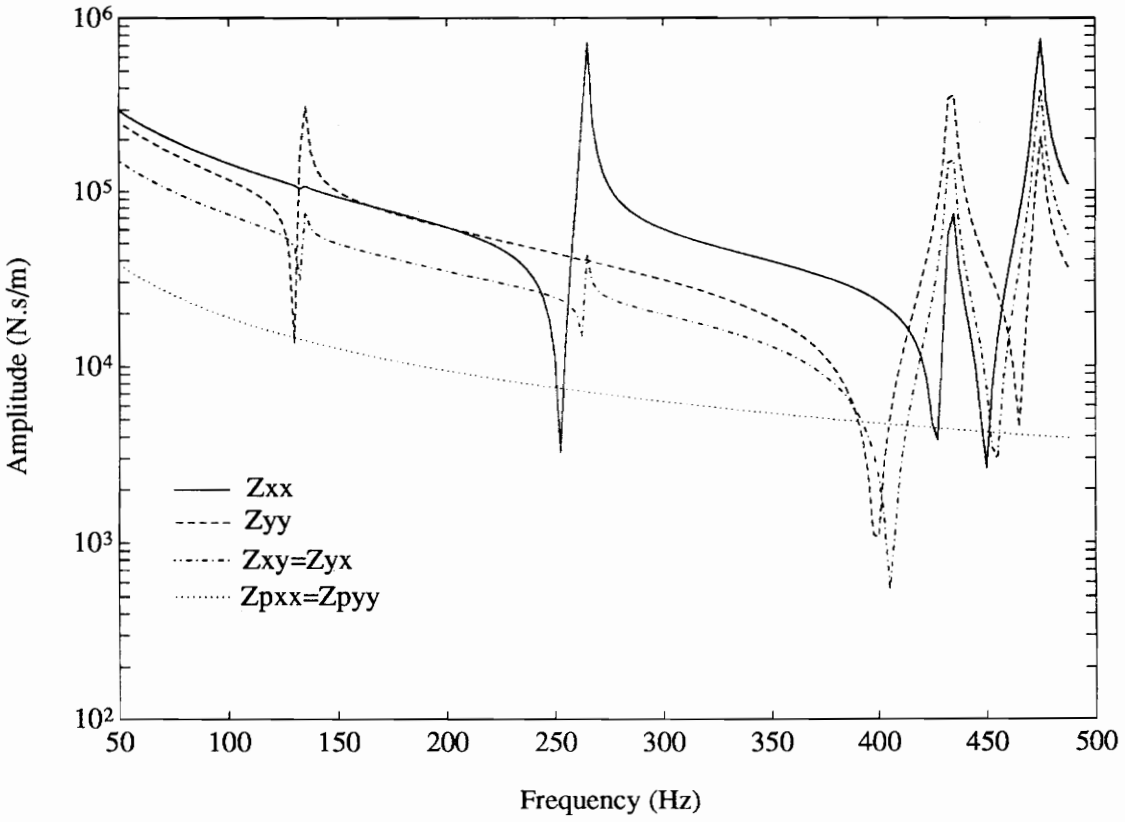

Figure 3.5: The input impedance of the PZT actuator and the mechanical impedance of the host plate.

Therefore, the actuation of the PZT actuator is not equal, that is, $\overline{M}_x \neq \overline{M}_y$.

To examine the utility and generality of the two-dimensional impedance model, the developed model above is applied to one-dimensional structures. It is assumed that the mechanical coupling terms of the host structure, i. e., the cross impedance Z_{xy} and Z_{yx} in Eq. (3.8) is zero and the Poisson effect of the piezoelectric material is also ignored. A decoupling analysis is then obtained. The force output of the PZT actuator predicted by Eq. (3.11) is reduced to:

$$F_{x(y)} = -\frac{Z_{xx(yy)}}{Z_{pxx(yy)}+Z_{xx(yy)}} Y_p^E S_{px(y)} d_{31} E \ , \tag{3.34}$$

where $S_{px(y)}$ is the cross section area of the PZT patch. This result is exactly same as that derived by Stein et al. (1993) and Liang et al. (1993a). Therefore, the two-dimensional impedance analysis presented in the previous section is more general and collates the results predicted by earlier publication for one-dimensional structures.

3.5 Experimental Verification

A simply-supported thin plate was built and tested to verify the dynamic model. The experimental setup of vibration excitation of the plate is illustrated in Fig. 3.6. The thin plate in the experiment is made of aluminum and the PZT material is G1195. Their geometric parameters are shown in Table. 3.1. The basic material properties are listed

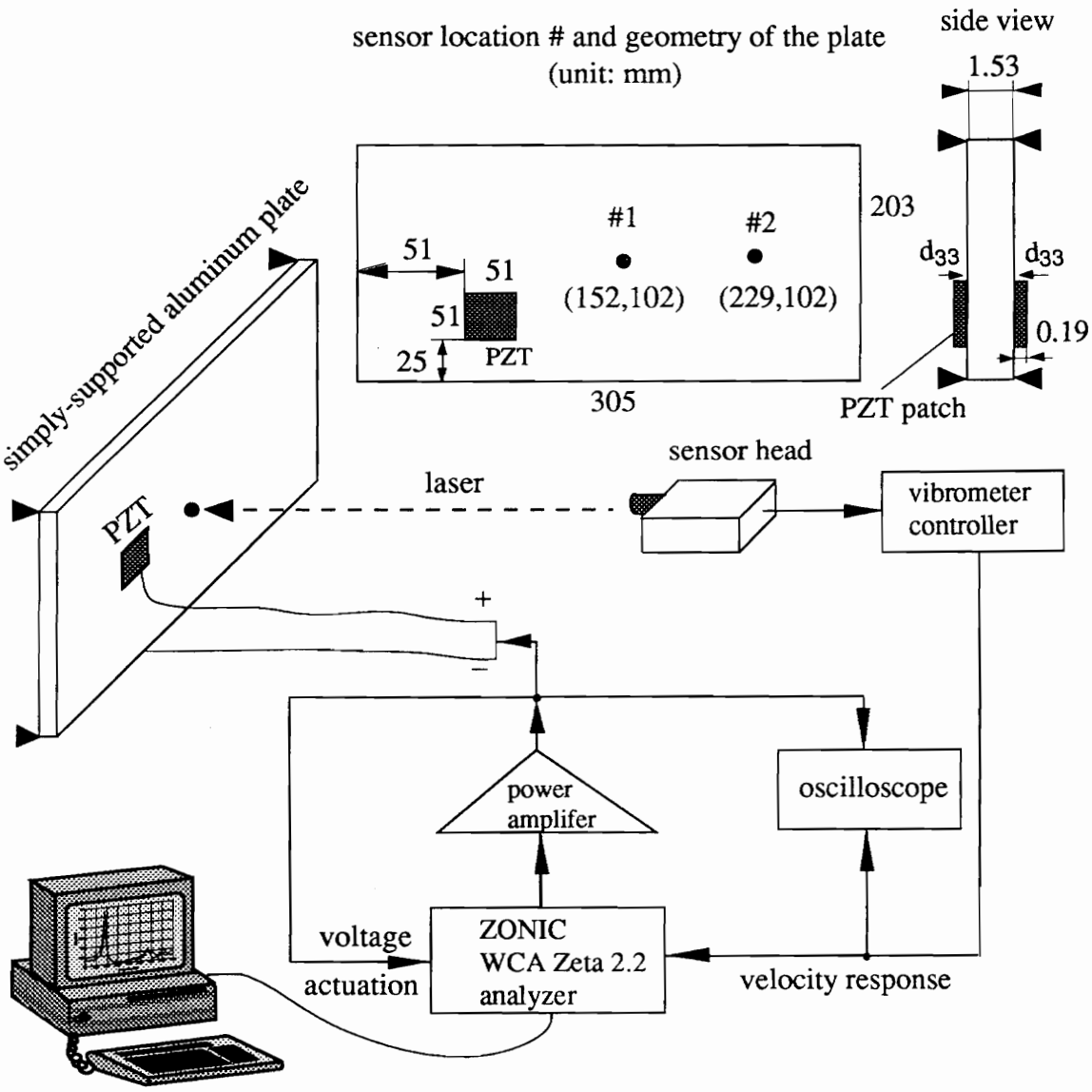

Figure 3.6: The experimental setup for the measurement of the velocity response of the host plate integrated with PZT actuators.

in Table 2.1.

A pseudo-random signal was used in a burst mode to activate the plate. The transverse velocity response of the plate is accurately measured using a noncontact laser sensor such that the effect of the added mass and stiffening effect of the sensor on the plate has been eliminated. The response is picked up at two different locations: $x=6''$, $y=4''$, and $x=9''$, $y=4''$, as shown in Fig. 3.6. The coherence of the actuation voltage and the velocity response is used to examine the accuracy of the excited modes.

Figure 3.7 illustrates the measured and predicted frequency response function of the plate at the sensor location #1. Two important results have been observed:

First, the theoretical prediction based upon the impedance analysis (dash line) agrees well with the experimental data (solid line). The static model (dashed-dotted line), however, misrepresents the normalized velocity response of the plate and is not able to predict the 2nd (2,1) mode and the 3rd mode (1,2). The reason was explained in previous Chapter 3 (Sec. 2.4, pp. 48-51). Since the sensor location #1 is on the nodal lines of these two modes, assuming a constant moment input in the static model misses these two modes in the pseudo-frequency response function. As a matter of fact, the input moment is a function of frequency and is maximized at the resonant frequencies of the integrated system. The 2nd and 3rd modes thus show up in the pseudo-frequency response function.

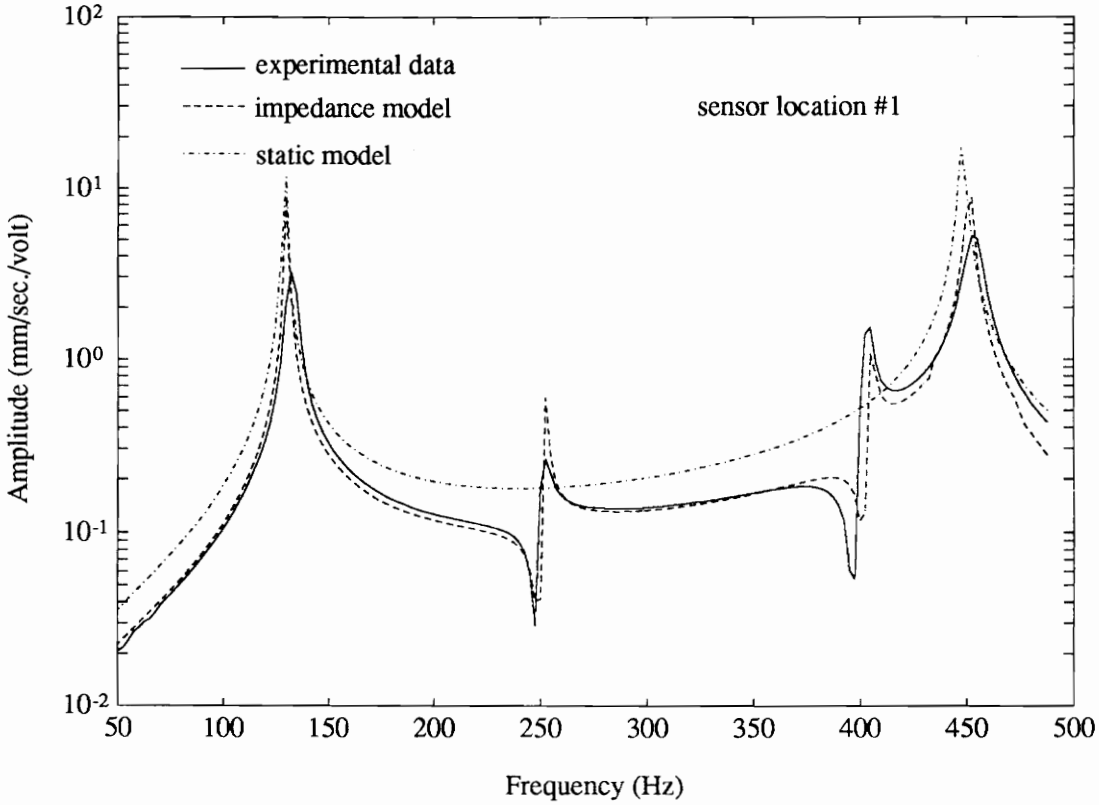

Figure 3.7: The predicted and measured velocity response of the host plate integrated with PZT actuators at sensor location #1.

Second, Figure 3.7 clearly demonstrates that the dynamic performance of the original system is altered due to the added PZT patches. The resonant frequency of the original plate is shifted to high values. The maximum frequency shift happens to be at 4th mode (1,3) and the resonant frequency increases about 15 Hz within the frequency band less than 1000 Hz. At the same time, the amplitude of the system response decreases. This may be explained by the observation that the PZT patches bonded on the surface of the plate stiffen the structure and add the parasitic mass in the original system. In general, the stiffening effectiveness will increase the resonant frequencies of the structure while the added mass has the opposite influence. However, the stiffening effect may have the greater impact on the dynamic characteristics of the plate than the added mass. Consequently, the resonant frequencies of the integrated system are shifted to the higher value. The intensity of the variation of the frequencies depends on the extent of the impedance matching between PZT and the plate. In static model, the dynamic behavior of the plate is assumed to be unchanged, hence, the phenomena of resonant frequency shift can't be observed in the experiment.

When the sensor location is moved from the location #1 to the location #2, the same phenomena as shown in Fig. 3.7 happens. This time, the sensor location #2 is placed on the nodal line of only 3rd mode (1,2). Thus, the static model picks up the 2nd mode but misses the 3rd mode, as shown in Fig. 3.8. The resonant frequency shift and the dynamic response variation of the original system caused by the bonded PZT actuators still exist.

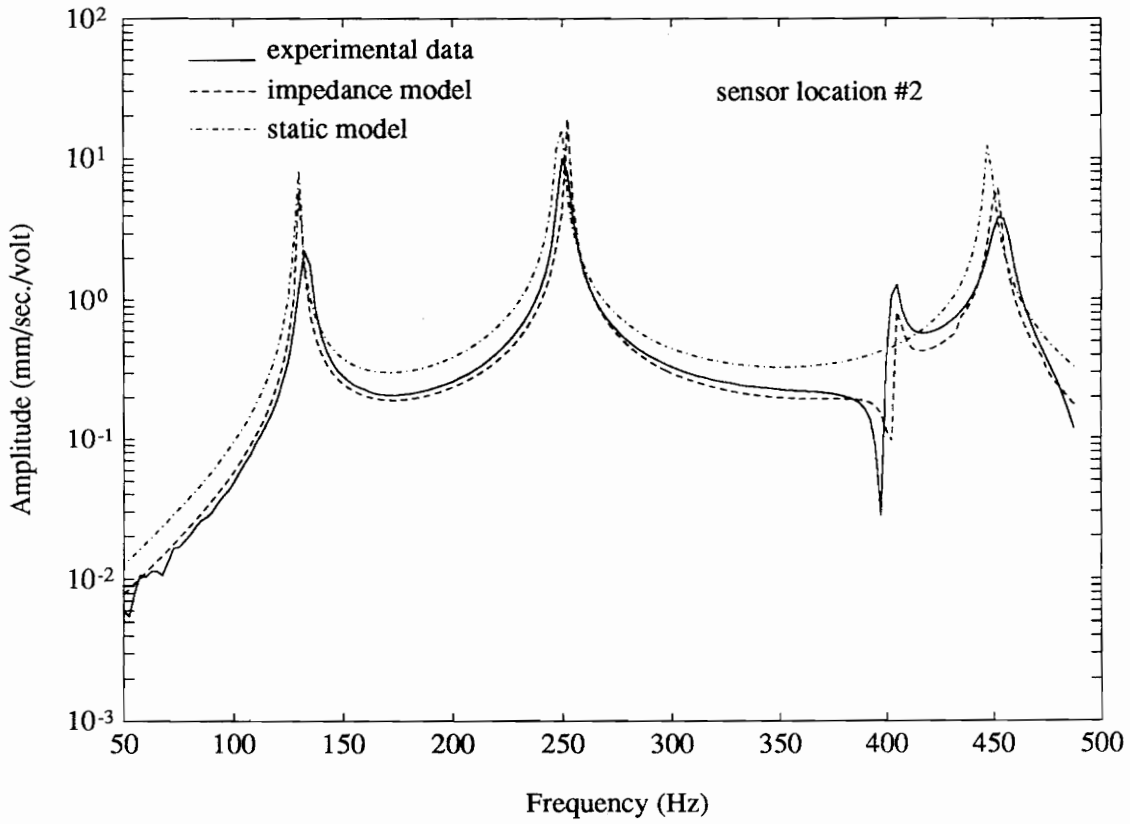

Figure 3.8: The predicted and measured velocity response of the host plate integrated with PZT actuators at sensor location #2.

However, these dynamic performance variations are not predicted by the static model.

3.6 Concluding Remarks

- A dynamic model for the actuation of two-dimensional structures has been developed using the mechanical impedance analysis. The impedance modeling approach has clearly demonstrated its advantage over conventional static models and its potential in the design and the application of PZT actuators. It reveals the dynamic essence of the actuation of the PZT actuators and offers more accurate prediction.

- The experiment has verified the accuracy of the impedance model to predict the dynamic outputs (forces or moments) of the induced strain actuators and the vibration response of the adaptive structures.

- The dynamic performance of the adaptive structures may be strongly affected by the stiffening effect of the distributed piezoelectric actuators.

3.7 References

Crawley, E. F. and K. B. Lazarus, 1991, "Induced Strain Actuation of Isotropic and Anisotropic Plates", AIAA Journal, Vol. 29, No. 6; pp. 944-951.

Dimitriadis, E. K., C. R. Fuller and C. A. Rogers, 1989, "Piezoelectric Actuators for Distributed Noise and Vibration Excitation of Thin Plates", ASME Failure Prevention and Reliability, DE-Vol. 16; pp. 223-233.

Kim, S. J. and J. D. Jones, 1991, "Optimal Design of Piezoactuators for Active Noise and Vibration Control", AIAA Journal, Vol. 29, No. 12; pp. 2047-2053.

Leissa, W., 1973, Vibration of Shells, NASA, U.S. Government Printing Office, Washington, DC; pp. 31-157.

Liang, C., F. P. Sun and C. A. Rogers, 1993a, 1993, "Dynamic Output Characteristics of Piezoceramic Actuators", Smart Structures and Materials '93, SPIE, Albuquerque, NM, VOL. 1917; pp. 286-298.

Liang, C., F. P. Sun and C. A. Rogers, 1993b, "An Impedance Method for Dynamic Analysis of Active Material Systems", Proceedings of the 34th SDM Conference, AIAA, La Jolla, CA; pp. 3587-3599.

Soedel, W., 1981, Vibrations of shells and Plates, Marcel Dekker Inc., New York; pp. 199-228 and 248-260.

Stein, S., C. Liang, and C. A. Rogers, "Power Consumption of Piezoelectric Actuators in Underwater Active Structural Acoustic Control", Proceedings of the Second Conference on Recent Advances in Active Control of Sound and Vibration, Blacksburg, VA, April 28-30, 1993; pp. 240-251.

Wang, B. T. and C. A Rogers, 1990, "Laminate Plate Theory for Spatially Distributed Induced Strain Actuators", Fifth Japan-U. S. Conference on Composite Materials, Tama City, Japan.

Zhou, S. W. and C. A. Rogers, 1994, "A System Modeling Method of Piezoelectric-Driven Adaptive Structures", accepted for the publication in Journal of Vibration and Acoustics, October, 1994.

Zhou, S. W., C. Liang, and C. A. Rogers, 1994, "A Dynamic Model of Piezoelectric

Actuator-Driven Thin Plates", Proceedings of Smart Structures and Materials, SPIE, Orlando, FL; Paper No: 2190-56; in press.

Chapter 4

Power Flow and Consumption in Piezoelectrically-Actuated Structures

Nomenclature

a	length of structure
A	electro-mechanical admittance of a system
b	width of structure
d	piezoelectric constant
E	electric field
F	force output of piezoelectric actuator
h	thickness of structure
Q	mechanical admittance
j	imaginary part of a complex number
I	current
k	wave number
P	dissipative power
R	reactive power
u	displacement in x direction
v	displacement in y direction
V	voltage
Y	Young's modulus

Z	mechanical impedance
W	complex power

Greek

ε	strain
η	structural loss factor
ν	Poisson's ratio
ρ	mass density
ω	angular frequency
σ	stress

Subscripts

p	parameters of piezoelectric actuator
x,y	physical coordinates
0	magnitude of electrical parameters
1,2,3	piezoelectric material directions

Superscript

*	complex parameter

4.1 Introduction

Piezoelectric actuator-driven adaptive structures are complex electro-mechanical coupling systems in which electrical energy is converted into mechanical energy and vice-versa. The ability and efficiency of the energy conversion of the actuators are always of concern in the design and application of intelligent structures, especially for aerospace applications. Large and complex aerospace structures may require a great number of relatively large actuators, which will dictate large, expensive power supplies. Minimizing power consumption and enhancing energy conversion efficiency of actuators will result in reductions in the cost and mass of the system, two of major objectives in designing

intelligent structures (Rogers, 1993). To achieve this, it is highly desirable to explore the nature and components of electro-mechanical power flow and consumption in active structures.

Liang et al. (1993a) suggested a coupled electro-mechanical analysis for a piezoelectric actuator-driven spring-mass-damper system and discussed the concept of actuator power factor and energy transfer of the system. Stein et al. (1993) investigated the power consumption of piezoelectric actuators integrated with an underwater structure that radiates sound, and considered the power requirements in the active acoustic control. Lomeno et al. (1993) developed a technique to maximize mechanical power transfer from stacked PZT actuators to host structures. A mechanical impedance model applicable to two-dimensional structures, developed in Chapters 2 and 3, now needs to be extended to include system electrical parameters to analyze electro-mechanical power flow in PZT actuator-driven active structures (Zhou et al., 1994a; and 1994b).

The concept of energy conversion in a PZT actuator-driven system involves a two-step conversion: one is the energy transfer from the support power electronics to the integrated PZT/substrate mechanical system; the other is the energy conversion from the electrical energy of the PZT actuator to the mechanical energy driving the host structure. The focus of this current work is on the analysis of the second-step energy conversion, i.e., the electro-mechanical power consumption and power flow in PZT actuator-driven active

structures. In this chapter, the formulation of a coupled electro-mechanical admittance for generic two-dimensional PZT actuator-driven structures will be derived. Then, the model will be used to predict and analyze the power consumption, power requirement, and energy conversion efficiency of the integrated PZT/substrate system. A parametric study will be presented to examine the effects of different factors in the system on power dissipation and energy transfer, including the effects of different damping factors and geometric parameters in the system. An experiment on a simply-supported thin plate using an impedance analyzer will be conducted. The experimental data will be compared with the analytical results from the coupled electro-mechanical impedance model so that the theoretical model could be verified.

4.2 A Coupled Electro-Mechanical System Model

A schematic of a two-dimensional PZT/substrate coupling system is shown in Fig. 4.1. When a voltage is applied to the piezoelectric patches along the polarization direction (3), a mechanical strain is induced in the PZT actuator in both the x (1) and y (2) directions. This induced strain generates the active forces, F_x and F_y, at the edge of the PZT actuator. The corresponding induced stress is thus expressed as:

$$\begin{pmatrix} \sigma_x \\ \sigma_y \end{pmatrix} = \begin{pmatrix} 1/(b_p h_p) & 0 \\ 0 & 1/(a_p h_p) \end{pmatrix} \begin{pmatrix} F_x \\ F_y \end{pmatrix}, \tag{4.1}$$

where F_x and F_y are equal and opposite to the reactions of the host structure, which can

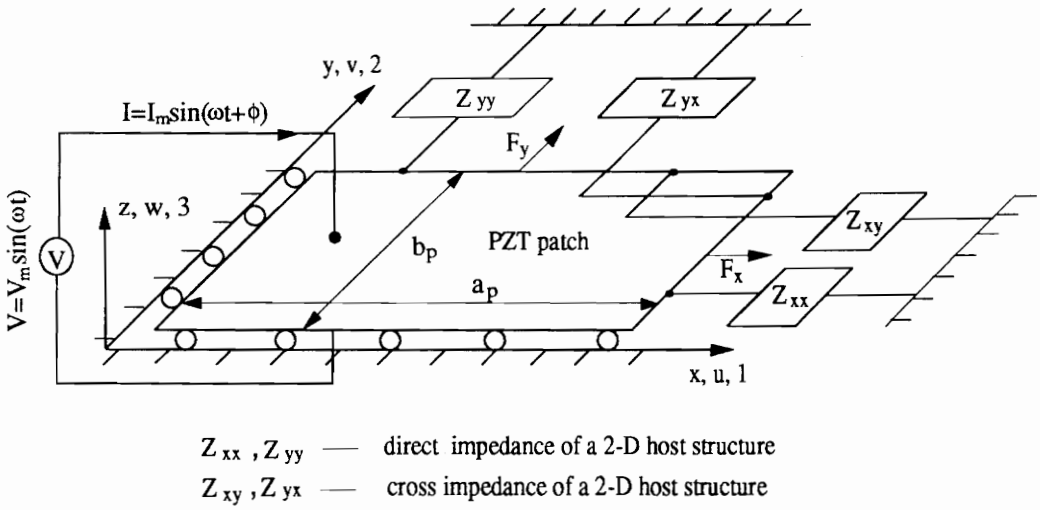

Figure 4.1: Schematic representation of a coupled electro-mechanical system model of an integrated PZT/substrate system.

be described in terms of the mechanical impedance of the host structure:

$$\begin{pmatrix} F_x \\ F_y \end{pmatrix} = -\begin{pmatrix} Z_{xx} & Z_{xy} \\ Z_{yx} & Z_{yy} \end{pmatrix}\begin{pmatrix} \dot{u} \\ \dot{v} \end{pmatrix}. \tag{4.2}$$

Eq. (4.1) is thus rewritten as:

$$\begin{pmatrix} \sigma_x \\ \sigma_y \end{pmatrix} = -\begin{pmatrix} 1/(b_p h_p) & 0 \\ 0 & 1/(a_p h_p) \end{pmatrix}\begin{pmatrix} Z_{xx} & Z_{xy} \\ Z_{yx} & Z_{yy} \end{pmatrix}\begin{pmatrix} \dot{u} \\ \dot{v} \end{pmatrix}, \tag{4.3}$$

The velocity response in Eq. (4.3) may be described by:

$$\dot{u} = j\omega\left[A\sin(k_{p11}x) + B\cos(k_{p11}x)\right]e^{j\omega t} \tag{4.4a}$$

$$\dot{v} = j\omega\left[C\sin(k_{p22}y) + D\cos(k_{p22}y)\right]e^{j\omega t}, \tag{4.4b}$$

where A, B, C, and D are unknowns and can be determined by the boundary conditions and the constitutive equation of the PZT material. The detailed derivation for determination of A, B, C, and D can be found in Chapter 3 (Sec. 3.2), and the results are directly given here:

$$\begin{pmatrix} A \\ C \end{pmatrix} = \begin{pmatrix} k_p\cos(k_p a_p)(1-\nu_p\frac{b_p}{a_p}\frac{Z_{xy}}{Z_{pxx}}+\frac{Z_{xx}}{Z_{pxx}}) & k_p\cos(k_p b_p)(\frac{a_p}{b_p}\frac{Z_{yx}}{Z_{pyy}}-\nu_p\frac{Z_{yy}}{Z_{pyy}}) \\ k_p\cos(k_p a_p)(\frac{b_p}{a_p}\frac{Z_{xy}}{Z_{pxx}}-\nu_p\frac{Z_{xx}}{Z_{pxx}}) & k_p\cos(k_p b_p)(1-\nu_p\frac{a_p}{b_p}\frac{Z_{yx}}{Z_{pyy}}+\frac{Z_{yy}}{Z_{pyy}}) \end{pmatrix}^{-1}\begin{pmatrix} d_{31} \\ d_{32} \end{pmatrix}E = M^{-1}\begin{pmatrix} d_{31} \\ d_{32} \end{pmatrix}E \tag{4.5}$$

and $B = D = 0$,

where Z_{pxx} and Z_{pyy} are the input mechanical impedance of the PZT actuator, as expressed in Eq. (3.9) in Chapter 3.

Substituting Eqs. (4.5) and (4.4) into Eq. (4.3), the dynamic stress output of the PZT actuator can be determined by:

$$\begin{pmatrix}\sigma_x\\ \sigma_y\end{pmatrix}=\frac{Y_p^* E}{1-\nu_p^2}\begin{pmatrix}1 & \nu_p\\ \nu_p & 1\end{pmatrix}\left[k_p\begin{pmatrix}\cos(k_p x) & 0\\ 0 & \cos(k_p y)\end{pmatrix}[M]^{-1}\begin{pmatrix}d_{31}\\ d_{32}\end{pmatrix}-\begin{pmatrix}d_{31}\\ d_{32}\end{pmatrix}\right]. \tag{4.6}$$

The constitutive equation of the PZT material is again revoked in terms of the electrical displacement field, D_3, in the z (3) direction:

$$D_3=\varepsilon_{33}^* E+d_{31}\sigma_x+d_{32}\sigma_y\ , \tag{4.7}$$

where

$$\varepsilon_{33}^*=\varepsilon_{33}(1-j\delta_p)\ , \tag{4.8}$$

is the complex dielectric constant at a zero stress. Substituting Eq. (4.6) into Eq. (4.7) and letting $d_{32}=d_{31}$ yields the electrical displacement field:

$$D_3=E\left\{\varepsilon_{33}^*+\frac{d_{31}^2 Y_p^*}{1-\nu_p}\left(k_p\left[\cos(k_p x)\ \ \cos(k_p y)\right][M]^{-1}\begin{pmatrix}1\\ 1\end{pmatrix}-2\right)\right\}, \tag{4.9}$$

where the applied electric field E can be expressed in terms of the applied voltage V:

$$E=\frac{V}{h_p}=\frac{V_0}{h_p}e^{j\omega t}\ . \tag{4.10}$$

The charge in the PZT patch can be obtained by integrating the displacement in Eq. (4.9) with respect to the area:

$$q=\int_0^{a_p}\int_0^{b_p} D_3\,dx\,dy\ . \tag{4.11}$$

The current is thus given by differentiating Eq. (11) with respect to time:

$$\begin{aligned} I &= I_0 e^{j\omega t}=\dot{q} \\ &= jV_0\omega\frac{a_p b_p}{h_p}\left\{\varepsilon_{33}^{*}-\frac{2d_{31}^2 Y_p^{*}}{1-\nu_p}+\frac{d_{31}^2 Y_p^{*}}{1-\nu_p}\left[\frac{\sin(k_p a_p)}{a_p}\quad\frac{\sin(k_p b_p)}{b_p}\right][M]^{-1}\begin{pmatrix}1\\1\end{pmatrix}\right\}e^{j\omega t}. \end{aligned} \tag{4.12}$$

When the PZT actuator is driven by an active voltage V, the current in the circuit, I, is related to the driven voltage through the coupled electro-mechanical admittance, $A^{*}=I/V$. Accordingly, rewriting Eq. (4.12) produces the coupled electro-mechanical admittance of the integrated PZT/substrate system:

$$A^{*}=j\omega\frac{a_p b_p}{h_p}\left\{\varepsilon_{33}^{*}-\frac{2d_{31}^2 Y_p^{*}}{1-\nu_p}+\frac{d_{31}^2 Y_p^{*}}{1-\nu_p}\left[\frac{\sin(k_p a_p)}{a_p}\quad\frac{\sin(k_p b_p)}{b_p}\right][M]^{-1}\begin{pmatrix}1\\1\end{pmatrix}\right\}. \tag{4.13}$$

It is noted that the admittance, A^{*}, represents the integrated electro-mechanical characteristics of a piezoelectric actuator-driven system, and it is frequency dependent. Apparently, the complex admittance, A^{*}, contains all of the parameters concerning the system electro-dynamics performance, including mass, stiffness, damping, material and physical properties, electrical parameters, and boundary conditions. Once these parameters are selected, the admittance will be determined and the power consumption of the system can be predicted. The input structural impedance of the PZT actuator is given by Eq. (3.9) in Chapter 3. The mechanical impedance matrix of the host structure

in Eq. (4.5) is determined by:

$$\mathbf{Z} = \begin{pmatrix} Z_{xx} & Z_{xy} \\ Z_{yx} & Z_{yy} \end{pmatrix} = \begin{pmatrix} Q_{xx} & Q_{yx} \\ Q_{xy} & Q_{yy} \end{pmatrix}^{-1}, \tag{4.14}$$

where Q_{xx} and Q_{yy} are the direct mechanical admittance of the host structure at the edge of the PZT patches, and Q_{xy} and Q_{yx} are the cross mechanical admittance. The structural impedance matrix can usually be developed from classic theory of elasticity. For example, under the actuation of the distributed moments, the analytical solution of the mechanical admittance matrix of a simply-supported plate at the mid-point of the edge of the PZT patch can be derived from plate theory, which was done at Chapter 3 [Eqs. (30)-(33)]. For complex structures, the mechanical impedance of host structures can be determined from either experiments or finite element analysis.

So far, the assumption made in the derivation is that the system is linear and the host structure is a generic two-dimensional structure. The formulation, Eq. (4.13), is a generic solution for coupled admittance of a integrated PZT/Substrate system and can be applied to general two-dimensional structures.

4.3 System Power Consumption and Energy Conversion Efficiency

Since a PZT actuator acts as a plate capacitor, when a voltage, $V=V_0e^{j\omega t}$, is applied to it to activate a host structure, the current in the circuit is expressed by:

$$I = I_0 e^{j(\omega t + \phi)} \ , \tag{4.15}$$

where ϕ is the phase between the current and voltage. The electrical power supplied to the PZT actuator is actually decomposed into two components: one is the real power,

$$P = \frac{I_0 V_0}{2} \cos\phi = \frac{V_0^2}{2} Re(A^*) \ , \tag{4.16}$$

where $cos\phi$ is called the power factor of the electrical system (Carlson and Gisser, 1990). The other is the reactive power,

$$R = \frac{I_0 V_0}{2} \sin\phi = \frac{V_0^2}{2} Im(A^*) \ . \tag{4.17}$$

Physically, the real power is the electrical power supplied to the PZT actuator and converted into mechanical power to drive the host structure. The reactive power is the power circulating between the electrical power source and the integrated PZT/substrate system. The total power may be expressed as:

$$W^* = P + jR \ . \tag{4.18}$$

The magnitude of the complex power is defined as the apparent power:

$$W_0 = \sqrt{P^2 + R^2} = \frac{I_0 V_0}{2} = \frac{V_0^2}{2} A_0 \ , \tag{4.19}$$

where A_0 is the magnitude of the admittance A^*. The apparent power reflects the power requirement of the system. The emphasis of the current work is on the analysis of the dissipative power consumption of a PZT actuator-driven structure. When power supplies

are considered in the system modeling, the reactive power in the system will exert an important influence on the power requirement. In that case, a large reactive power is usually expected as a high current demand is required from the power supply. In addition, the dissipative power consumed in the power supply itself should also be considered in the power requirement for the integrated system as a whole. Future work will include the electronics of power supplies in order to determine the overall power requirement.

Substituting Eq. (4.19) into Eq. (4.16), the power factor is rewritten as:

$$\cos\phi = FP = \frac{Re(A^*)}{A_0} = \frac{P}{W_0} \quad . \tag{4.20}$$

The power factor, FP, is thus defined as the ratio of the dissipative power to the apparent power and represents the energy conversion efficiency of the system. It is noticed that the dissipative power consumption, the power requirement, and the energy conversion efficiency of the system, are strongly related to the coupled electro-mechanical admittance, A^*.

The dissipative (real) power in an integrated PZT/substrate system includes three parts:

(1) the power dissipated by the structural damping of the host structure, which is related to the structural loss factor η in the complex Young's modulus.

This power is proportional to the mechanical vibration power of the host structure;

(2) the power consumed by the structural damping of the PZT actuator, which is associated with the mechanical loss factor η_p of the PZT actuator.

(3) the power consumption caused by the dielectric loss of the PZT actuator, which is related to the dielectric loss factor δ_p in the complex dielectric constant.

The consumed power is eventually converted into internal heat in the system, resulting in actuator temperature rise and possible thermal damage in the PZT actuator. These issues will be addressed in Chapter 6. The first two parts of the system power consumption mentioned above are directly used in driving the host structure. They may be considered to represent the total mechanical power dissipation in the system. An actuator power factor, PF_a, suggested by Liang et al. (1993a), is defined as:

$$PF_a = \frac{dissipative\ mechanical\ power}{apparent\ power} = \frac{Re(A_a^*)}{|A_a^*|}, \tag{4.21}$$

in which A^*_a is calculated by assuming the dielectric loss factor (δ_p) to be zero in Eq. (4.13). Apparently, the difference between the system power factor [Eq. (4.20)] and the actuator power factor [Eq. (4.21)] is that the former includes the dielectric power consumption of the PZT actuator in the dissipative power consumption. When the power factor is experimentally determined, the system power factor should be used because the

dielectric loss of the PZT actuator is usually not zero in a real system. In this chapter, the system power factor is used in the following numerical examples. A comparison between the system power factor and the actuator power factor will also be performed.

4.4 Parametric Studies and Discussion

A parametric study is conducted in this section to quantitatively examine how the dissipative power is consumed by the different components in the system and how much power is required to drive the system. The influence of the thickness and the location of the PZT actuator is also discussed.

A thin plate made of aluminum is used in the numerical example. The PZT material is G1195. It is assumed that the geometric configuration of the integrated PZT/plate system in the current case studies is sam as that used in Chapter 3 such that the analysis in this chapter can directly use the previous results. The basic electrical properties of the PZT material is listed in Table 4.1 and the corresponding mechanical properties are given in Table 2.1. The geometric parameters of the integrated are shown in Fig. 3.1 and Table 3.1. The magnitude of the voltage applied to the PZT actuator is assumed to be 20 volt.

Figure 4.2 illustrates the constitution and distribution of the dissipative (real) power in the frequency domain. The solid line represents the total dissipative power. The dashed line

Table 4.1: Electric Parameters of the Piezoelectric Material

piezoelectric constants d_{31},d_{32} (m/volt)	dielectric constant ε_{33} (Farads/m)	dielectric loss factor δ_p
-1.66×10^{-10}	1.5×10^{-8}	0.015

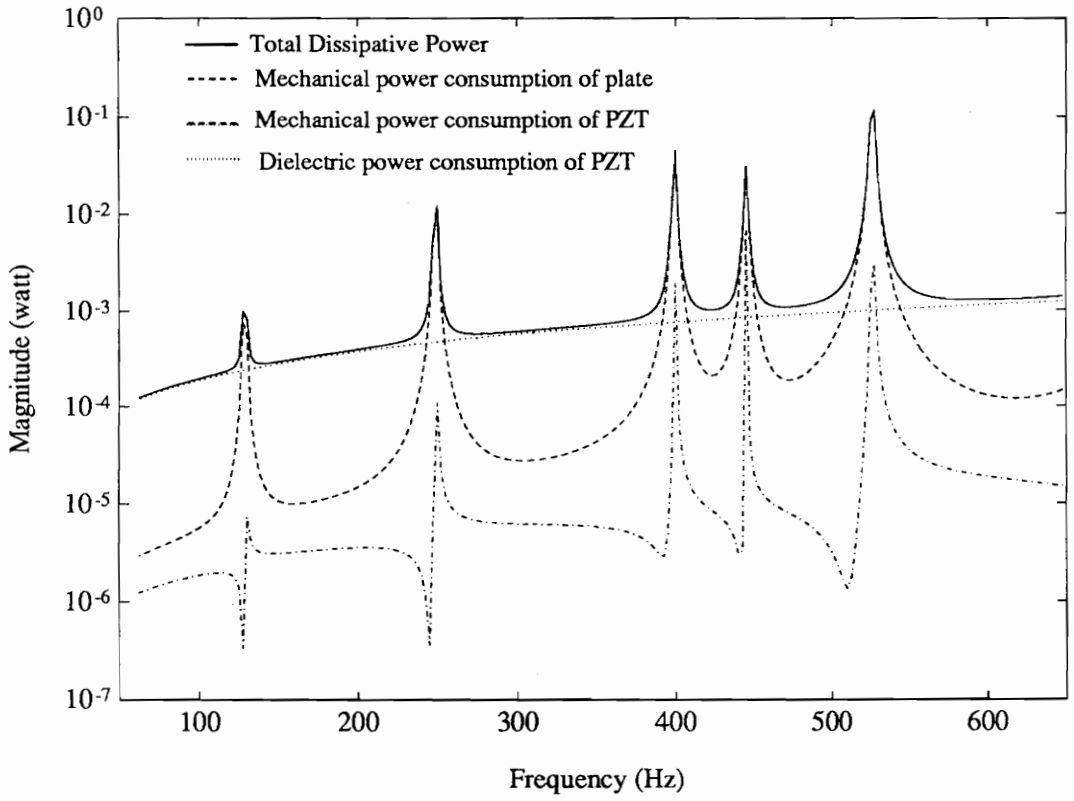

Figure 4.2: The components of the dissipative power of an integrated PZT/substrate system.

is the power consumption only due to the mechanical loss of the plate, obtained from Eqs. (4.13) and (4.16) assuming $\delta_p=\eta_p=0$. The dash-dotted line is the power consumption only from the mechanical loss of the PZT actuator, found by setting $\delta_p=\eta=0$ in Eqs. (4.13) and (4.16). The dotted line is the power consumed only by the dielectric loss of the PZT actuator, found by assuming $\eta=\eta_p=0$ in Eqs. (4.13) and (4.16). It is clearly seen in Fig. 4.2 that at the resonant frequencies, the dissipative power is primarily consumed by the structural damping of the plate, while at off-resonance, it is significantly affected by the dielectric loss of the PZT itself. The mechanical damping of the PZT, however, has a slight influence on the real power consumption because of its small size.

Figure 4.3 shows the characteristics of apparent power of the system. The peak power appears at the 5th mode in the arrange of less than 650 Hz and it can be used to estimate the power requirement of the system. Obviously, the power consumption significantly goes up when the excitation frequency increases. Once the interesting frequency band is determined, the power requirement of the system can be numerically predicted.

Figure 4.4 demonstrates the difference of the power factor predicted from Eq. (4.20) and Eq. (4.21), respectively. At resonant frequencies, the power factor is maximized because of the minimum resistance to the structural vibration. Both the system power factor and the actuator power factor gives the same prediction. At off-resonance, however, the actuator power factor is much smaller than the system power factor. The reason is that

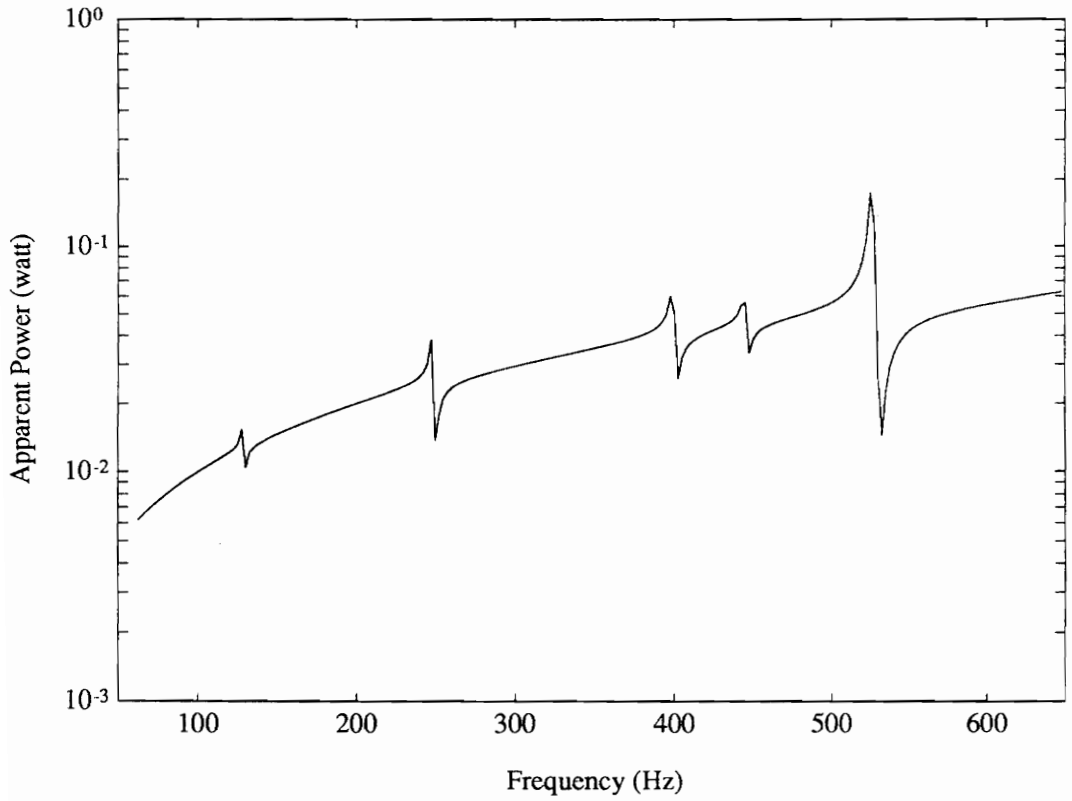

Figure 4.3: Apparent power of an integrated PZT/plate system.

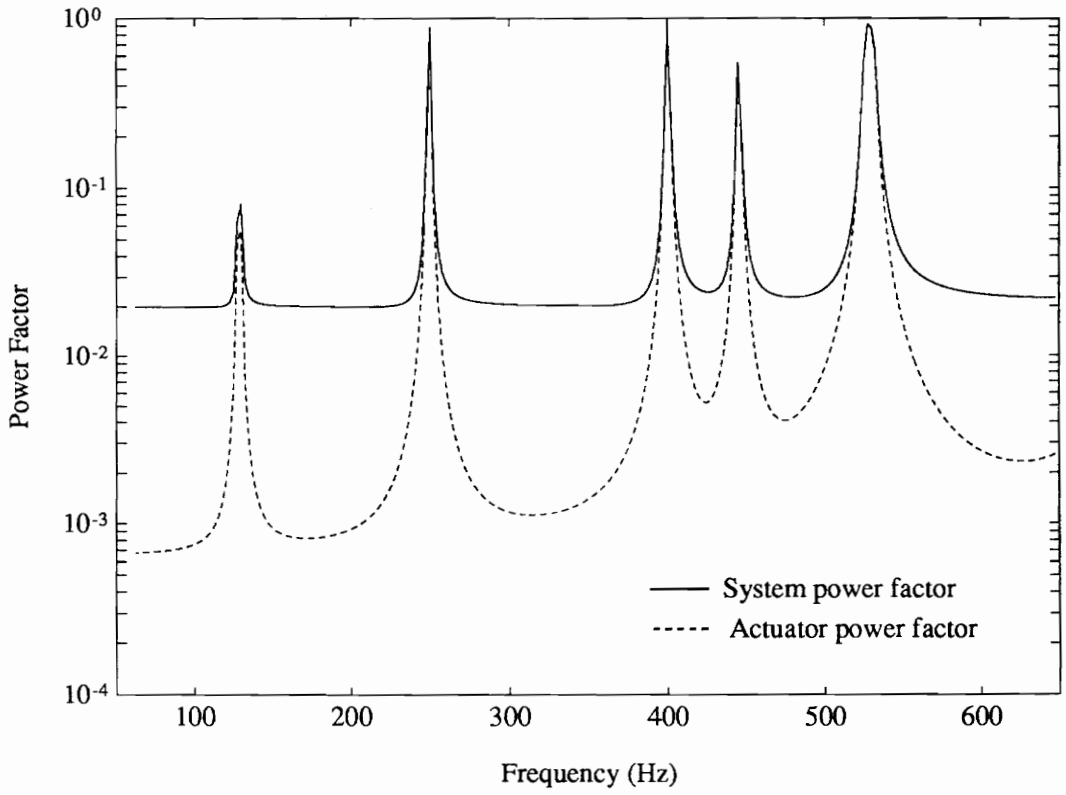

Figure 4.4: Comparison of the system power factor and the actuator power factor.

the dissipative power is dominated by the dielectric loss behavior of the PZT actuator at off-resonance. Assuming a zero dielectric loss gives a very low power consumption, resulting in a low actuator power factor.

When the damping value in the system changes, the basic relations of the power consumption as shown in Fig. 4.2 are still applicable. Figure 4.5 illustrates that if the loss factor of the plate increases from 0.001 to 0.005, the dissipative power goes up at resonant frequencies and increases slightly at off-resonance. In contrast, if the dielectric loss factor of the PZT actuator doubles from the 0.015 to 0.03, the dissipative power and the power factor increase by about 50% at off-resonant frequencies and remain the same at the resonant frequencies, as displayed in Fig. 4.6.

The geometric parameters of the PZT actuator, such as the thickness and location, have significant influence on the dissipative power and the power factor because the mechanical impedance of the system strongly varies with these geometric parameters. Under the assumption of the constant magnitude of the applied voltage (v_0=20 volt), when the thickness of the PZT patch increases from 0.19 mm to 2 × 0.19 mm and 4 x 0.19 mm, the real power consumption decreases on the whole frequency band, as displayed in Fig. 4.7. The power factor also decreases at off-resonance. However, the power factor has a complicated variation at the resonant frequencies. This observation indicates that when the thickness of the PZT actuator varies, the maximum power factor

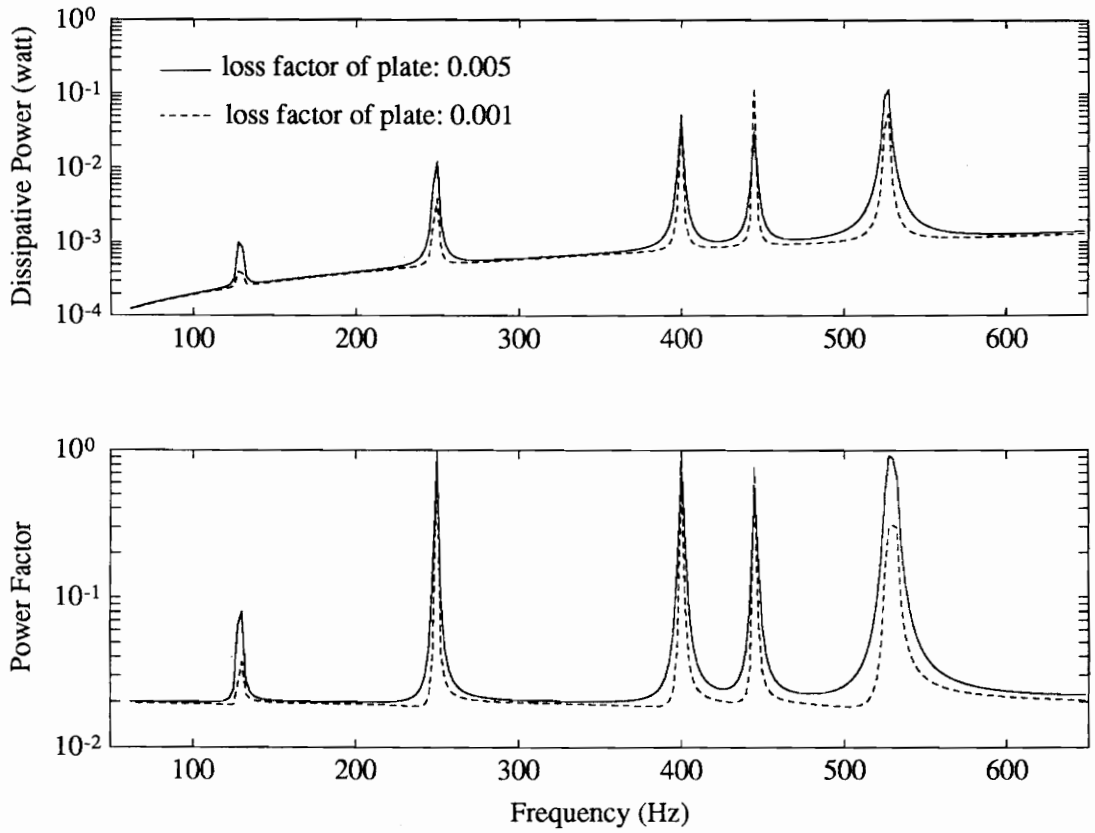

Figure 4.5: Influence of the loss factor of the plate on the dissipative power and power factor of an integrated PZT/plate system.

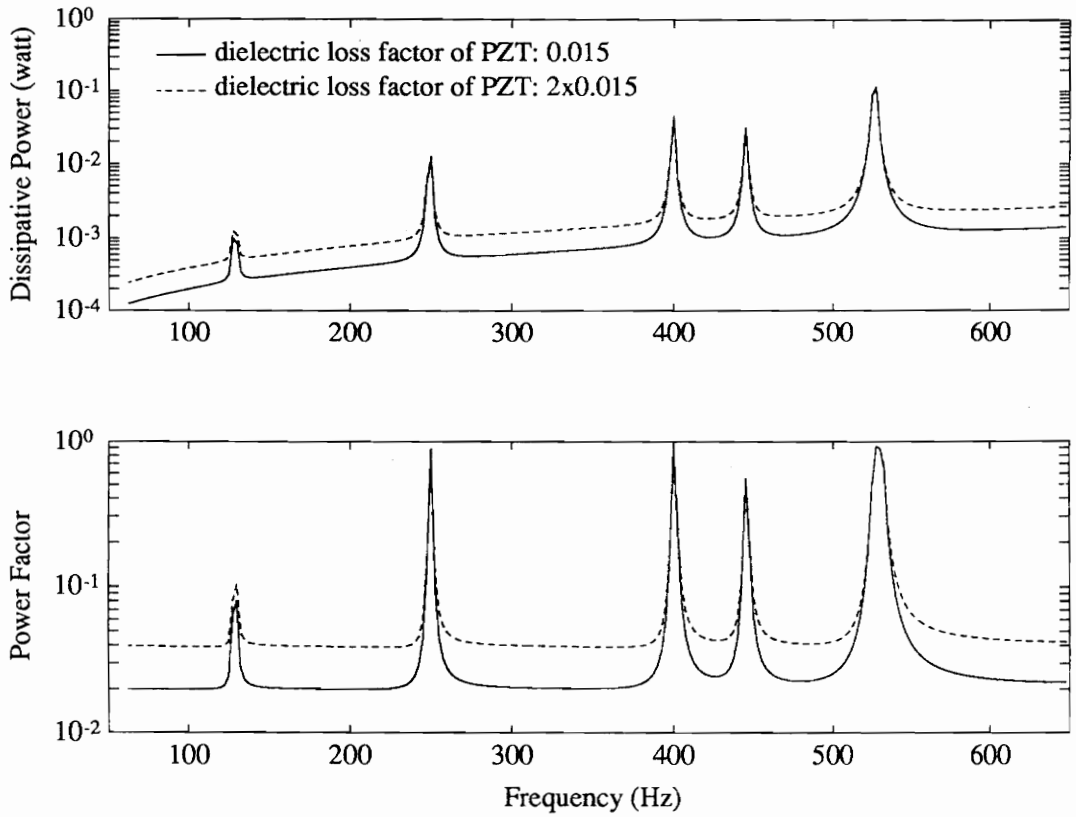

Figure 4.6: Influence of the dielectric loss factor of the PZT actuator on the dissipative power and power factor of an integrated PZT/plate system.

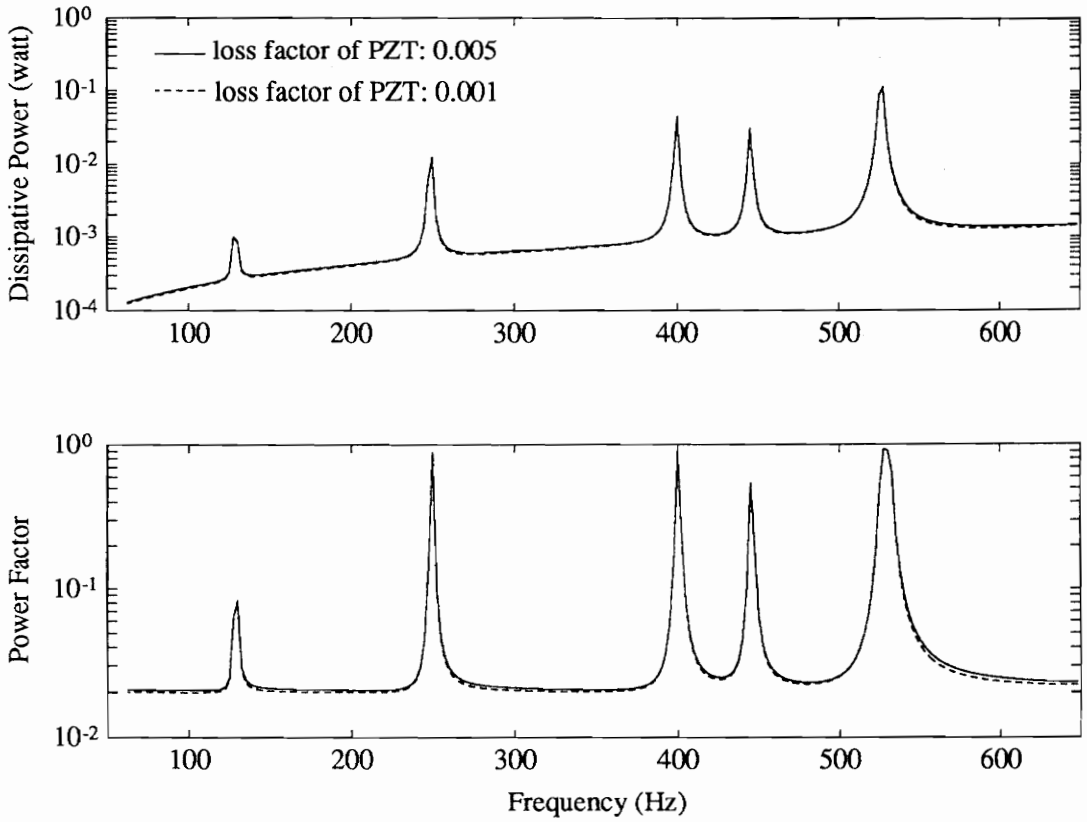

Figure 4.7: Influence of the thickness of the PZT actuator on the dissipative power and power factor of an integrated PZT/plate system.

will depend on the individual mode. Another important observation in Fig. 4.7 is that the resonant frequencies of the system apparently shift to higher values when the thickness of the PZT actuator increases. It can be explained that the added PZT patches stiffen the original plate and shift the resonant frequencies to the high values.

Figure 4.8 shows that when the location of the PZT actuator on the structure varies, the mechanical impedance changes and so does the power consumption of the system. Note that when the center of the PZT actuator locates at the node line position in the x direction (location #2), the corresponding modes, i.e., the 2nd and the 5th modes, are tailored off since little mechanical vibration energy is supplied to these vibrational modes.

4.5 Experimental Verification

A simply-supported thin plate integrated with surface-bonded PZT patches was built and tested to validate the coupled electro-mechanical impedance model. The size and physical properties of the plate and the PZT material are the same as those used in the numerical calculation in the previous section, as listed in Tables 3.1 and 4.1. An HP 4194A Impedance/Gain-Phase Analyzer was used to directly measure the coupled electro-mechanical admittance of the piezoelectric actuator-driven plate. Then, a comparison between the theoretical model and the experimental results was performed.

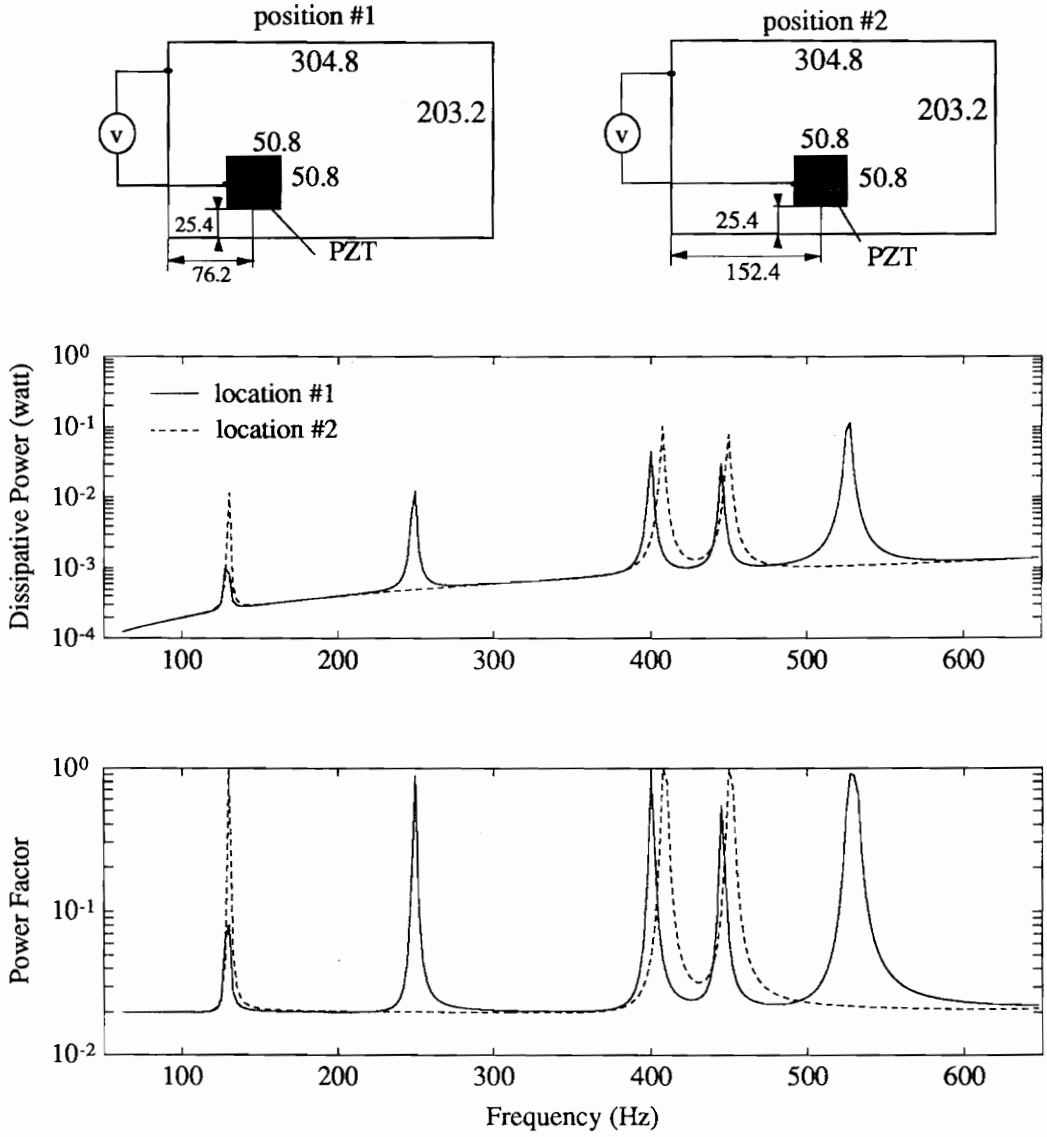

Figure 4.8: Influence of the location of the PZT actuator on the dissipative power and power factor of an integrated PZT/plate system.

Figure 4.9 illustrates the measured and predicted complex admittance of the system in terms of the real part and the imaginary part, respectively. The first eight modes are excited. The corresponding power factor, calculated from the experimental data using Eq. (4.20), is displayed in Fig. 4.10. In both figures, the theoretical prediction based upon the complex impedance model (dashed line) agrees well with the experimental data (solid line). The coupled electro-mechanical impedance model has provided a reasonably accurate prediction of the power consumption and the energy conversion efficiency of the integrated PZT/Plate system. It should be noted that the maximum difference between the theoretical model and the experimental results appears at the 5th mode, i.e., (2,2) mode. It may be explained that when the geometric center of the PZT actuator locates on the anti-node position of the host plate (x=76.2 mm, y=50.8 mm), the excitation of that mode is maximized. The inertial effect caused by the added mass loading of the PZT patch is then intensified. The measured resonant frequency and the response of this mode [the 5th mode (2,2)] are thus smaller than those predicted by the theoretical model.

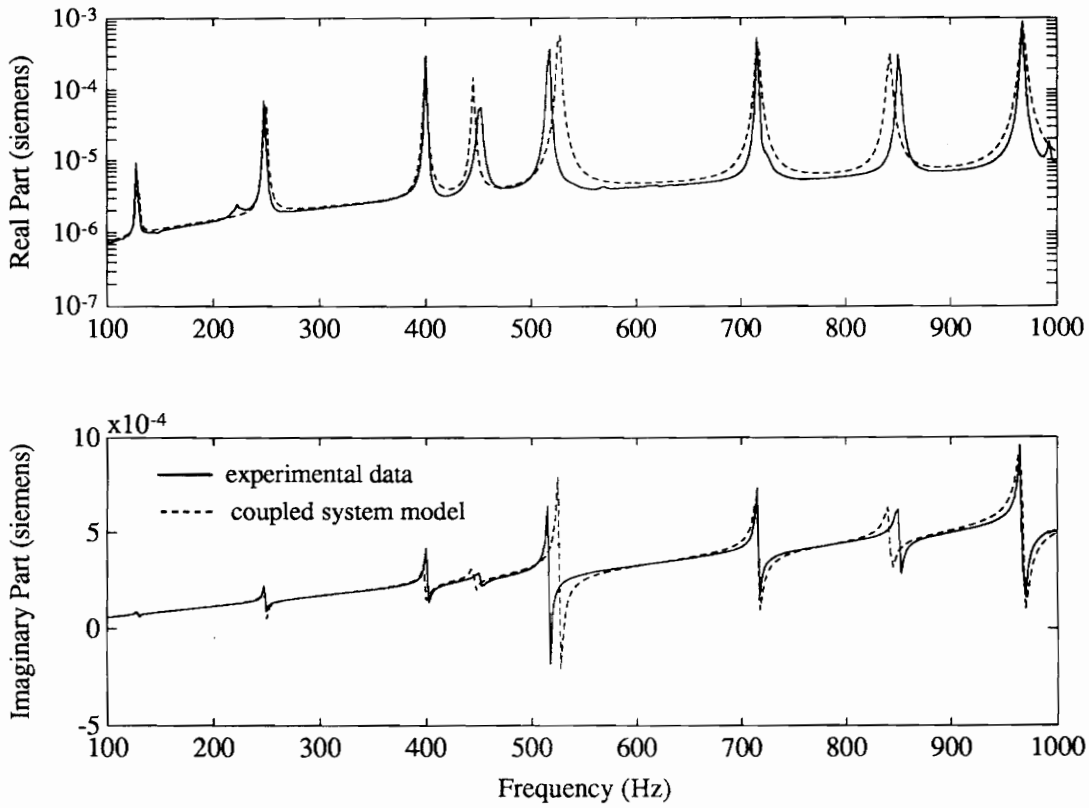

Figure 4.9: The measured and predicted complex electro-mechanical admittance of an integrated PZT/plate system.

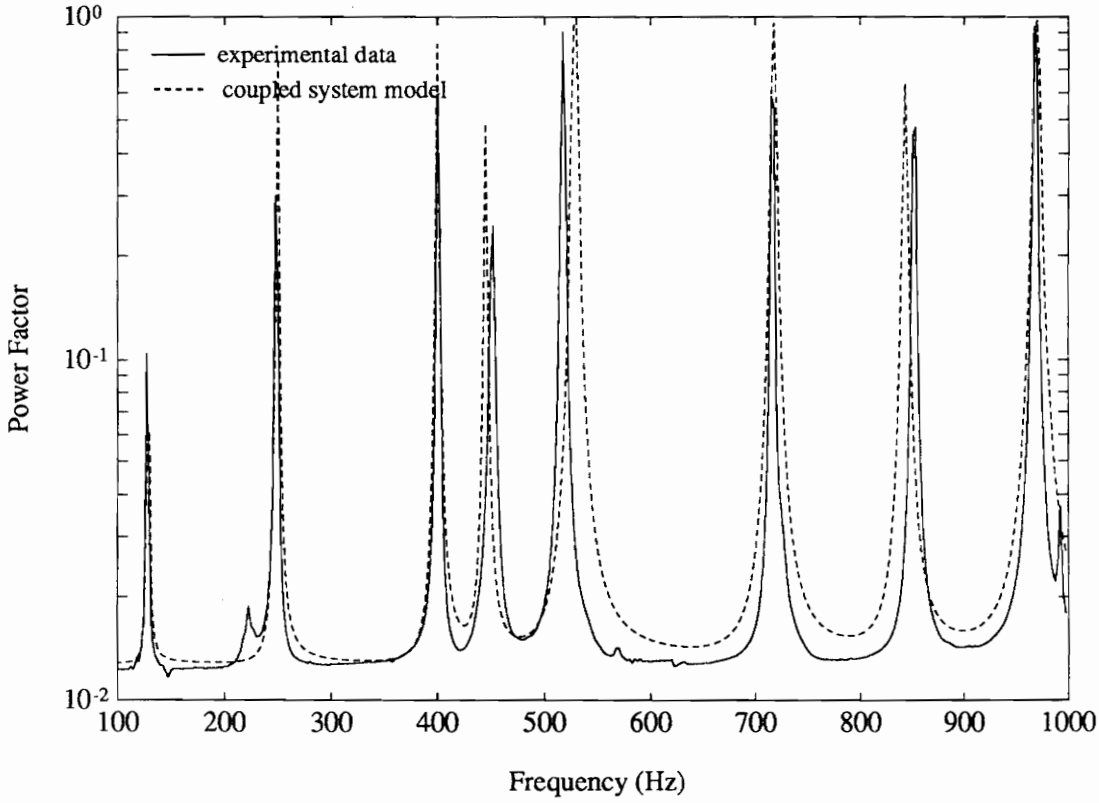

Figure 4.10: The measured and predicted power factor of the integrated PZT/plate system.

4.6 Concluding Remarks

- A coupled electro-mechanical impedance model for a generic two-dimensional piezoelectric actuator-driven structure has been developed to analyze the power flow and its components in active structures, and to predict the power requirement and the energy conversion efficiency of the system. This modeling approach is helpful in designing energy-efficient intelligent structures.

- The parametric study has demonstrated that the dissipative power supplied to the PZT actuator is primarily consumed by the mechanical damping of the host structure at the resonant frequencies and is dissipated by the dielectric loss of the PZT itself at the off-resonance.

- The thickness and location of the PZT actuator have an impact on the dissipative power consumption and the energy efficiency of integrated system because these geometric parameters may cause significant changes in the mechanical impedance of systems.

4.7 References

Carlson, A. B. and D. G. Gisser, 1990, Electrical Engineering: Concepts and applications, Addison-Wesley, California.

Ikeda, T., 1990, Fundamentals of Piezoelectricity, Oxford University Press, New York.

Lomenzo, R. A., H. Sumali, and H. H. Cudney, 1993, "Maximizing Mechanical Power Transfer from Piezoelectric Stacked Actuators to Structures", Proceeding of the Adaptive Structures and Material Systems, ASME, New Orleans; pp. 229-235.

Liang, C., F. P. Sun, and C. A. Rogers, 1993a, " Coupled Electro-Mechanical Analysis of Piezoelectric Ceramic Actuator-Driven Systems—Determination of the Actuator Power Consumption and System Energy Transfer", Proceedings of Smart Structures and Materials '93, SPIE, Albuquerque, NM; pp.229-235.

Niezrecki, C., and Cudney, H., 1993, "Power Factor Correction Method Applied to Piezoelectric Actuators", Proceedings of Structures, Structural Dynamics and Materials Conference, La Jolla, CA; pp.3261-3268.

Rogers, C. A., 1993, Intelligent Material Systems: The Dawn of a New Materials Age", Journal of Intelligent Material Systems and Structures, Vol. 4, No. 1; pp. 4-12.

Stein, S. C., C. Liang, and C. A. Rogers, 1993, "Power Consumption of Piezoelectric Actuators in Underwater Active Structural Acoustic Control", The Second Conference on Recent Advances in Active Control of Sound and Vibration, Blacksburg, VA; pp. 189-203.

Wang, B. T., 1991, "Active Control of Sound Transmission/Radiation from Elastic Plates Using Multiple Piezoelectric Actuators", Ph.D. Dissertation, Department of Mechanical Engineering, Virginia Polytechnic Institute and State University, Blacksburg, VA.

Zhou, S. W., C. Liang, and C. A. Rogers, 1994, "A Coupled Electro-Mechanical Analysis to Predict Power Requirement and Energy Conversion of Piezoelectric Actuators Driven-Plate Like Structures", Proceedings of AIAA/ASME Adaptive Structures Forum, Hilton Head, SC; pp. 259-269

Zhou, S. W. and C. A. Rogers, 1994, "Power Flow and Consumption in Piezoelectrically-Actuated Structures", accepted for the publication in AIAA Journal, September, 1994.

Chapter 5

Dynamic Stress Characteristics and Design Issues of Integrated Piezoelectric Patch Actuators

5.1 Introduction

Distributed piezoelectric (PZT) actuators have been widely used in various applications. Compared with conventional "point" actuators (shakers, etc.), PZT patch actuators have demonstrated competitive characteristics, such as light weight, small size, and good dynamic output performance, and relatively simple experimental setup. When these actuators are used in scientific research and industrial processes, several basic and important issues are raised.

First, the actuation ability of such small and thin patch actuators must be primarily considered. The question is whether host structures can be sufficiently excited using these actuators. This issue involves the quantitative prediction of output performance of PZT actuators, such as displacement output, forces, or moments. As a matter of fact, the issue was noticed in the early development and implementation of PZT actuators. Several static strain (or stress)-based approaches were developed to determine static forces or moments (Bailey and Hubbard, 1985; Crawley and de Louis, 1987; Crawley and Lazarus, 1991; Dimitriadis et al., 1989; Wang and Rogers, 1990). However, the static approaches are limited to analyzing the static output behavior of the actuators. An approximate dynamic analysis using static models is not accurate because active forces provided by PZT actuators are usually alternate forces. The dynamic interaction between the host structures and the active elements always exists and affects the performance of both the structures and the actuators. An impedance-based system model developed in Chapters 2 and 3 provides a better understanding of the dynamic essence of PZT actuator-driven systems. The frequency-dependent force output behavior is accurately predicted in the impedance model.

Second, designers of engineering and space structures are concerned with how efficiently a PZT actuator, as a transducer, transforms electrical energy into mechanical energy. The reason is that minimizing power consumption and enhancing energy conversion efficiency can directly reduce the requirement for power supplies, resulting in a reduction in the cost

and mass of systems. In Chapter 4, a coupled electro-mechanical system analysis was presented to quantitatively determine the power consumption, power requirement, and the energy conversion efficiency for generic integrated PZT/Substrate systems. The influence of different dissipators on the system power factor and the system power requirement was discussed.

Third, PZT patch actuators are most often placed under a certain amount of alternate stress. The question is how to quantitatively predict the alternate stress so that a safety design can be effectively conducted. However, investigations done to date on this issue have been limited. As PZT actuators are induced strain actuators, intensive strain or stress is expected for the structural actuation, while piezoelectric materials may be degraded or broken under such a dynamic stress level. Especially, piezoelectric materials are brittle materials, and their tensile strength is much lower than the compressive strength. Hence, it is very important to estimate the dynamic stress level in design stage.

The focus of this chapter is on the investigation of mechanical dynamic stress characteristics and the corresponding design consideration of integrated PZT patch actuators. The important design parameters, such as actuator thickness and actuator location, will be discussed. Some recommendation on the design of PZT actuators will be addressed. A piezoelectric actuator-driven thin plate will be used in the parametric study. An experiment will be conducted on a simply-supported aluminum plate to validate the

theoretical model. A comparison will be made to demonstrate the significant difference between conventional static approaches and the impedance method in physical concept and numerical results.

5.2 Dynamic Stress Characteristics of Integrated PZT Patch Actuators

The dynamic stress, $\sigma_{x,(y)}$, can be derived from the impedance-based system model, which was developed in Chapters 3 and 4. The formulation is repeated here:

$$\begin{pmatrix}\sigma_x\\ \sigma_y\end{pmatrix}=\frac{Y_p^* V_m}{h_p(1-\nu_p^2)}\begin{pmatrix}1 & \nu_p\\ \nu_p & 1\end{pmatrix}\left[k_p\begin{pmatrix}\cos(k_p x_p) & 0\\ 0 & \cos(k_p y_p)\end{pmatrix}M^{-1}-I_{2x2}\right]\begin{pmatrix}d_{31}\\ d_{32}\end{pmatrix}e^{j\omega t}, \tag{5.1}$$

where the subscript p refers to the parameters of a PZT actuator; h_p is the thickness; V_m denotes the magnitude of applied voltage; ν_p is the Poisson's ratio; k_p is the wave number; Y_p^* is the complex Young's modulus at a constant electrical field: $Y_p^*=Y_p(1+j\eta_p)$; η_p is the structural loss factor; d_{31} and d_{32} are the piezoelectric constants; ω is the input angular frequency; x_p and y_p are the location coordinate of the stress point; I_{2x2} is a identical matrix; and M is the 2x2 matrix described by:

$$M=\begin{pmatrix}k_p\cos(k_p a_p)(1-\nu_p\frac{b_p}{a_p}\frac{Z_{xy}}{Z_{pxx}}+\frac{Z_{xx}}{Z_{pxx}}) & k_p\cos(k_p b_p)(\frac{a_p}{b_p}\frac{Z_{yx}}{Z_{pyy}}-\nu_p\frac{Z_{yy}}{Z_{pyy}})\\ k_p\cos(k_p a_p)(\frac{b_p}{a_p}\frac{Z_{xy}}{Z_{pxx}}-\nu_p\frac{Z_{xx}}{Z_{pxx}}) & k_p\cos(k_p b_p)(1-\nu_p\frac{a_p}{b_p}\frac{Z_{yx}}{Z_{pyy}}+\frac{Z_{yy}}{Z_{pyy}})\end{pmatrix}, \tag{5.2}$$

in which a_p and b_p are the length and width of the PZT actuator; Z_{pxx} and Z_{pyy} are the input impedance of the actuator itself; Z_{xx} and Z_{yy} are the direct impedance of the host structure;

Z_{xy} and Z_{yx} are the cross impedance of the host structure.

It can be clearly seen from Eq. (5.1) that the mechanical stress induced in the PZT actuator is a complex stress and alternate stress. The magnitude of the dynamic stress is a function of frequency, the mechanical impedance of the host structure, and the actuator input impedance. In addition, the induced stress varies along the location coordinate (x_p, y_p).

In the following discussion, a simply-supported aluminum thin plate is used. The size of the plate is *381 x 228.6 x 1.5 mm (15" x 9" x 0.06")*. Two PZT patches are bonded on the top and the bottom surface of the plate and located at x_1=*158.75 mm* and y_1=*80.55 mm* on the plate. Figure 5.1 shows the geometric configuration of the integrated PZT/plate system. The size of the PZT patch (SPI-5H) is *63.5 x 38.1 x 0.19 mm (2.5" x 1.5" x 0.0075")*. Table 2.1 lists the basic material properties of the PZT and the plate. A static model developed by Dimitriadis et al. (1989) is used here in comparison with the dynamic model. The formulation is expressed by (Dimitradis et al., 1989):

$$\sigma_x = \sigma_y = -\frac{1+\nu}{1-\nu_p}\frac{d_{31}Y_pV}{h_p[1+\nu-(1+\nu_p)\tau]}, \tag{5.3}$$

where

$$\tau = -\frac{Y_p}{Y}\frac{1-\nu^2}{1-\nu_p^2}\frac{6hh_p(h+h_p)}{h^3+8h_p^3+6hh_p^2}. \tag{5.4}$$

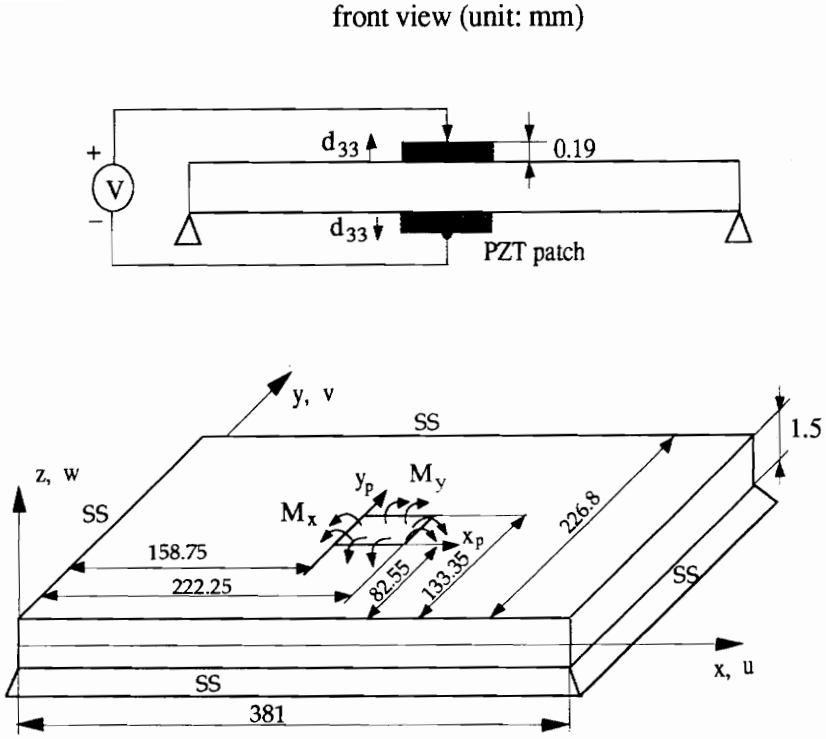

Figure 5.1: The geometric configuration of a simply-supported (ss) aluminum plate with surface-bonded PZT patch elements.

5.2.1 Frequency-Dependent Behavior

Figure 5.2 shows the frequency-dependent behavior of the PZT actuator. It is assumed that the stress is measured at the location: x_p=*3 mm* and y_p=*19 mm*. At the integrated system resonance, the dynamic stress is quite high and has a peak value, while at the off-resonance it is relatively low and looks like a constant. It is implied from this observation that the host structural dynamics applies a significant influence on the induced stress of the actuator. It can be explained that the structure has the minimum dynamic resistance at its resonance frequency, leading to the maximum actuator force output and peak stress. At the off-resonance of the integrated system, the performance of the host structure is dominated by its static behavior. Therefore, the conventional static model always predicts the induced stress as a constant stress in the frequency domain without considering the influence of structural dynamics. Obviously, when compared to the static approach, the impedance-based system model can give a more accurate prediction of the induced stress. When PZT actuators are operating at the off-resonance, the static model could be used as an approximation solution of the dynamic stress.

5.2.2 "Point" Stress Behavior

It is noted that the location coordinate, (x_p, y_p), exerts an influence on the stress distribution in Eq. (5.1), however, this influence depends on the ratio of the wavelength

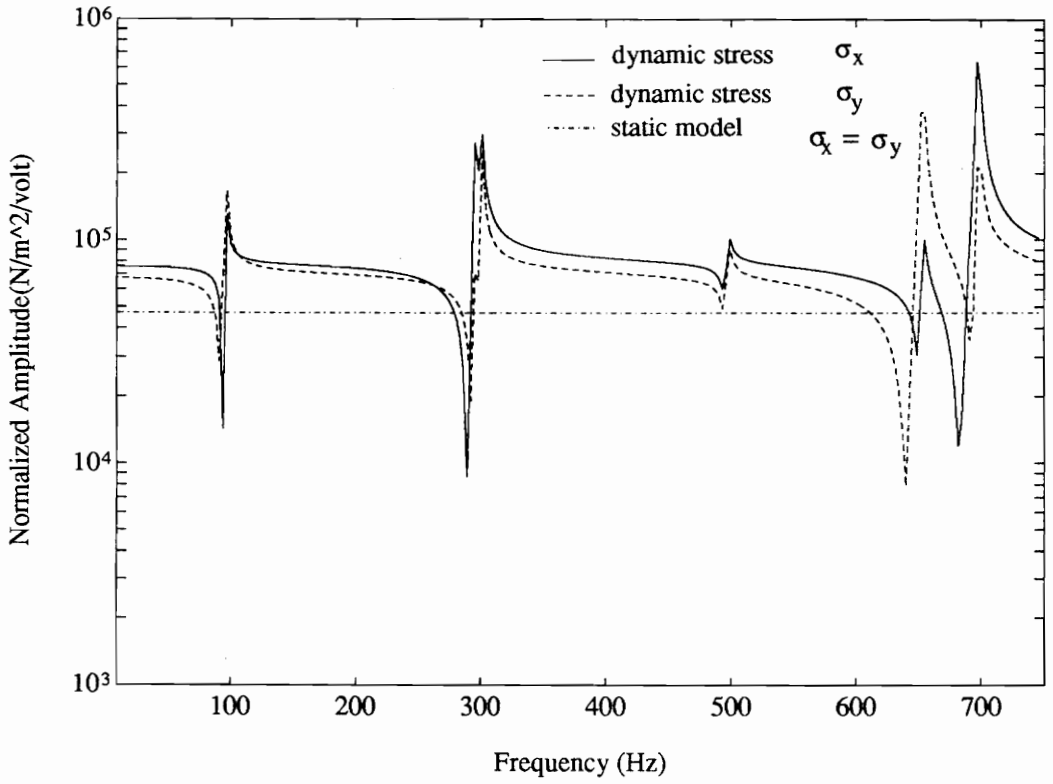

Figure 5.2: The induced mechanical stress characteristics of the PZT element, predicted by the static model and dynamic system model, respectively.

λ_p of the PZT patch to its maximum length. The wavelength, λ_p, is defined as:

$$\lambda_p = \frac{2\pi}{k_p} = \frac{1}{f}\left(\frac{Y_p}{\rho_p}\right)^{1/2} , \tag{5.5}$$

where f is the input frequency and ρ_p is the mass density of the PZT material. Usually, commercial segmented PZT actuators have a small size, for example, *38.1 x 63.5 mm (2.5"x1.5")*. If the excitation frequency is operated at 2,000 Hz, the ratio of the wavelength to the maximum length of the PZT patch is:

$$\beta = \frac{\lambda_p}{a_p} = 46 >> 1 . \tag{5.6}$$

In this case, the wavelength is much longer than the maximum size of the PZT patch. The coordinate (x_p, y_p) does not significantly influence the dynamic stress distribution on the PZT patch. It is assumed that the stress is measured at two different location points: x_{p1}=*25.4 mm*, y_{p1}=*25.4 mm*; and x_{p2}=*55.9 mm*, y_{p2}=*11.4 mm*. Figure 5.3 shows that the induced dynamic stress is almost same at the different locations of the stress points. The PZT actuator, thus, can be treated as a "point" stress source in this situation. At very high frequency, or in the case of a relatively large PZT patch, the ratio coefficient, β, approaches one. The dynamic strain or stress may significantly change along the coordinate location (x_p, y_p). The PZT patch then becomes a "line" or a "plane" stress source.

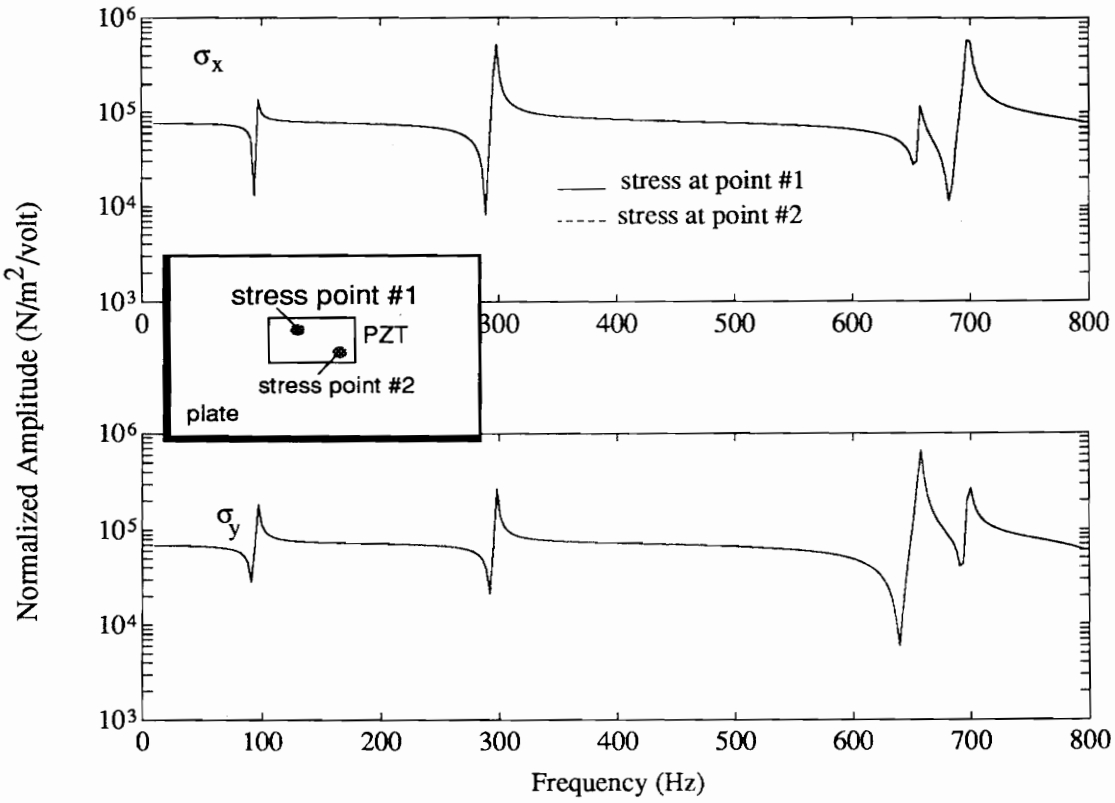

Figure 5.3: The induced mechanical stress of the PZT element is almost same at the different stress points, resulting in a "point" stress behavior.

5.2.3 Tensile Stress Strength

Since piezoelectric materials are brittle materials, the dynamic tensile strength is much lower than the static strength. Table 5.1 lists the strength of the typical piezoelectric material. The dynamic tensile strength is about only one-fourth of the static tensile strength, and the one-twenty fifth of the compressive strength. When piezoelectric materials are used as actuators, they are most commonly operated at broad band excitation frequency range. Thus, the dynamic stress should be limited to a value less than the dynamic tensile strength, $\sigma_{tensile}$:

$$Max.\,\sigma_{x,(y)} \leq \sigma_{tensile} \ , \tag{5.7}$$

where $Max.\sigma_{x(y)}$ is the maximum stress allowed in the safe design. Otherwise, there is a danger of degrading the performance. Figure 5.2 shows that the tensile stress is above $3x10^5$ (N/M^2/volt) at some resonant frequencies. When the plate is excited at the 2nd mode and a driving voltage of 100 volt is applied across each PZT patch, the mechanical stress level will exceed the tensile strength of the PZT material. The damage of PZT actuator will take place. In practice, the safety factor, SF, should be considered by:

$$Max.\,\sigma_{x(y)} = \frac{\sigma_{tensile}}{SF} \ . \tag{5.8}$$

It is worthy to point out that when other stress factors degrading the performance of PZT actuators are considered in the design procedure, the thermal stress should be included. The electrical energy, supplied to PZT actuators in driving host structures, is eventually

Table 5.1: Stress Strength of the PZT Material*

compressive strength (N/m^2)	tensile strength (N/m^2)	
	static	dynamic
5.2×10^8	6.3×10^7	2.1×10^7

*SPI-5A-S3 (Piezo Systems, Inc.)

transformed into internal heat in the PZT patches and structures. The dissipators in the system include structural damping loss and dielectric loss, which creates a distributed heat generation throughout the PZT patch and the host structure. The temperature increase in the integrated system is inevitable, resulting in thermal stress and possible thermal damage in the PZT actuators. In this case, a principal stress, σ_1, or equivalent Von Mises stress, σ_e, should be used in the safety design of the actuator:

$$Max.\sigma_{x(y)} = \frac{\sigma_{1(e)}}{SF} \quad . \tag{5.9}$$

The issues of temperature rise and thermal damage of PZT actuators will further be addressed in Chapter 6.

5.3 Important Design Parameters: Actuator Thickness and Location

When a piezoelectric patch, as an actuator, is considered in a design process, its geometric configuration integrated with a host structure should be first determined. The sandwich-type of integrated PZT/substrate systems has been widely used in intelligent structures. Once the geometry of an integrated PZT/substrate structure is selected, the formulations derived earlier can be directly utilized to quantitatively predict the performance of the PZT actuator. For different types of architectures of PZT actuator-driven structures, the mechanical impedance of the system is different and needs to be numerically or experimentally determined.

For structural actuation, the actuator outputs (forces or moments) are expected to be at a high level, however, as mentioned above, the induced stress is limited by the material strength. To conduct the safe design of PZT actuators, important design parameters, such as the actuator thickness and actuator location, should be carefully selected. One way to reduce the induced stress level is to limit the active voltage, while declination of the actuation force then results. The other way is to increase the thickness of a PZT patch as the voltage increases. Figure 5.4 displays that when the thickness of a PZT patch doubles from *0.19 mm* to *2x0.19 mm*, the overall moment output increases at most of frequency range (10—750 Hz). While Figure 5.5 shows that the dynamic stress decreases as the actuator thickness goes up. This observation indicates that increasing the thickness of PZT actuators can amplify the moment output for structural actuation, and at the same time, it can relieve the peak stress level in the PZT actuators. The relatively thick PZT actuators, therefore, are recommended in the actuator design.

In addition to the thickness, another important design parameter is the location of the PZT actuator. When the PZT actuator is placed in different locations on a host structure, as shown in Fig. 5.6, the mechanical impedance at the edge of the actuator changes, and so does the dynamic output performance of the actuator. Figure 5.7 clearly shows that the moment actuation is strongly related to the location of the PZT patch. When the center of the PZT patch is placed on the nodal lines of the host structure, the maximum moment output corresponding this mode cannot be achieved. For instance, when the center of the

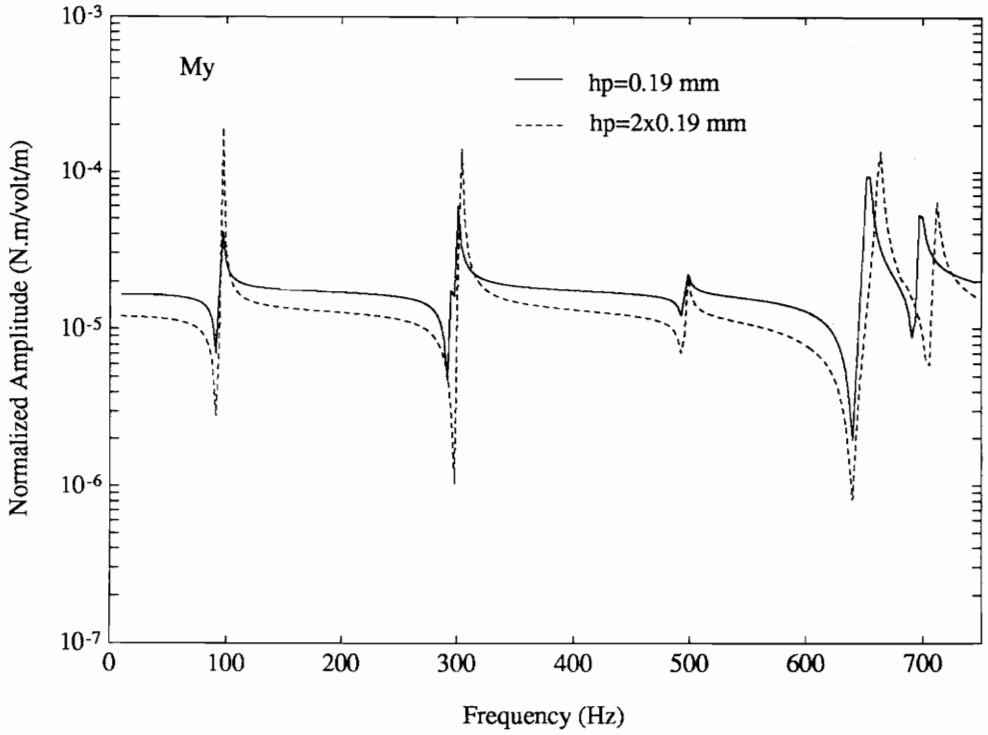

Figure 5.4: The moment output of the PZT actuator goes up as the actuator thickness increases.

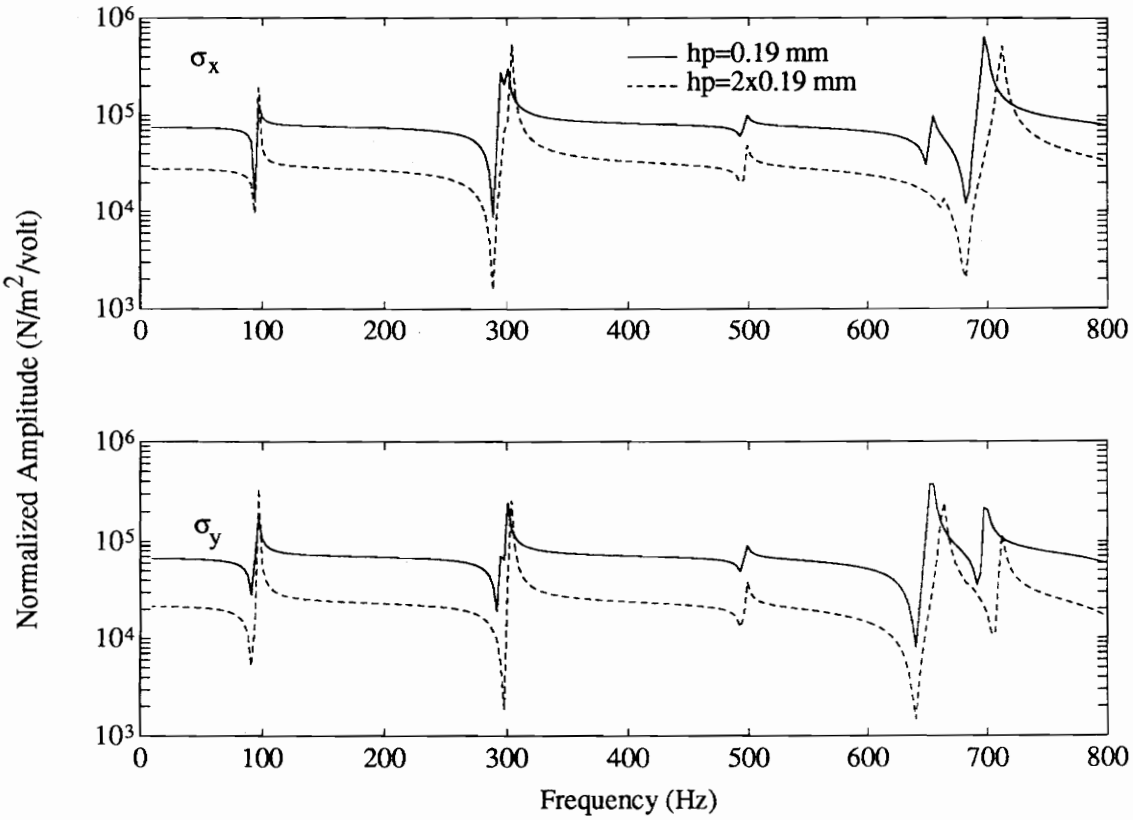

Figure 5.5: The induced dynamic stress of the PZT actuator decreases as the actuator thickness increases.

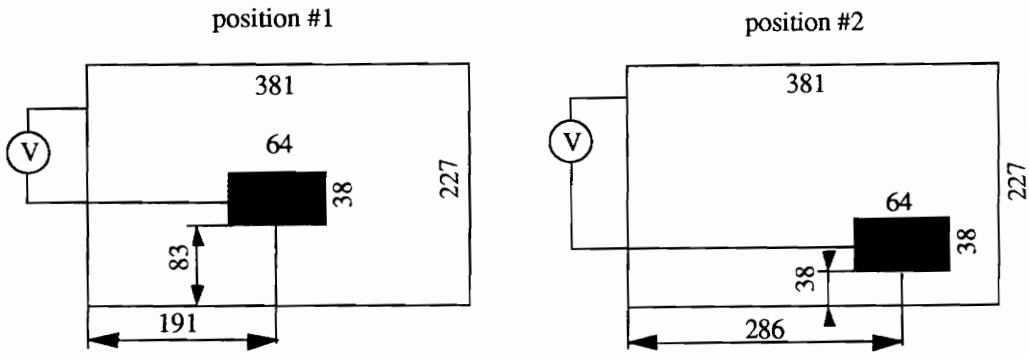

Figure 5.6: The geometric location coordinate of the PZT actuator on the plate.

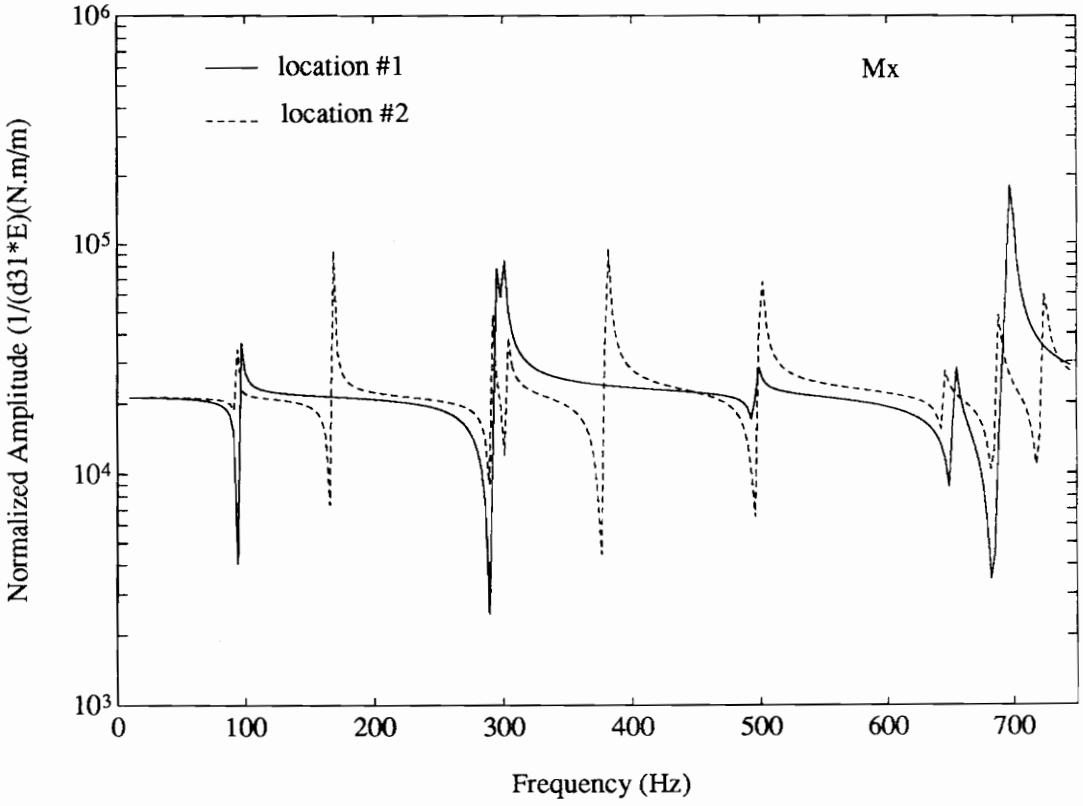

Figure 5.7: The variation of the location of the PZT actuator on the plate changes the actuator moment output (M_x).

PZT patch is on location #1, which is the center of the plate, the moment actuation on the 2nd mode (2,1) is limited, as illustrated in Fig. 5.7. This mode may be missed in the frequency response function. To actuate modes at a broad frequency band, the PZT actuator should be intentionally placed off the nodal lines of any interesting modes; otherwise, some of them may be lost in the response. The influence is similar for the dynamic stress, as shown in Fig. 5.8.

5.4 Experimental Verification

A simply-supported thin plate was built and tested to verify the design model. The experimental setup to excite the plate is illustrated in Fig. 5.9. The thin plate in the experiment is made of aluminum and the PZT material is G1195. The basic material properties are same as those listed in Table 2.1. The geometric size of the PZT patch is *50.8 x 50.8 x 0.19 mm*, and the size of the plate is *305 x 203 x 1.5 mm*.

A pseudo-random signal was used in a burst mode to activate the plate. The dynamic strain of the PZT actuator was directly measured using a strain gage. Two strain gages were placed on each surface of a PZT patches at right angeles to measure the induced strain in the x and y directions, respectively, as shown in Fig. 5.9. A half-bridge configuration was used to improve the ratio of the signal to the noise in the measurement. The coherence of the active voltage signal and the response voltage signal obtained from

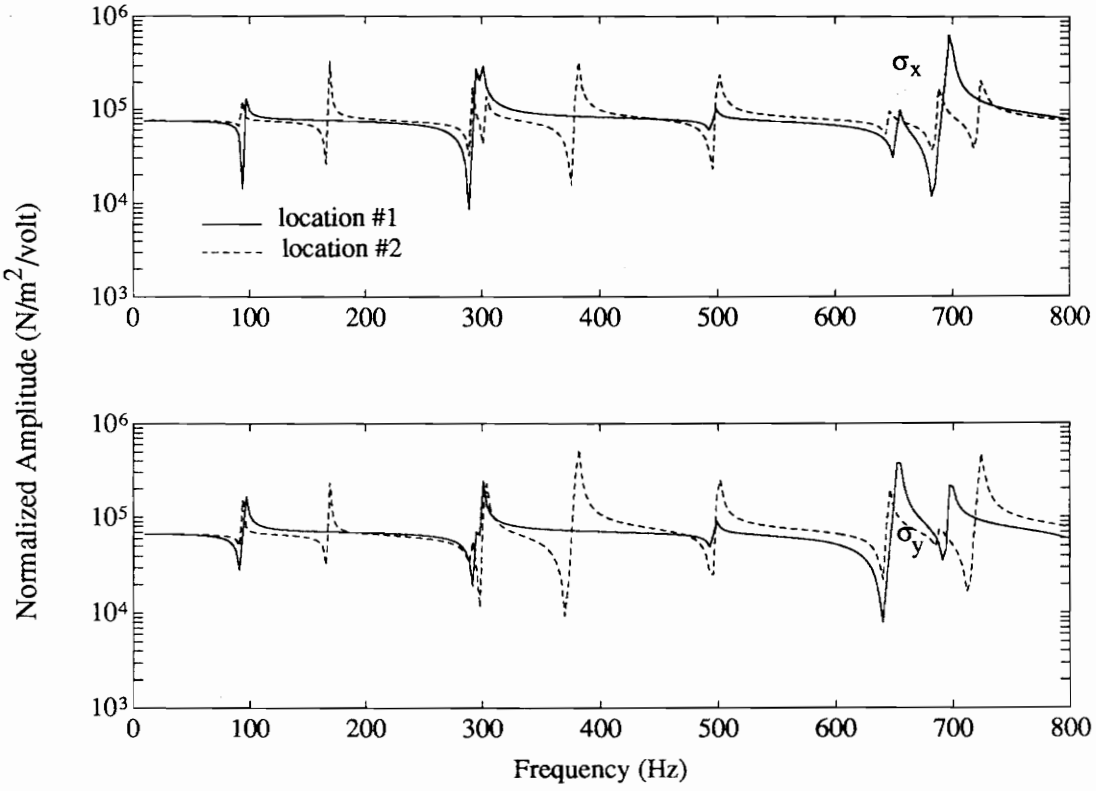

Figure 5.8: The variation of the location of the PZT actuator on the plate changes the induced dynamic stress of the PZT actuator.

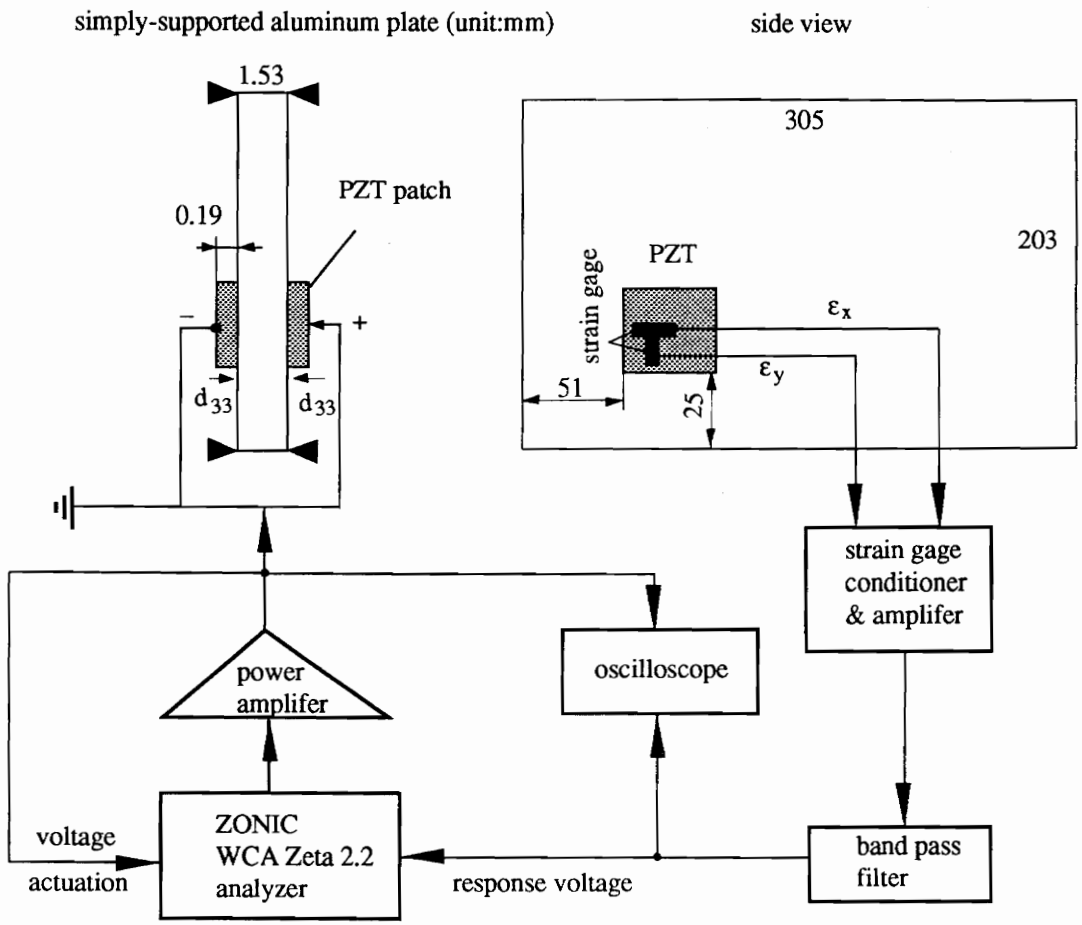

Figure 5.9: The experimental setup for measuring the dynamic strain of the PZT actuator.

the strain gage was used to examine the accuracy of all of the excited modes.

Figures 5.10 and 5.11 illustrate the measured and predicted strain in the x direction and y direction, respectively. The theoretical prediction based upon the dynamic system analysis (dashed line) agrees well with the experimental data (solid line). Compared with the static model, the impedance-based model provides an accurate prediction of dynamic stress behaviors of a PZT patch actuator. The design model has thus been validated.

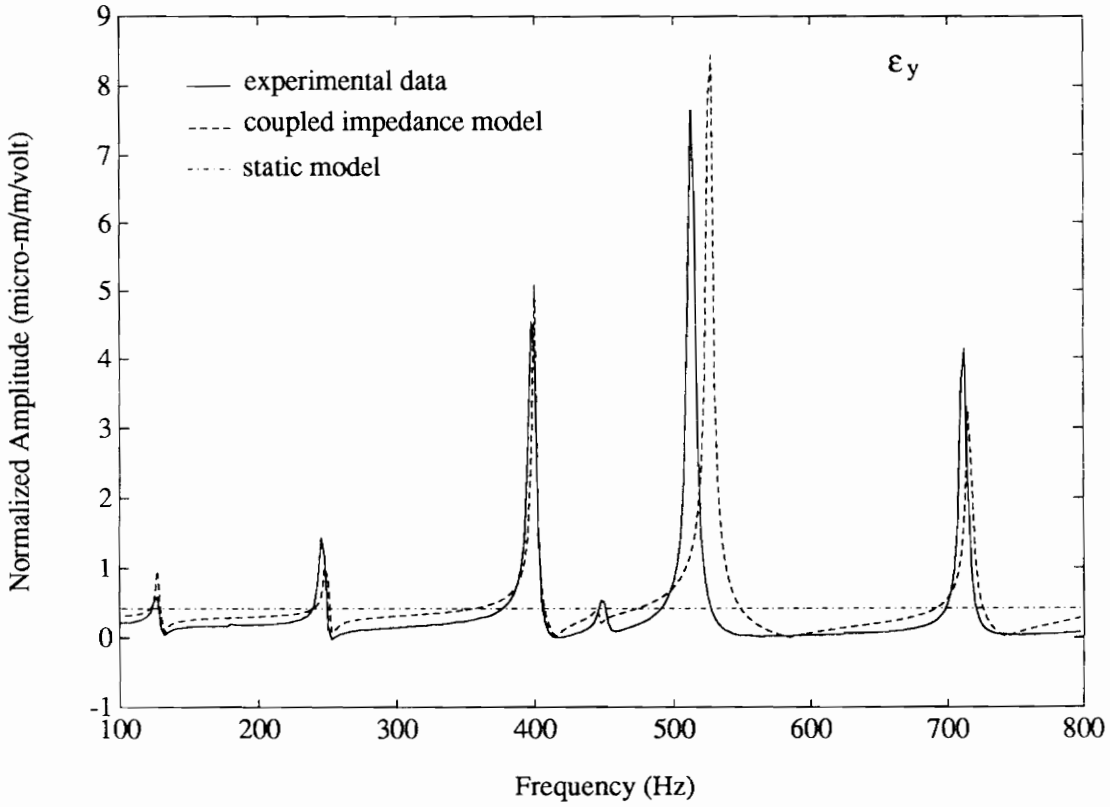

Figure 5.10: The predicted and measured dynamic strain of the PZT patch actuator in the y direction.

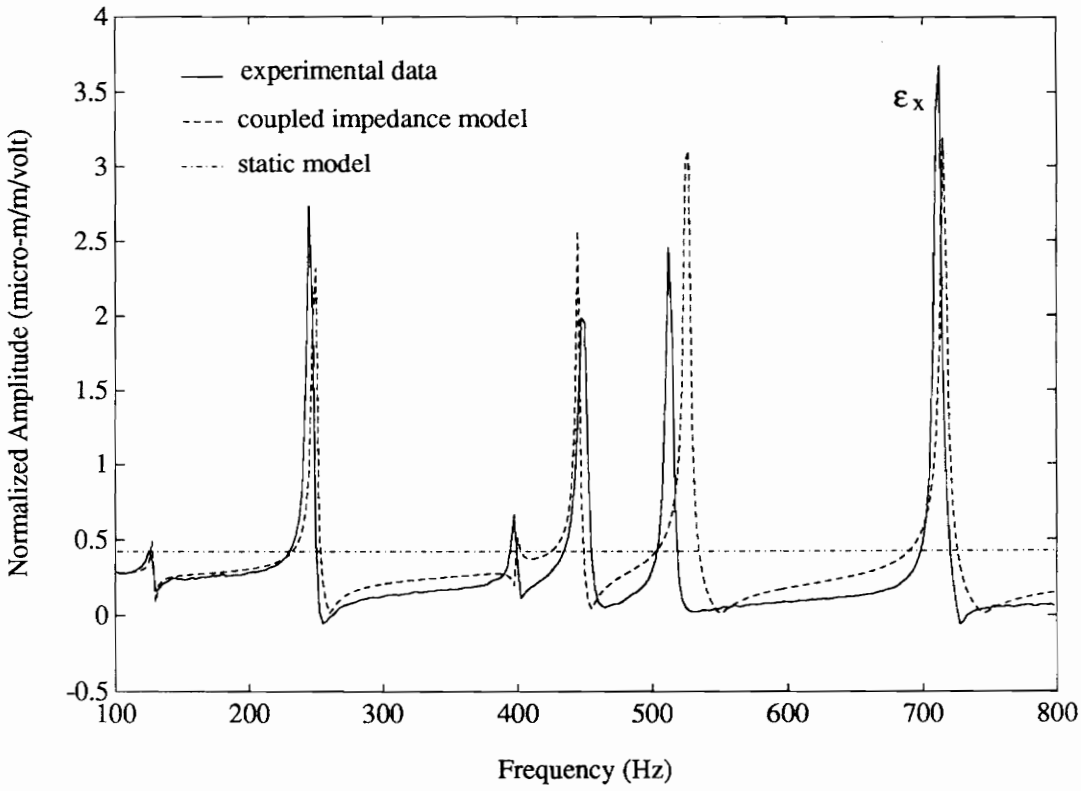

Figure 5.11: The predicted and measured dynamic strain of the PZT patch actuator in the x direction.

5.5 Concluding Remarks

- An impedance-based design model has been developed for the performance prediction and the parametric design of two-dimensional PZT patch actuators. The model can be used to quantitatively predict the dynamic outputs and the induced strain or stress, and to provide a effective tool to conduct the safety design of piezoelectric patch actuators.

- The induced mechanical stress in PZT patch actuators is a complex stress, a frequency-dependent stress, and a "point" stress. At the system resonance of integrated PZT/substrate structures, the dynamic stress is very high and has a peak value, while at the off-resonance the dynamic stress is relatively low and looks like a constant. The conventional static models may be used at off-resonance as an approximation of the dynamic system model.

- The parametric study shows that increasing the thickness of the PZT actuator not only intensifies actuator moment outputs for structural actuation, but also decreases the

induced dynamic stress levels. The actuation of the vibrational modes of the integrated system is strongly related to the location of the PZT actuator on the host structure. When the center of a PZT actuator happens to be located at the nodal line of a specific mode, this mode is hard to be excited because little actuation is applied to this mode.

- The experiment of measuring the induced dynamic strain of the PZT actuator integrated with a plate has verified the ability and utility of the impedance-based design model to predict the behaviors of PZT patch actuators.

5.6 References

Bailey, T. and J. E. Hubbard, "Distributed Piezoelectric-Polymer Active Vibration Control of a Cantilever Beam", AIAA Journal of Guidance and Control, 6 (5), 1985; pp. 605-611.

Crawley, E. F. and J. de Louis, 1987, "Use of Piezoelectric Actuators as Elements of Intelligent Structures", AIAA Journal, Vol. 29, No. 6; pp. 1373-1385.

Crawley, E. F. and K. B. Lazarus, 1991, "Induced Strain Actuation of Isotropic and Anisotropic Plates", AIAA Journal, Vol. 29, No. 6; pp. 945-951.

Dimitriadis, E. K., C. R. Fuller, and C. A. Rogers, 1989, "Piezoelectric Actuators for Distributed Noise and Vibration Excitation of Thin Plates", ASME Failure Prevention and Reliability, DE-Vol. 16; pp. 223-233.

Ikeda, T., 1990, Fundamentals of Piezoelectricity, Oxford University Press, New York.

Piezo Systems, In., 1993, Piezoelectric Product Catalog

Rogers, C. A., 1993, "Intelligent Material Systems: The Dawn of a New Materials Age", Journal of Intelligent Material Systems and Structures, Vol. 4, No. 1, pp. 4-14.

Wang, B. T. and C. A. Rogers, 1990, "Laminate Plate Theory for Spatially Distributed Induced Strain Actuators", Proceedings of the Fifth Japan-U. S. Conference on Composite Materials, Tama City, Japan.

Dimitriadis, E. K., C. R. Fuller, and C. A. Rogers, 1989, "Piezoelectric Actuators for Distributed Noise and Vibration Excitation of Thin Plates", ASME Failure Prevention and Reliability, DE-Vol. 16; pp. 223-233.

Ikeda, T., 1990, Fundamentals of Piezoelectricity, Oxford University Press, New York.

Zhou, S. W., C. Liang, and C. A. Rogers, 1994a, "A Dynamic Model of a Piezoelectric Actuator-Driven Thin Plates", Proceedings of Smart Structures and Materials, SPIE, Orlando, FL; in press.

Zhou, S. W., C. Liang, and C. A. Rogers, 1994, "Dynamic Design and Stress Characteristics of Integrated Piezoelectric Patch Actuators", Proceedings of the 2nd International Conference of Intelligent Materials, Williamsburg, VA; pp. 1360-1374.

Zhou, S. W., C. Liang, and C. A. Rogers, 1994, "Integration and Design of Piezoelectric Patch Actuators", accepted for the publication in Journal of Intelligent Material System and Structures, August, 1994.

Chapter 6

Temperature Rise and Thermal Stress of Piezoelectric Elements in Active Structures

6.1 Introduction

Piezoelectric (PZT) materials have been most commonly used as active elements in adaptive structures for various industrial and research applications. For the purpose of structural actuation, the mechanical output performance and dynamic behaviors of PZT elements have been widely investigated, as discussed in Chapters 2, 3, and 5. For space applications, system power consumption is one of the major concerns. Enhancing energy conversion efficiency results in a reduction in the cost and mass of systems, two of the major objectives of adaptive structures. Chapter 4 performed a coupled electro-

mechanical impedance analysis for two-dimensional PZT actuator-driven systems and discussed the influence of different dissipators on the system power factor and the system power requirement.

The system dissipative power is eventually transformed into internal heat energy in PZT elements. An increase in the temperature of the actuators is thus inevitable. The phenomenon of temperature rise of PZT actuators has often been noticed in the experiments. When PZT elements operate at a certain temperature, the aging process is accelerated, and piezoelectric properties, such as the dielectric constant and piezoelectric constant, change because of the strong temperature dependency. Figures 6.1 and 6.2 show the variation of the piezoelectric constant d_{31} and relative dielectric constant (K) with temperature, respectively (Piezo Systems, Inc., 1993). The material of SPI-5H displays a stronger temperature sensitivity than SPI-5A.

If the temperature is close to the Curie temperature of PZT materials, which represents a maximum operating temperature before suffering a permanent loss of piezoelectricity, the maximum safe stress of PZT elements is reduced and the thermal damage may take place. The Curie temperature is about 350 C for PSI-5A and 200 C for PSI-5H, respectively. In practice, as PZT elements are used for structural actuation at the system resonance or with a large electrical field, the heat generation throughout PZT actuators may be significant. Sometimes, the tin solder points on the surface of PZT actuators even

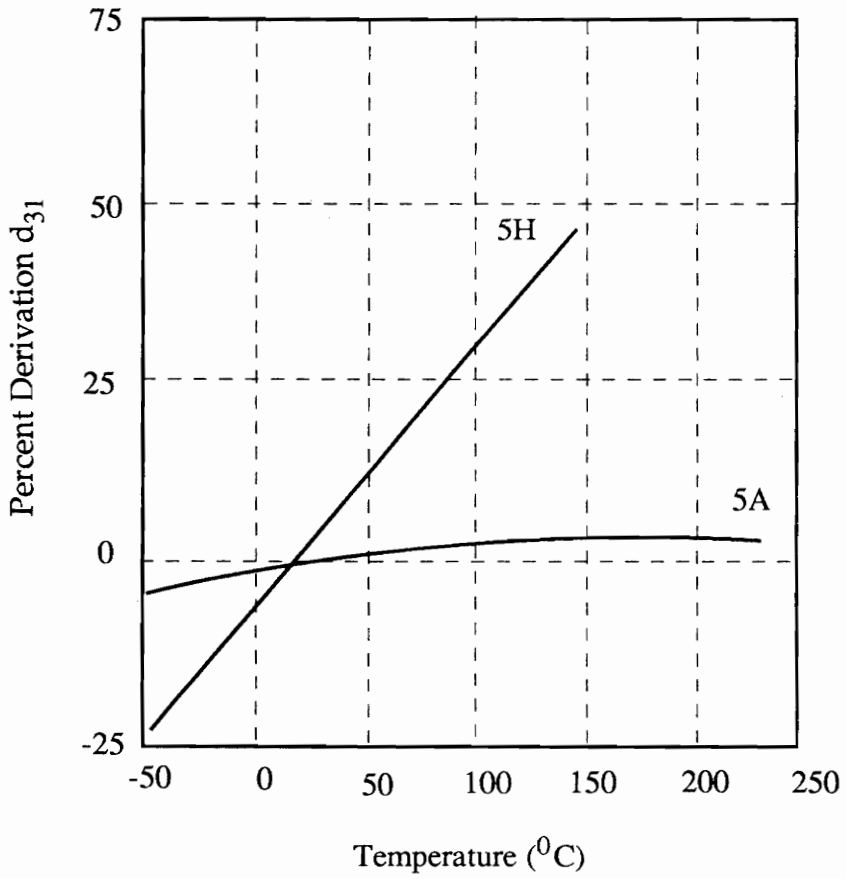

Figure 6.1: Influence of temperature on the piezoelectric constant, d_{31}, for typical piezoelectric materials: PSI-5A and PSI-5H (Piezo Systems, Inc).

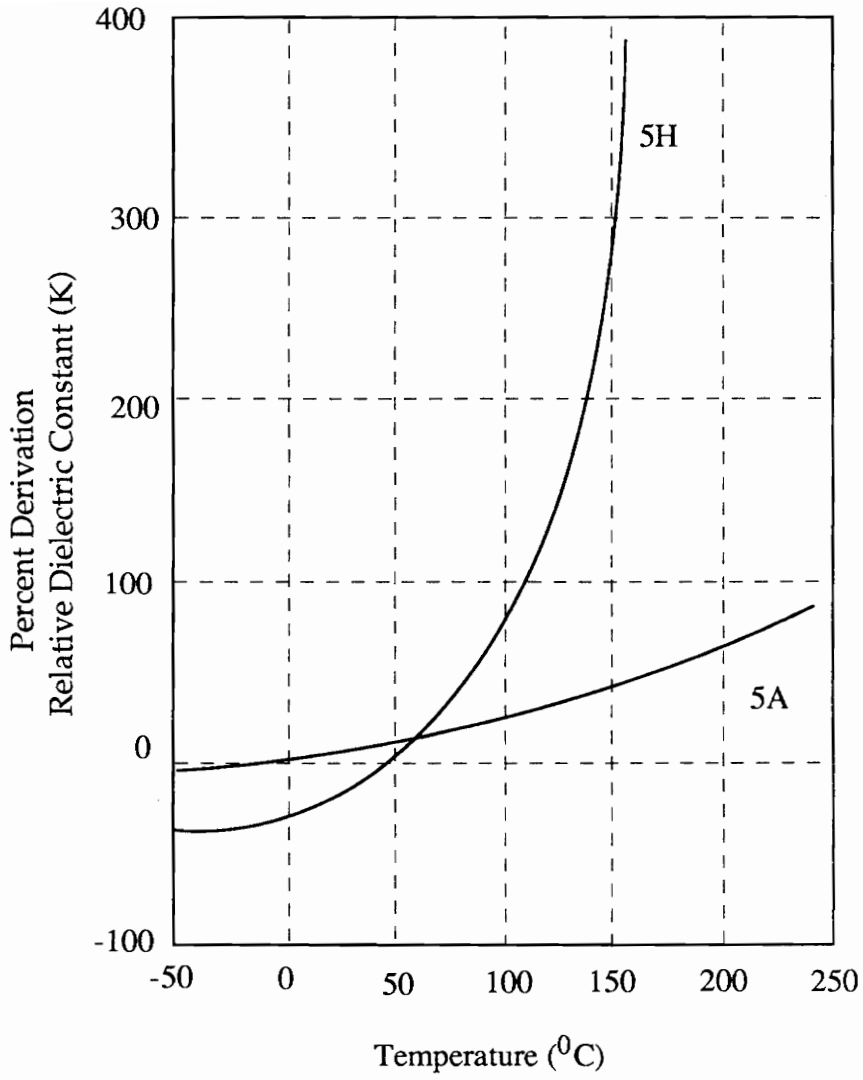

Figure 6.2: Influence of temperature on the relative dielectric constant, K, for typical piezoelectric materials: PSI-5A and PSI-5H (Piezo Systems, Inc.).

melt down. The situation becomes worse if actuated host structures are made of thermal resistant-materials, such as polymeric matrix composites or glass. In the meantime, the temperature gradient existing in PZT elements induces thermal stress, which may have an impact on the overall mechanical stress. Therefore, the heat transfer analysis of integrated PZT elements in structural actuation is of practical engineering importance. Investigation of these issues, however, has been limited.

The emphasis of this chapter is on the development of a simple approach to analyze and estimate temperature rise of PZT elements because of internal heat dissipation. A one-dimensional heat transfer model will be applied to integrated PZT/plate structures. The temperature field of the PZT actuators will be analytically found and the corresponding thermal stress will be quantitatively estimated. To determine the rate of internal heat generation in PZT actuators, a coupled electro-mechanical system model developed by the authors is directly used. The system dissipative power will then be predicted and treated as equivalent thermal dissipation to generate a distributed heat source throughout PZT actuators and host structures. A piezoelectric actuator-driven simply-supported plate will be used in the case studies. A comparison between the thermal stress level and the mechanical stress level is made to identify the impact of the thermal stress on the overall stress level. The effects of the actuator thickness, the magnitude of applied voltage, and material properties on the actuator temperature and the thermal stress level will be investigated.

6.2 Analytical Model

Figure 6.3 illustrates the schematic geometry of an integrated PZT/plate structure. Two PZT patches are bonded on the top and bottom surfaces of the plate. The integrated PZT/plate system is exposed to ambient room air without an external cooling source. It is assumed that the thickness of the plate and PZT actuator is much smaller than the sizes in the other coordinate directions. The flow of heat through the plate and the PZT element thus depends only on the coordinate measured normal to the x-y plane, resulting in a one-dimensional heat transfer problem with no edge effects. Figure 6.4(a) shows such an one-dimensional model. The internal heat generation, $q_{(p)}$, is assumed to be uniform throughout the PZT element and the plate, respectively. The steady state temperature distribution of the PZT element needs to be found, and thermal stress induced in the PZT element can then be estimated.

Considering the symmetrical condition of heat transfer, the problem shown in Fig. 4(a) may be simplified to the equivalent situation displayed in Fig. 6.4(b). The mid-plane of the plate is isolated, that is, $Dt/dz=0$. The governing differential equation of the temperature distribution cross the PZT element is depicted by:

$$\frac{d^2T_p}{dz^2}+\frac{Q_p}{k_p}=0\ , \tag{6.1}$$

where the subscript p denotes the parameters of the PZT element; k symbolizes the

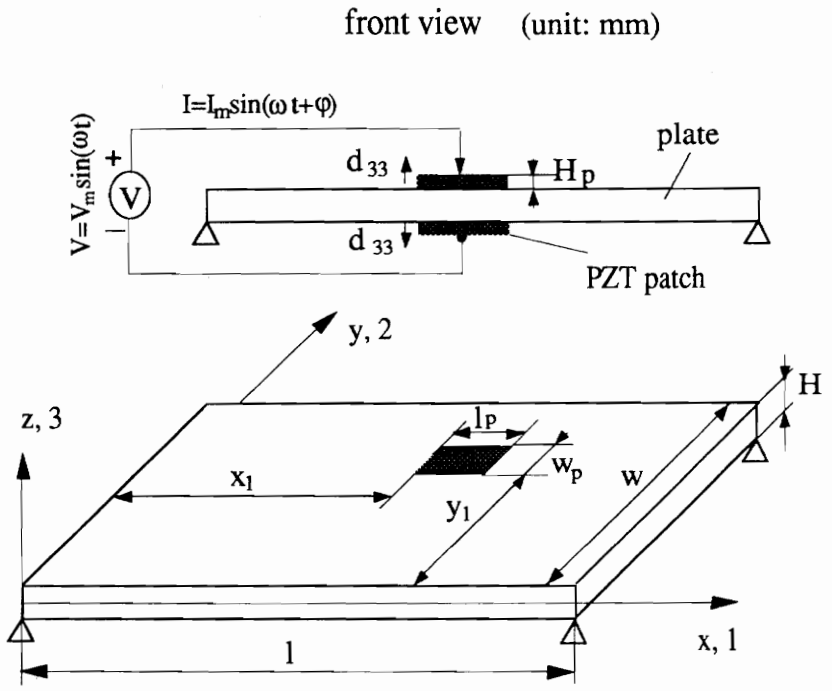

Figure 6.3: Schematic geometry of an integrated PZT/plate structure.

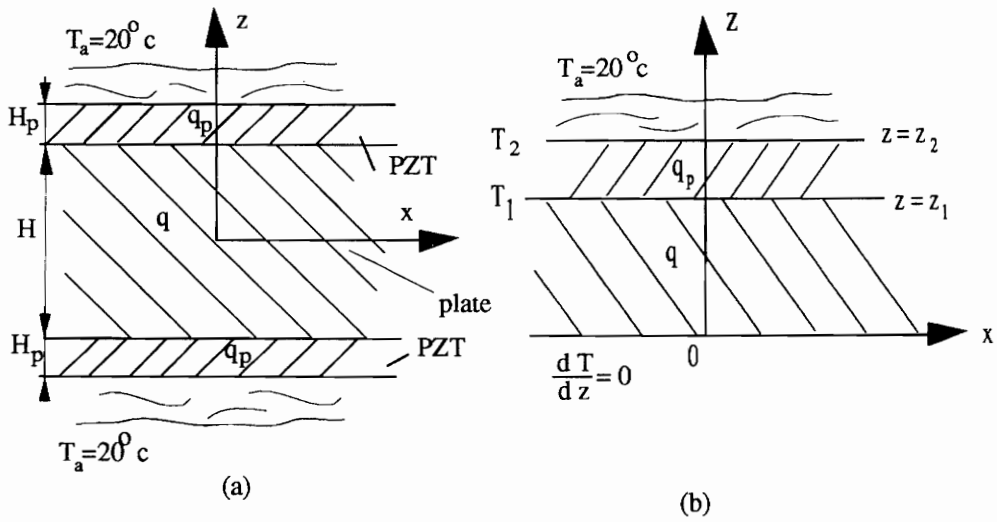

Figure 6.4: A schematic diagram of a heat transfer model for the analysis of temperature distribution of PZT elements integrated with a plate structure.

thermal conductivity; Q represents the rate at which heat is being internally generated in the PZT patch per unit volume (watt/m^3); and T is the temperature distribution in the PZT element. Twice integrating Eq. (6.1) with respect to the coordinate z obtains:

$$T_p = a_1 + b_1 z - \frac{Q_p}{2k_p} z^2 \ , \tag{6.2}$$

where a_1 and b_1 are the integration constants.

For the host plate, the governing differential equation of the temperature distribution and the corresponding solution are similar to Eqs. (6.1) and (6.2):

$$\frac{d^2T}{dz^2} + \frac{Q}{k} = 0 \ , \tag{6.3}$$

and

$$T = a_2 + b_2 z - \frac{Q}{2k} z^2 \ , \tag{6.4}$$

where a_2 and b_2 are integration constants. To determine a_1, b_1, a_2, and b_2, one may use the boundary conditions,

$$\begin{cases} \left(\frac{dT}{dz}\right)_{z=0} = 0 \\ \left(\frac{q_p}{s_p}\right)_{z=z_2} = h(T_2 - T_a) \ , \end{cases} \tag{6.5}$$

and the temperature continuity and heat transfer continuity at the interface of the PZT element and the plate,

$$\begin{cases} T_{z=z_1} = (T_p)_{z=z_1} \\ (q/s)_{z=z_1} = (q_p/s_p)_{z=z_1} \ , \end{cases} \tag{6.6}$$

s in Eqs. (6.5) and (6.6) is the surface area of the plane structure; h is the convection heat

transfer coefficient, or film coefficient. For free convection in air, h=5—25 $w/(m^2.C)$ (Chapman, 1974); T_2 and T_a are the surface temperature of the PZT element and the air temperature at the ventilated room, respectively; and the heat flow q can be found by using Fourier's law:

$$q = -ks\frac{dT}{dz}\ , \tag{6.7}$$

in which the minus sign indicates that the heat flow is taken to be positive if Dt is negative in the direction of increasing z. Substituting Eqs. (6.2), (6.4), and (6.7) into Eqs. (6.5)-(6.6) and solving for the integration constants yield:

$$\begin{cases} a_1 = -\dfrac{Q_p - Q}{k_p} z_1 z_2 + \dfrac{Q_p}{2k_p} z_2^2 + \dfrac{1}{h}[Qz_1 + Q_p(z_2 - z_1)] + T_a \\ b_1 = \dfrac{z_1}{k_p}(Q_p - Q) \\ a_2 = \dfrac{z_1^2}{2}\left(\dfrac{Q}{k} - \dfrac{Q_p}{k_p}\right) + a_1 + b_1 z_1 \\ b_2 = 0 \quad , \end{cases} \tag{6.8}$$

where z_1 and z_2 are the coordinates of the two surfaces of the PZT element; and the heat generation rate, Q_p in the PZT actuator and Q in the plate, can be obtained from a coupled electro-mechanical system model and will be developed later. Substituting Eq. (6.8) into Eq. (6.2), the surface temperature of the PZT element, T_2, can be obtained by:

$$T_2 = \frac{1}{h}[Qz_1 + Q_p(z_2 - z_1)] + T_a\ . \tag{6.9}$$

Eq. (6.9) indicates that the temperature in a PZT element increases with the rate of the internal heat generation, Q_p and Q, respectively. In addition, the temperature is inversely proportional to the heat conductivity of host structures. The induced thermal stress, σ_T,

is estimated by:

$$\sigma_T = \gamma_p Y_p (T_1 - T_2) \ , \tag{6.10}$$

where Y_p and γ_p denote the real Young's modulus and the coefficient of thermal expansion of piezoelectric materials, respectively. For PSI-5A-S3 material (Piezo System, Inc., 1993), $\gamma_p = 4x10^{-6}$ (m/m.C).

6.3 Heat Generation of the Integrated System

To estimate the heat generation in integrated PZT/plate systems, a coupled electro-mechanical system model is needed to quantitatively predict dissipative power consumption in the system. The power supplied to the PZT actuator is actually decomposed into two components (Zhou et. al., 1994): one is the dissipative power,

$$P = \frac{I_m V_m}{2} \cos\phi = \frac{V_m^2}{2} Re(A^*) \ , \tag{6.11}$$

and the other is the reactive power,

$$R = \frac{I_m V_m}{2} \sin\phi = \frac{V_m^2}{2} Im(A^*) \ , \tag{6.12}$$

where A^* is the electro-mechanical admittance of the system and the superscript * symbolizes a complex number. The subscript m denotes the magnitude of the electrical parameters: the applied voltage, $V = V_m e^{j\omega t}$ and the current in the circuit, $I = I_m e^{j(\omega t + \phi)}$; ϕ denotes the phase between the current and voltage; j symbolizes the imaginary part of a complex number; and ω is the input angular frequency; and the total electrical power, i.e.,

apparent power, is expressed by:

$$W=\sqrt{P^2+R^2}\ . \tag{6.13}$$

The power requirement of the system can be estimated from the maximum value of the apparent power.

It is clearly seen that the system power consumption is essentially dominated by the coupled electro-mechanical admittance of the system. The complex electro-mechanical impedance of the integrated PZT/plate system was derived by the authors. The detailed theoretical development can be found in a separate reference (Zhou et al., 1994). The relevant formulations are directly given here. When an electrical field, $E=V/H_p$, is applied cross a PZT element along the polarization direction (3), the current passing through the PZT actuator can be derived based upon the capacitor behavior for the PZT material. Then, following the definition of coupled electro-mechanical admittance gives:

$$A^*=\frac{I}{V}=j\omega\frac{l_p w_p}{H_p}\left[\epsilon_{33}^*-\frac{2d_{31}^2 Y_p^*}{1-\nu_p}+\frac{d_{31}^2 Y_p^*}{1-\nu_p}\left(\frac{\sin(\alpha_p l_p)}{l_p}\quad\frac{\sin(\alpha_p w_p)}{w_p}\right)N_{2\times 2}^{-1}\begin{pmatrix}1\\1\end{pmatrix}\right], \tag{6.14}$$

where l_p, w_p, and H_p are the length, width, and thickness of the PZT element, respectively; d_{31} and d_{32} are the piezoelectric constants; ν_p is the Poisson's ratio of the PZT material; $\epsilon^*_{33}=\epsilon_{33}(1-j\delta_p)$ is the complex dielectric constant at zero stress; δ_p is the dielectric loss factor of the PZT actuator; $Y_p^*=Y_p(1+j\eta_p)$ is the complex Young's modulus at a constant electrical field; η_p is the structural loss factor. The wave number, α_p, is defined as:

$$\alpha_p = \omega \sqrt{\frac{\rho_p}{Y_p^*}}, \tag{6.15}$$

where ρ is the mass density. The matrix N_{2x2} in Eq. (15) is depicted by:

$$N_{2\times 2} = \begin{pmatrix} \alpha_p \cos(\alpha_p l_p)(1 - \nu_p \frac{w_p}{l_p}\frac{Z_{yx}}{Z_{pxx}} + \frac{Z_{xx}}{Z_{pxx}}) & \alpha_p \cos(\alpha_p w_p)(\frac{l_p}{w_p}\frac{Z_{xy}}{Z_{pyy}} - \nu_p \frac{Z_{yy}}{Z_{pyy}}) \\ \alpha_p \cos(\alpha_p l_p)(\frac{w_p}{l_p}\frac{Z_{yx}}{Z_{pxx}} - \nu_p \frac{Z_{xx}}{Z_{pxx}}) & \alpha_p \cos(\alpha_p w_p)(1 - \nu_p \frac{l_p}{w_p}\frac{Z_{xy}}{Z_{pyy}} + \frac{Z_{yy}}{Z_{pyy}}) \end{pmatrix}, \tag{6.16}$$

in which Z_{xx} and Z_{yy} are the direct impedance, and Z_{xy} and Z_{yx} are the cross impedance of the plate at the mid-point of the edge of the PZT element, respectively. For simply-supported plates, the analytical solutions of the mechanical impedance of the system have been derived in Chapter 3. For complex structures, a finite element analysis or experimental approaches is helpful to determine the mechanical impedance of the system.

Our current interest is in the system dissipative power. It basically includes three parts in an integrated PZT/substrate system : (1) the power dissipated by the structural damping of the host structure, which is related to the structural loss factor in the complex Young's modulus; (2) the power consumed by the material damping of the PZT actuator; (3) the power consumption caused by the dielectric loss of the PZT actuator. The dissipative power is assumed to be totally converted into thermal energy to heat the system. The heat generation rate in the PZT element may be obtained by setting a zero structural loss factor for the plate in Eqs. (6.11) and (6.14):

$$Q_p = \frac{P_{\eta=0}}{l_p w_p H_p} \quad . \tag{6.17}$$

Similarly, assuming a zero mechanical loss and dielectric loss of the PZT element in Eqs. (6.11) and (6.14) gives the heat generation rate in the plate:

$$Q = \frac{P_{\eta_p=\delta_p=0}}{lwH} \quad , \tag{6.18}$$

where l, w, and H are the length, width, and thickness of the plate, respectively.

6.4 Numerical Cases and Discussion

A simply-supported aluminum thin plate integrated with PZT patch elements is used in the current case studies. The geometric configuration of the integrated PZT/plate system is shown in Fig. 6.3. The PZT elements are located on the plate at x_1=*158.8 mm (6.25")* and y_1=*82.6 mm (3.25")*. The size of the plate is *228.6 x 127 x 1 mm (9" x 5" x 0.04")*. The size of the PZT patch is *38.1 x 25.4 mm (1.5" x 1")*. The basic material properties of the PZT (PSI-5A-S3) and the plate are listed in Table 2.1.

The effect of the applied electrical field on the surface temperature of the PZT element is first examined. The actuator thickness is selected as H_p=*0.1*, *0.2*, and *0.4* (mm). The free convection heat-transfer coefficient h in air at the ventilated room temperature, T_a=*20 C*, is chosen as *7 (w/m^{2}C)*. The integrated system is excited at the 5th mode that is at a frequency of about 800 Hz. The surface temperature of the PZT actuator is calculated

using Eq. (6.9). Figure 6.5 shows the numerical results. The temperature rapidly increases with the applied voltage because the internal heat generation rises with the order of the square of the applied voltage. At a constant voltage, decreasing the actuator thickness produces a stronger electrical field, resulting in an increment of the surface temperature. When a voltage of 120 volts is applied to the PZT actuator with the thickness of 0.2 mm to excite the 5th mode, the temperature is up to 216^0C which exceeds the melting point of the tin solder. A simple experiment was conducted to actuate an aluminum plate of the size 203 x 101.6 x 1 mm (8" x 4" x 0.04") using the PZT patches (Hp=0.19mm). The phenomenon of melting the tin solder was observed.

To identify the impact of the thermal stress on the overall stress level of the PZT actuator, the mechanical stress needs to be determined. The induced mechanical stress in the PZT element, σ_x and σ_y, can be calculated as follows (see Chapter 4 for the details):

$$\begin{pmatrix}\sigma_x\\ \sigma_y\end{pmatrix} = \frac{Y_p^* V_m}{H_p(1-\nu_p^2)}\begin{pmatrix}1 & \nu_p\\ \nu_p & 1\end{pmatrix}\left[\alpha_p\begin{pmatrix}\cos(\alpha_p x_p) & 0\\ 0 & \cos(\alpha_p y_p)\end{pmatrix}N_{2\times 2}^{-1} - I_{2\times 2}\right]\begin{pmatrix}d_{31}\\ d_{32}\end{pmatrix}e^{j\omega t}, \tag{6.19}$$

where I_{2x2} is an identical matrix; and x_p and y_p are the location coordinates of the stress point on the PZT actuator. The mechanical stress is a function of excitation frequency and the mechanical impedance of the system. It is assumed that the stress is measured at x_p=*3 mm* and y_p=*19 mm*. The size of the plate is again *228.6 x 127 x 1 mm (9" x 5" x 0.04")*. The size of the PZT element is *38.1 x 25.4 x 0.2 mm (1.5" x 1" x 0.04")*. Figure 6.6 illustrates the mechanical stress characteristics. The induced dynamic stress

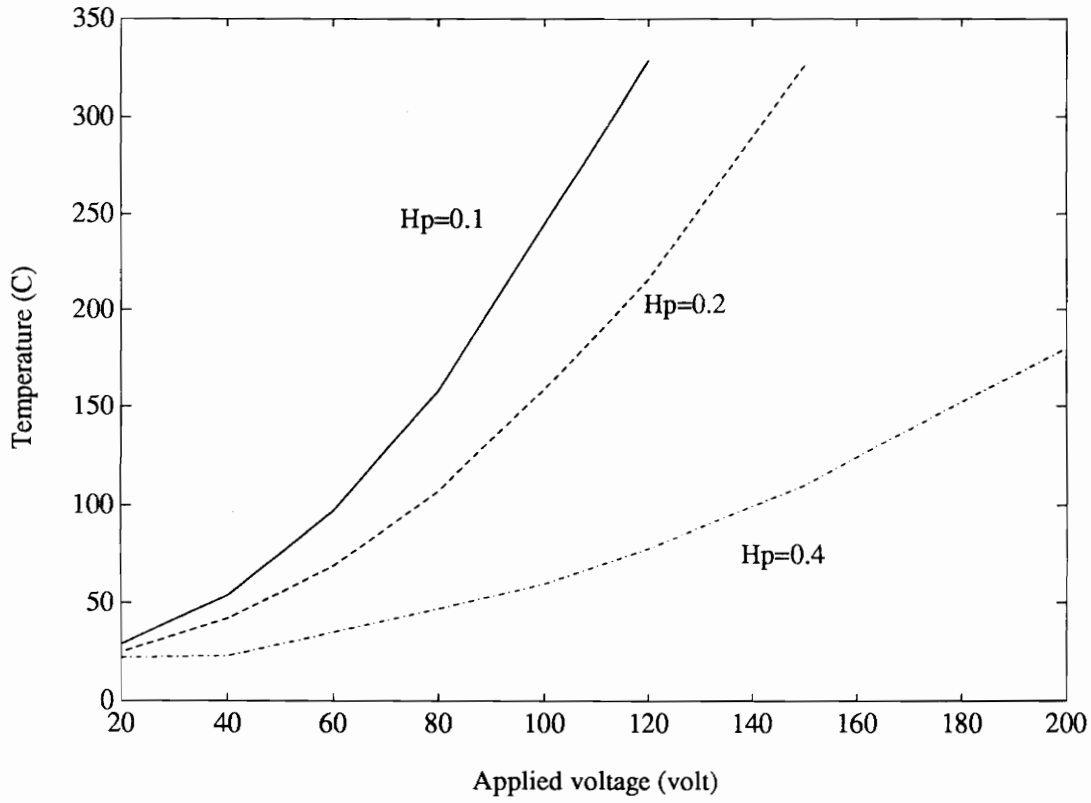

Figure 6.5: Effect of an applied electrical field on the surface temperature of PZT elements.

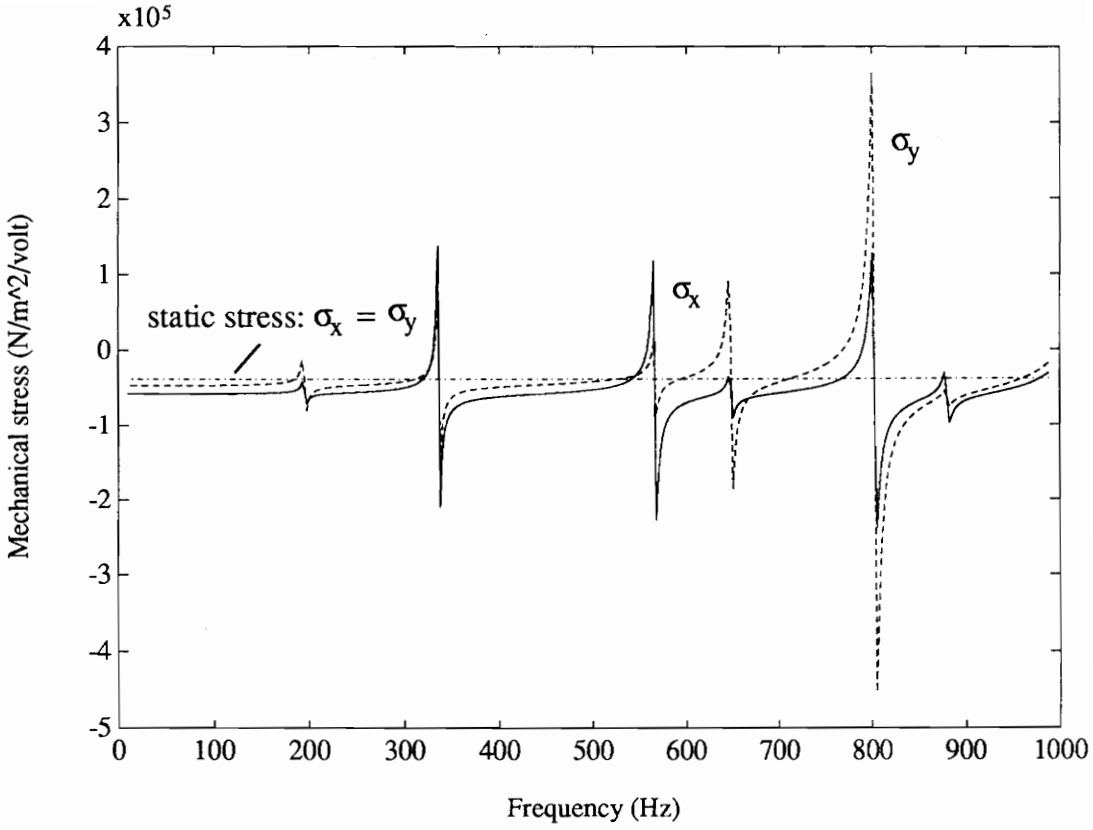

Figure 6.6: Mechanical stress characteristics of an integrated PZT element.

is a complex stress. At the resonant frequencies of the integrated system, the induced stress levels are very high because of the minimum structural impedance. While at off-resonance the induced dynamic stress approaches the static stress that is calculated using the static model developed by Dimitriadis et al. (1989).

If a *228.6 x 127 x 4 mm (9" x 5" x 0.16")* plate is excited at the 5th mode and the applied electrical field is maintained at 250 (volt/mm), Eqs. 6.10 and 6.19 can be used to obtain the thermal stress and mechanical stress of the PZT element, respectively. Figures 6.7 and 6.8 show the numerical results. The thermal stress induced in the PZT element increases when the element becomes thicker and thicker, as displayed in Fig. 6.7. The mechanical stress, however, significantly declines when the thickness of the PZT element goes up, as displayed in Fig. 6.8. It can be explained that the thicker PZT element has a larger cross sectional area that relieves the mechanical stress. On the other hand, the thicker element produces a larger temperature difference, leading to a higher thermal stress. This observation implies that the thermal stress in a stack PZT actuator (or a multilayer actuator) may become a major factor to influence the overall stress levels. It is also noted that the stress in Figs. 6.7 and 6.8 do not linearly change with the actuator thickness because structural mechanical impedance is not simple linear function of the actuator thickness.

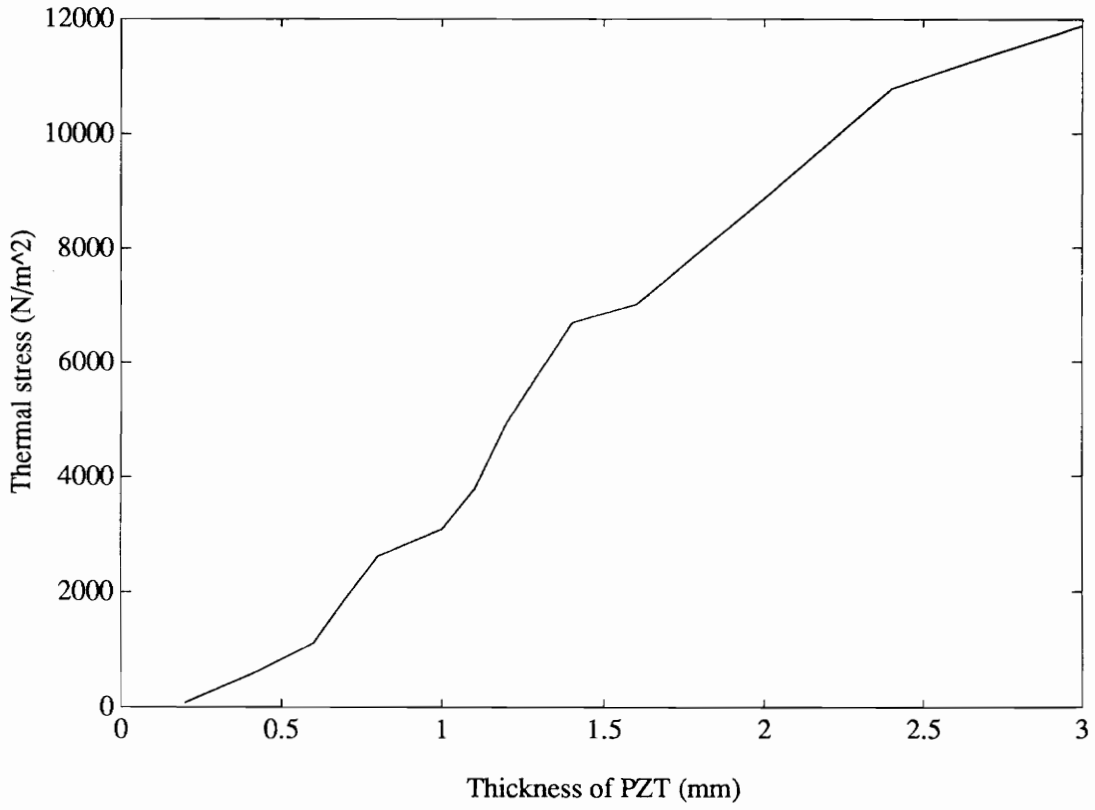

Figure 6.7: Thermal stress goes up as the thickness of an integrated PZT element increases (E=250 volt/mm; H=4 mm).

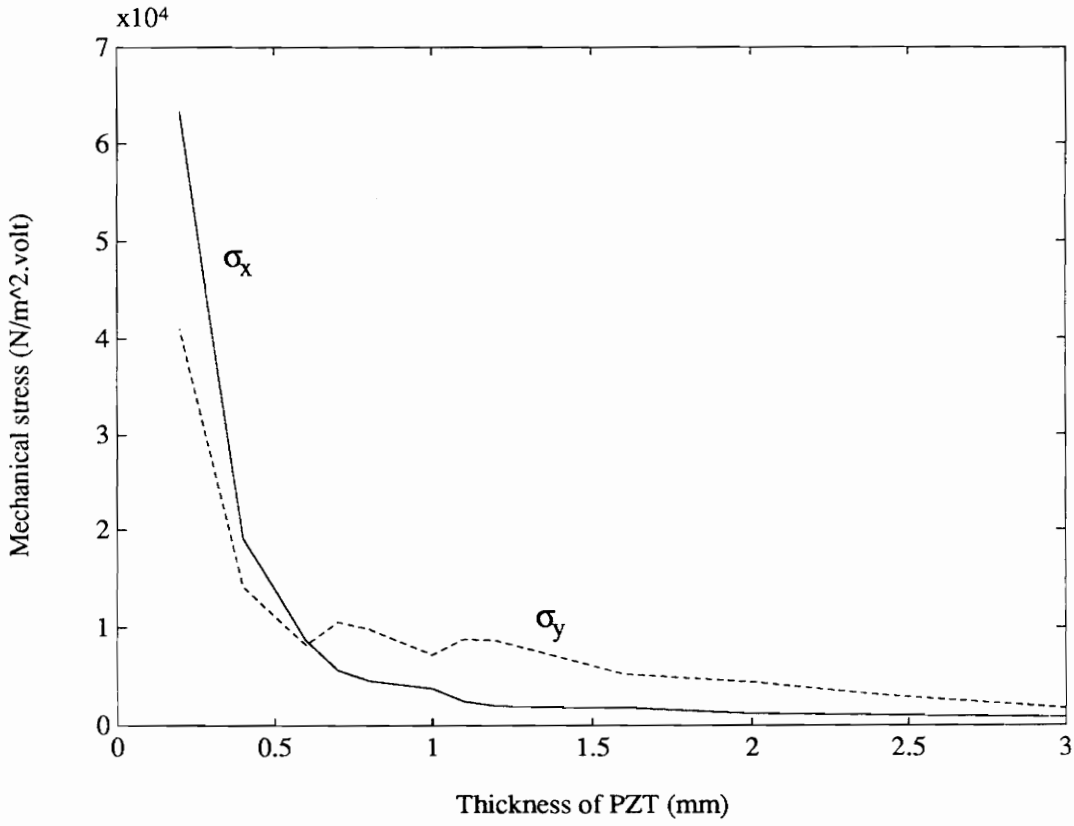

Figure 6.8: Mechanical stress decreases as the thickness of an integrated PZT element increases (E=250 volt/mm; H=4 mm).

From a design point of view, one way to reduce the induced stress level in PZT elements is to limit the active voltage, leading to a decline in both the mechanical and thermal stress. In this case, the actuation force also decreases. The other way is to increase the cross-sectional area of PZT elements as the voltage increases so that the electrical field is maintained at a relatively low level to avoid possible thermal damage and mechanical degradation in the PZT elements. In general, when a thin PZT patch is used for the structural actuation, the induced mechanical stress is of major concern and the surface temperature of the actuator should also be considered. While a multilayer actuator or a stack actuator is applied for the actuation, the thermal stress may become an important factor in the actuator design and application.

To examine the influence of the thermal conductivity of the host plate on the surface temperature of PZT elements, three types of materials with different thermal conductivity are selected: aluminum, nickel steel, and glass. Table 6.1 lists the basic properties of the materials. For simplification, it is assumed that the investigated plates have the same geometric size and the structural damping. Figure 6.9 shows the numerical results. As PZT actuators are used to excite thermal resistant material, such as glass and nickel steel, the temperature rises quickly and the thermal degradation of the actuator may speed up. Under the condition of a certain rate of heat generation, host structures with a good conductivity can slow down the temperature hike of PZT actuators and relieve the possible thermal degradation.

Table 6.1: Material Properties of the Different Host Plates and the PZT Actuators

	Young's modulus (N/m^2)	mass density (kg/m^3)	thermal conductivity (w/-m.c)
Nickel steel	$21x10^{10}$	8800	18.6
Glass plate	$6.4x10^{10}$	2300	0.76
Aluminum	$6.9x10^{10}$	2700	112.5
PZT (SPI-5A-3S)	$5.7x10^{10}$	7700	23

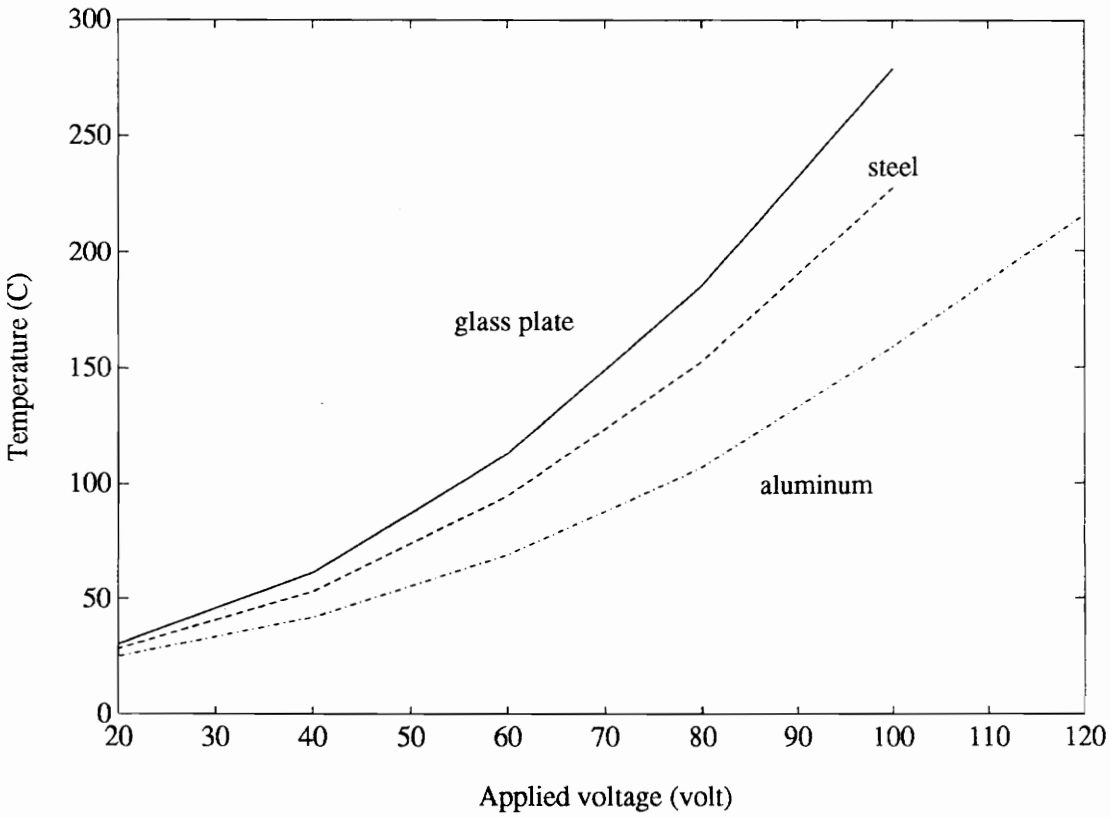

Figure 6.9: Influence of the thermal conductivity of the host structures on the surface temperature of an integrated PZT element (*E=250 volt/mm; H=4 mm; and* H_p*=0.2 mm*).

6.5 Concluding Remarks

- A simple one-dimensional heat transfer model for piezo-electric elements for structural actuation has been suggested . The analytical model has been developed to quantitatively estimate the temperature rise and the induced thermal stress of the PZT elements.

- The heat generation of the integrated PZT/plate system has been determined from the dissipative power consumption using the electro-mechanical system model.

- Case studies have demonstrated that when the PZT actuator operates at the system resonance, or with a relatively high electrical field, the heat generation and temperature rise of PZT actuators is significant and may cause the thermal degradation, even damages of PZT elements. The temperature of PZT actuators increases with the applied voltage because the heat dissipation is proportional to the square of the applied voltage. Under the excitation with a constant voltage, the thinner PZT actuator gains higher temperature rise due to the higher electrical field.

- The thermal stress increases with the thickness of PZT actuators. When a thicker PZT patch or a multilayer or a stacked PZT actuator is used for structural actuation, the thermal stress may become a significant factor influencing the strength design of the PZT actuator.

- When the thermal resistant materials are used for host structures, the temperature in PZT elements increases quickly, and cooling measures may be needed to avoid the possible thermal damage.

6.6 References

Chapman, A. J., 1974, Heat Transfer, Macmillan Publishing Co., New York.

Dimitriadis, E. K., C. R. Fuller, and C. A. Rogers, 1989, "Piezoelectric Actuators for Distributed Noise and Vibration Excitation of Thin Plates", ASME Failure Prevention and Reliability, DE-Vol. 16; pp. 223-233.

Holman, J. P., 1976, Heat Transfer, MaGraw-Hill Inc., New York.

Piezo Systems, In., 1993, Piezoelectric Product Catalog

Zhou, S. W., C. Liang, and C. A. Rogers, 1994, "Temperature Rise and Thermal Stress of Integrated Piezoelectric Elements for Structural Actuation", Adaptive Structures and Composite Materials, ASME, AD-Vol. 45, MD-Vol. 54, Chicago, MI, Nov. 6-11, 1994; pp. 183-191.

Zhou, S. W. and C. A. Rogers, 1994, "Heat Generation, Temperature, and Thermal Stress of Structurally Integrated Piezo-Actuators", accepted for the publication in Journal of Intelligent Material Systems and Structures, August, 1994.

Chapter 7

Conclusions and Recommendations

7.1 Conclusions

In this dissertation, an impedance-based electro-mechanics analytical method and experimental investigation have been performed for generic piezoelectric actuator-driven adaptive structures. The newly developed system model has been used to quantitatively predict the actuator outputs (forces, moments, or displacements), the actuator energy conversion efficiency, the system power requirement and consumption, the induced dynamic stress characteristics, and the actuator temperature rise and thermal damage. When compared with the conventional static models, the coupled system modeling method has provided a new interdisciplinary viewpoint on adaptive structures and a more accurate description of complex electro-mechanical active material systems. The dynamic essence and the interconnections among the intelligent elements and supporting structures

have been revealed. Another advantage of this modeling technique is the potential for designing energy-efficient smart structures, actuators, and their associated power electronics and for optimizing the actuator location and thickness. The concept and method developed from this study will benefit the implementation and innovation of other induced strain actuators, such as shape memory alloy actuators, electrostrictive actuators, and magnetostrictive actuators.

The major conclusions from this study are summarized as follows:

- The theoretical model of integrated PZT/substrate systems was developed for generic two-dimensional smart structures based on the system mechanical impedance characteristics and the piezoelectric constitutive equation. The actuation force was evaluated as a result of the dynamic interaction between the actuator and the host structure. The added stiffening and mass loading of PZT actuators were considered in the system modeling. The model was then extended to include the electrical parameters of the PZT actuators. A close form solution of the coupled electro-mechanical admittance of the integrated system was derived from the capacitor behavior of the PZT materials. The power factor, the power dissipation, and the power requirement of the system were thus numerically predicted. Once the system power consumption was determined, the

dissipative power was treated as the equivalent thermal dissipation to evaluate a temperature rise and thermal stress of the actuators.

- To examine the utility and generality of the system modeling method, the developed model was applied to typical two-dimensional intelligent structures such as thin plates and thin shells, and to one-dimensional structures such as circular rings and beams. The detailed parametric studies were conducted including the actuator thickness, size, location, and material properties, and the geometrical and physical parameters of the host structures. The frequency-dependent and structural impedance-dependent output behaviors of the PZT actuators were quantitatively predicted. The phenomenon of the frequency response shift of the original system due to the "planted" PZT actuators was accurately reflected in the model. The physical implication was reasonably interpreted using the concept of the impedance matching. The actuation of the vibration modes of the integrated system is strongly related to the location of the PZT actuator on host structures. When the center of a PZT actuator happens to be located at the nodal line of a specific mode, this mode is hard to be excited because little actuation force or energy is supplied to this mode.

- The analysis of power consumption has demonstrated that the dissipative

power supplied to PZT actuators is primarily consumed by the mechanical damping of host structures at resonant frequencies and is dissipated by the dielectric loss of the PZT actuator itself at off-resonance. The system power requirement was also estimated.

- The modeling method was then applied to design the PZT patch actuators. The induced mechanical stress characteristics were specifically investigated. The complex, "point", frequency-dependent stress performance of the commercial segmented patch actuators was discussed. The significant difference between the static stress level and the dynamic stress level was clearly demonstrated. The low dynamic tensile strength of PZT materials was considered in the design. From the standpoint of safety design, the recommendation of increasing actuator thickness was made to amplify the moment output for structural actuation and to decrease the induced stress levels.

- A one-dimensional heat transfer model was suggested for the integrated PZT/plate structures. The rate of internal heat generation in PZT actuators was determined using the developed electro-mechanical system model. The temperature of PZT actuators increases with the applied voltage. Under the excitation with a constant voltage, the thin PZT actuator gains

higher temperature rise due to the higher electric field. The induced thermal stress increases with the thickness of PZT actuators. When a thicker PZT patch or a multilayer or a stacked PZT actuator is used for structural actuation, the thermal stress becomes a significant factor influencing the strength design of PZT actuators.

- The experimental techniques were explored in this research. The PZT actuator-driven simply-supported plate was built and tested. Two PZT patches were bonded on the top and bottom surfaces of the plate to create a pure bending excitation. The vibrational displacement and velocity of the integrated plate, and the dynamic strain of the PZT actuators were measured, respectively. The coupled electro-mechanical admittance of the real system was also directly measured using the impedance analyzer. The power factor representing the energy conversion efficiency was thus directly determined. An extensive comparison of experimental results and the corresponding theoretical solutions was made to demonstrate the ability and accuracy of the system model. The predicted results have a good match with the experimental data so that the theoretical model has been validated. In addition, the various sensors, including the laser sensor, PZT sensors, the accelerometer, and the strain gauge were used in the testing to identify the effect of the different sensing on the experimental results.

7.2 Recommendations

Further study and research efforts are recommended to expand the coupled electro-mechanical system modeling approach into a wider scope of applications.

- The coupled electro-mechanical system modeling approach has been very well established and experimentally verified for typical small scale structures in the laboratory. Although there is no limitation applied on the developed theory, the future investigation is required to apply this modeling technique to large-scale complex structures, such as aircraft cabins and shell structures of submarines.

- Since integrated PZT actuators stiffen host structures and put added mass in the system, the frequency shift of the system resonance occurs, resulting in the change of the system poles. When piezoelectric actuator-driven adaptive structures are used in structural vibration and acoustic control, the pole shift may cause the instability of the integrated system. The developed system model, which can accurately predict the frequency shift, should be further extended to be incorporated into a control algorithms. The influence of the frequency shift on the system stability should also be investigated.

- An optimization algorithm needs to be developed based upon the maximum system power factor or the maximum actuator outputs (force, moment or displacement) to determine the optimal actuator location, actuator thickness, and actuator sizes.

- The expansion of the electro-mechanical system model should include the acoustic impedance and fluid loading such that a coupled eletro-acousto-mechanical analysis will be developed for 2-D underwater structural acoustic control.

- The present analysis of integrated actuator and system power consumption focuses on the damping factors in PZT/substrate systems. The further power consumption analysis should include the electronics of the power supply in order to determine the overall system power requirement. The effect of the actuator power factor on energy efficiency of an active vibration and acoustic control system should be further investigated.

- To more accurately predict the actuator temperature field and the possible thermal damage, a coupled electro-thermo-mechanical model is needed to consider the dynamic couplings of heat transfer with the structural mechanics and electrical field. The pyroelectric effect and the thermal

strain effect can then be incorporated into the system model.

Vita

Su-Wei Zhou was born in Nanjing, China on September 17, 1958. He grew up in Nanjing and graduated from First Jurong High School in 1975. He did not start his undergraduate study until 1978 when the universities in China were reopened after being closed for ten years. He enrolled in Mechanical Engineering at Nanjing Institute of Technology, where he earned a Bachelor's degree in 1982, and a Master's degree in 1985. After graduation, he joined the faculty of the Department of Mechanical Engineering, Southeast University, Nanjing, China, and worked as an Assistant Professor and later as a Lecturer from 1985 to 1991. During this time, he conducted research in impact vibration and noise control, especially in passive damping technologies. He also taught courses on Control, Vibration of Mechanical Systems, Machine Design, Tool and Die Design, and Manufacturing Technologies of Machine Tools. He then decided to continue his education at Virginia Polytechnic Institute and State University (Virginia Tech), in Blacksburg, VA, U.S.A. He came to Virginia Tech in the Fall of 1991 to pursue a doctoral degree in the Department of Mechanical Engineering, where his research work has centered on adaptive structures. He graduated with a Ph.D. degree in Mechanical Engineering in August, 1994.